

AN EXPERIMENTAL AND NUMERICAL STUDY ON THE COMBUSTION
CHARACTERISTICS OF POOL FIRES IN TUNNELS

A THESIS SUBMITTED TO
THE GRADUATE SCHOOL OF NATURAL AND APPLIED SCIENCES
OF
MIDDLE EAST TECHNICAL UNIVERSITY

BY

SINA SHAFEE

IN PARTIAL FULFILLMENT OF THE REQUIREMENTS
FOR
THE DEGREE OF DOCTOR OF PHILOSOPHY
IN
MECHANICAL ENGINEERING

JULY 2017

Approval of the thesis:

**AN EXPERIMENTAL AND NUMERICAL STUDY ON THE COMBUSTION
CHARACTERISTICS OF POOL FIRES IN TUNNELS**

submitted by **SINA SHAFEE** in partial fulfillment of the requirements for the degree
of **Doctor of Philosophy in Mechanical Engineering Department, Middle East
Technical University** by,

Prof. Dr. Gülbin Dural Ünver
Dean, Graduate School of **Natural and Applied Sciences**

Prof. Dr. Raif Tuna Balkan
Head of Department, **Mechanical Engineering**

Assoc. Prof. Dr. Ahmet Yozgatlıgil
Supervisor, **Mechanical Engineering Dept., METU**

Examining Committee Members:

Assoc. Prof. Dr. M. Metin Yavuz
Mechanical Engineering Dept., METU

Assoc. Prof. Dr. Ahmet Yozgatlıgil
Mechanical Engineering Dept., METU

Prof. Dr. Murat Köksal
Mechanical Engineering Dept., Hacettepe University

Assoc. Prof. Dr. Murat Kadri Aktaş
Mechanical Engineering Dept., TOBB ETÜ

Assist. Prof. Dr. Feyza Kazanç
Mechanical Engineering Dept., METU

Date: 07.07.2017

I hereby declare that all information in this document has been obtained and presented in accordance with academic rules and ethical conduct. I also declare that, as required by these rules and conduct, I have fully cited and referenced all material and results that are not original to this work.

Name, Last Name: Sina, SHAFEE

Signature:

ABSTRACT

AN EXPERIMENTAL AND NUMERICAL STUDY ON THE COMBUSTION CHARACTERISTICS OF POOL FIRES IN TUNNELS

Shafee, Sina

Ph.D., Department of Mechanical Engineering

Supervisor: Assoc. Prof. Dr. Ahmet Yozgatlıgil

July 2017, 136 pages

This work presents the results of experimental and numerical analysis on tunnel fires in an attempt to improve existing knowledge on the fire dynamics and related safety measures in various tunnel fire scenarios. Results are grouped into four parts in which the effects of tunnel wall coating, inclination, tunnel obstruction and existence of secondary fire source in close vicinity were investigated on tunnel fire characteristics. A 1/13 longitudinally ventilated scaled tunnel model constructed based on Froude modeling was used in the experiments with ethanol pools as the fire source. Numerical simulations were carried out using Fire Dynamics Simulator code. The focus was on critical factors in the safety research community including heat release rate (fire load), burning rate of fire and tunnel temperature distribution, which were measured across a wide range of ventilation conditions, pool size and depth. Results emphasized that the overall variations in the burning rates of fires at different ventilation conditions was a function of competing factors that affect the heat release rate, mass transfer coefficient and cooling effect of the airflow. The application of absorptive wall coating led to considerable reduction of radiative heat flux to upstream of fire. Burning rate and the heat release rate of fire showed an increase as high as 125 % under the effect of the secondary fire source, emphasizing the need to account for

possible secondary fires in tunnel safety design. In case of blocked fire tests, the results from experiments as well as simulations indicated that due to changes in local ventilation velocity and flow pattern upstream of the fire, heat release rates tend to increase as high as 0.7 MW/m^2 compared to un-blocked fire under certain test conditions. It was also shown that tunnel inclination is an influential parameter that affects the smoke movement and ventilation requirements of tunnel considerably.

Keywords: Scaled tunnel model, pool fire, heat release rate, burning rate, Fire Dynamics Simulator

ÖZ

TÜNELLERDE GERÇEKLEŞEN HAVUZ YANGINLARININ YANMA KARAKTERİSTİKLERİ ÜZERİNE DENEYSEL VE SAYISAL ÇALIŞMA

Shafee, Sina

Doktora, Makine Mühendisliği Bölümü

Tez Yöneticisi: Doç. Dr. Ahmet Yozgatlıgil

Temmuz 2017, 136 sayfa

Bu çalışmada tünel yangınlarının dinamiği ve ilgili güvenlik önlemlerinin daha iyi incelenmesi amacıyla, çeşitli yangın senaryoları deneysel ve sayısal olarak analiz edilmiştir. Bu kapsamda, tünelin duvar kaplama malzemesinin, eğiminin, yangının akış yukarısındaki blokajın ve olası ikincil yangın kaynaklarının tünel yangınlarının karakteristikleri üzerinde etkisi dört ayrı bölümde irdelenmiştir. Deneysel çalışmalar Froude modelleme yöntemi ile inşa edilmiş 1/13 ölçekli tünel modeli üzerinde etanol havuz yangınları kullanılarak gerçekleştirilmiştir. Yangın simülasyonu ise Fire Dynamics Simulator kodu ile modellenmiştir. Yangın güvenliği açısından oldukça önem taşıyan ısı salınım hızı (yangın yükü), yanma hızı ve sıcaklık dağılımı gibi kritik parametreler değişen havalandırma hızı, havuz boyutu ve derinliğinde incelenmiştir. Sonuçlar yangının yanma hızının farklı havalandırma hızlarında değişmesinin havalandırmanın soğutucu etkisini, yangının ısı salınım hızını ve yanma kütle transferi katsayısını etkileyen yarışan faktörlere bağlı olduğunu göstermektedir. Soğurucu tünel kaplama malzemesi uygulanarak, yangının akış yukarısındaki ışımsal radyasyon yükü önemli biçimde düşürülmüştür. Bitişik yangının ana yangın ile etkileşiminden dolayı, yangının yanma hızı ve ısı salınım hızı yaklaşık % 125'e kadar artış göstererek, olası ikincil yangın etkisinin güvenlik sistemleri gereksinimlerinin tasarımında

muhtak hesabata katılması gerektiğini vurguladı. Tünel blokajı etkisini inceleyen deneyler ve sayısal modelleme sonuçları serbest yangın sonuçları ile karşılaştırılmış ve ısı salınım hızının 0.7 MW/m^2 'ye varan artışı gözlemlenmiştir. Ayrıca tünel eğiminin tüneldeki duman hareketi ve havalandırma gereksinimleri üzerinde önemli ölçüde etkili olduğu tespit edilmiştir.

Anahtar kelimeler: Ölçekli tünel modeli, havuz yangını, ısı salınım hızı, yanma hızı, Fire Dynamics Simulator

To my soulmate, Sadaf
My parents, Houshang and Farah
And to my brother, my friend, Ashkan

ACKNOWLEDGEMENTS

First and foremost, I want to express my sincerest gratitude towards my thesis supervisor, Professor Ahmet Yozgatlıgil for his continuous support and recommendations throughout the course of my studies. Not only his trusting and encouraging attitude immensely helped me instill the belief I needed in facing the various adversaries along the way, but also the numerous opportunities that he has given me to express myself, has lead me reach where I am today. His priceless mentorship always taught me how to drive forward and past any ordeal by becoming an independent, more intuitive researcher throughout these years, while his caring father figure always makes me feel welcome.

I would like to sincerely thank Professor Metin Yavuz and Professor Murat Aktaş whose insightful suggestions and guidance throughout the course of my research is highly appreciated. The funding from Orta Doğu Teknik Üniversitesi Bilimsel Araştırma Projeleri (BAP-03-02-2015-004) is acknowledged. The PhD scholarship from TÜBİTAK 2215 program is highly acknowledged.

Special thanks goes to Mr. Rahmi Ercan and Mr. Mehmet Özçiftçi from Fluid Mechanics Laboratory of METU for their technical assistance with the experimental setup. I would also like to thank my dear friends in the Internal Combustion Engine laboratory; Mr. Levent Şahin, Mr. Ramin Barzegar, Mr. Tuğberk Keçeçoğlu and Mr. Majd Abu Aisheh for their support during this research.

I am indeed in a lifelong debt to my parents, Houshang and Farah, without whom, I would not be where I am today,

And finally, I would like to thank my wife, Sadaf, for being there for me through the thick and thin, always...and forever.

TABLE OF CONTENTS

ABSTRACT	v
ÖZ	vii
ACKNOWLEDGEMENTS	x
TABLE OF CONTENTS	xi
LIST OF TABLES	xiv
LIST OF FIGURES	xv
LIST OF SYMBOLS	xvix
CHAPTERS	
1 INTRODUCTION	1
1.1 AIMS OF THIS RESEARCH	2
1.1.1 Effect of tunnel wall coating.....	2
1.1.2 Adjacent pool fire	2
1.1.3 Effect of tunnel blockage.....	3
1.1.4 Effect of tunnel inclination	3
1.2 THESIS OUTLINE	4
2 LITERATURE SURVEY	5
2.1 SAFETY MEASURES.....	6
2.2 STATE OF FIRE RESEARCH	10
2.2.1 Scaling in fire research	10
2.2.2 Heat release rate.....	14
2.2.3 Critical ventilation velocity	15
2.3 LARGE SCALE EXPERIMENTS.....	16
2.4 REDUCED SCALE EXPERIMENTS	22
2.5 NUMERICAL STUDIES	32
3 EXPERIMENTAL SETUP AND METHODS.....	37

3.1	INSTRUMENTS	39
3.1.1	Gas temperature	39
3.1.2	Burning rate	41
3.1.3	Species concentration.....	42
3.1.4	Radiative heat flux	43
3.1.5	Visualization	43
3.2	POOL FIRES	44
3.3	EXPERIMENT PROCEDURE AND SELECTION OF PARAMETERS	46
3.3.1	Effect of tunnel wall coating material.....	47
3.3.2	Adjacent pool fires	49
3.3.3	Effect of tunnel blockage	51
3.3.4	Effect of tunnel inclination	53
3.3.5	Uncertainty of calculations	55
4	NUMERICAL MODEL	61
4.1.1	Fundamental governing equations	61
4.1.2	The combustion model	64
4.1.2	Radiative transport equation.....	66
4.1.2	Numerical grid	67
5	RESULTS AND DISCUSSION	71
5.1	EFFECTS OF TUNNEL WALL COATING	71
5.1.1	Effect of pool depth and ventilation velocity.....	71
5.1.2	Effect of tunnel wall coating material.....	81
5.2	ADJACENT POOL FIRES	83
5.2.1	Burning rate behavior	84
5.2.2	HRR flux.....	96
5.3	EFFECT OF TUNNEL BLOCKAGE	98
5.3.1	HRR and burning rate behavior	98

5.3.2	Temperature distribution	105
5.4	EFFECT OF TUNNEL INCLINATION.....	109
6	CONCLUSIVE REMARKS	117
	REFERENCES.....	123
	CURRICULUM VITAE	135

LIST OF TABLES

Table 2.1. Major road tunnel fires from 1949 to 2007 [6].....	5
Table 2.2. Major railroad and underground fire incidents [1]	6
Table 2.3. Comparison of ventilation systems [10].....	8
Table 2.4. Full scale versus model HRR comparison.....	13
Table 2.5. Summary of large scale tunnel fire experiments in literature.....	17
Table 2.6. Peak HRR and fire growth rate from Runehammar tunnel tests [44]	21
Table 2.7. Summary of normalized HRR for fire tests in tunnels [41]	21
Table 2.7. Continued	22
Table 2.8. Global non-dimensional correlations for blocked fire [23].....	28
Table 3.1. Ethanol fuel properties	46
Table 3.2. Experiment variables due to tunnel wall coating tests	49
Table 3.3. Experiment variables due to multiple pool fire experiments.....	51
Table 3.4. Experiment variables due to tunnel blockage tests.....	52
Table 3.5. Experiment variables due to inclination tests.....	54
Table 3.6. Relative and combined uncertainties associated with burning rate measurements	56
Table 3.7. Relative and combined uncertainties associated with HRR measurements	59

LIST OF FIGURES

Figure 2.1. Formation of stagnation point in the backlayering flow due to longitudinal ventilation and the backlayering length	9
Figure 2.2. Evolution of compartment fire [13]	9
Figure 2.3. Propagating smoke in Benelux experiments [43]	18
Figure 2.4. Fire development of a car and small truck fire [43]	19
Figure 2.5. Test commodity used in large-scale tests of Runehamar tunnel [44]	20
Figure 2.6. Configuration and dimensions of model tunnel used in [47]	23
Figure 2.7. Non-dimensional burning rate vs. non-dimensional ventilation velocity for n-heptane pool fire [47]	23
Figure 2.8. Schematics of wind tunnel used in experiments [48]	24
Figure 2.9. Flame stretching in 20 x 10 cm pool fires [48]	25
Figure 2.10. Flame stretching in 10 x 40 cm pool fires [48]	25
Figure 2.11. Effect of tunnel slope on ventilation velocity [4]	26
Figure 2.12. Schematics of the experimental setup [23]	27
Figure 2.13. HRR as a function of blockage ratio [26]	29
Figure 2.14. Temperature distribution at different longitudinal ventilations [26]	29
Figure 2.15. Fuel layer temperature profiles [51]	30
Figure 2.16. Average burning rates as a function of distance to wall and pool aspect ratio [53]	31
Figure 2.17. Comparison of the calculated temperature to the experimental data downstream the fire using different combustion models and boundary conditions at a low ventilation rate of 0.5 m/s (a) at x = 18 m, (b) at x = 30 m, (c) at x = 40 m boundary	

condition: (a) at a ventilation rate of 0.85 m/s, (b) at a ventilation rate of 2.0 m/s [56]	33
Figure 2.18. Evolutions of the backlayering length obtained from prediction and correlation as a function of the wind velocity [58]	34
Figure 2.19. Blockage effect on iso-temperatures under a critical velocity condition, (a) smooth tunnel, (b) blockage upstream the fire source, and (c) blockage downstream the fire source [58]	35
Figure 3.1. Schematics of the real tunnel and model cross section.....	38
Figure 3.2. Experimental setup.....	38
Figure 3.3. Thermocouple configuration along the tunnel (dimensions are in cm) ..	39
Figure 3.4. Data acquisition pack with connected thermocouple.....	40
Figure 3.5. Typical temporal evolution of ceiling temperature.....	40
Figure 3.6. A&D GX-K and RADWAG APP-R.2 precision load cells.....	41
Figure 3.7. Typical mass history and calculated burning rate curves taken from experiments	42
Figure 3.8. TESTO 350-S gas analyzer.....	43
Figure 3.9. Hukseflux SBG-01 radiative heat flux sensor	43
Figure 3.10. Main heat transfer regimes in a pool fire [68]	45
Figure 3.11. Modified experimental setup due to wall coating tests.....	47
Figure 3.12. Horizontal and vertical radiometer orientations used in wall coating experiments	49
Figure 3.13. Model cross section and pool orientation in the combustion zone	50
Figure 3.14. Schematics of modified combustion zone at tunnel blockage experiments	53
Figure 3.15. Modified model for tunnel inclination experiments	54

Figure 4.1. HRR comparison between experiments and numerical simulations using different mesh sizes.....	69
Figure 4.2. The numerical grid and thermocouple locations.....	70
Figure 5.1. Effect of pool depth on incident radiation upstream of fire for (a) 0.5 m/s (b) 1 m/s (c) 1.5 m/s (d) 2.5 m/s ventilation velocity	73
Figure 5.2. Effect of ventilation velocity on incident radiation upstream of fire for (a) 100 ml (b) 200 ml (c) 300 ml fuel.....	74
Figure 5.3. Ethanol flames at 10 cm leading edge of pool fire 30 s after ignition....	77
Figure 5.4. Variation of (a) HRR flux and (b) burning rate of ethanol pool fires as a function of pool depth and ventilation velocity – Experiments versus FDS predictions	78
Figure 5.5. Maximum ceiling temperature along the tunnel axis for (a) 0.1 cm (b) 0.2 cm and (c) 0.3 cm pool depth (d) FDS simulations vs. experiment (0.2 cm pool depth case).....	80
Figure 5.6. Effect of wall coating type on the radiative heat flux upstream of the pool	81
Figure 5.7. Effect of wall coating type on maximum ceiling temperature along the tunnel axis for (a) reflective coating and (b) emissive coating material.....	82
Figure 5.8. Effect of wall coating type on NTHR (0.2 cm pool depth)	83
Figure 5.9. Observed temporal evolution of burning rates under tested conditions (a) single 10 cm pool, 1.5 m/s airflow, 40 g fuel (b) dual 10 cm pools, 0.5 m/s airflow, 40 g fuel (c) dual 10 cm pools, 1.5 m/s, 80 g fuel (d) dual 15 cm pools, 0.5 m/s airflow, 80 g fuel.....	86
Figure 5.10. Burning rates of single and dual pool fires as a function of pool depth (a) 0.5 m/s (b) 1 m/s (c) 1.5 m/s	90

Figure 5.11. Burning rates of single and dual pool fires as a function of airflow velocity (a) 40 g initial fuel (b) 80 g initial fuel	92
Figure 5.12. Burn duration of single and dual pool fires as a function of airflow velocity for (a) 40 g (b) 80 g initial fuel mass	94
Figure 5.13. Flame captures of dual 10 cm pool fires at 1.5 m/s for S = 4 cm	95
Figure 5.14. Flame captures of dual 10 cm pool fires at 1.5 m/s for S = 8 cm	96
Figure 5.15. HRR flux of single and dual pool fires as a function of pool depth and airflow velocity (a) 0.5 m/s (b) 1 m/s (c) 1.5 m/s	97
Figure 5.16. Effect of blockage and separation distance on HRR flux from the pool	99
Figure 5.17. Effect of blockage and separation distance on burning rates from the pool fires.....	101
Figure 5.18. Flame images and FDS predicted velocity field for (a) L/S = 3 and (b) L/S = 0.5 (c) velocity vectors at the wake of blockage at 1.5 m/s ventilation velocity for car blockage at 80 s after ignition.....	103
Figure 5.19. Flame images and FDS predicted velocity field for (a) L/S = 3 and (b) L/S = 0.5 and (c) velocity vectors at the wake of blockage at 0.5 m/s ventilation velocity for car blockage at 80 s after ignition.....	104
Figure 5.20. Maximum ceiling temperature along the tunnel for car and metro blockage as a function of tunnel ventilation velocity.....	106
Figure 5.21. Predicted vs. measured excess smoke layer temperature due to Kurioka [83] and Li et al. [50] models for (a) free fire and (b) blocked fire	108
Figure 5.22. Effect of positive and negative inclination on the burning rates and HRR flux from fires and the oxygen concentration at probe location	110

Figure 5.23. Effect of positive and negative inclination on the maximum ceiling temperature distribution as a function of ventilation velocity and inclination percentage	112
Figure 5.24. Temperature over ambient upstream of the pool fire as a function of ventilation velocity and tunnel slope at distances 0.7, 1.4 and 2.2 times height of the tunnel.....	113
Figure 5.25. Comparison of measured normalized critical velocity with existing empirical model.....	115

LIST OF SYMBOLS

A	: Pool surface area	[m ²]
A	: Cross sectional area of the tunnel	[m ²]
B	: Spalding mass transfer number	
c	: Specific heat	[W/m ² K]
D	: Pool depth, Diffusion coefficient, Characteristic flame diameter	[cm], [m ² /s], [m]
E	: Energy release	[J]
F	: View factor	
g	: Gravitational acceleration	[m/s ²]
h	: Convective heat transfer coefficient, Heat of vaporization, Heat of combustion	[W/m ² K], [J]
H	: Tunnel height	[m]
I	: Radiation intensity	[W/m ²]
k	: Thermal conductivity	[W/mK]
L	: Length scale, Pool size	[m], [cm]
MW	: Molecular weight	[g/mol]
m	: Mass	[kg]
\dot{m}	: Mass flow rate	[kg/s]
m'''	: Burning rate	[kg/m ² s]
p	: Pressure	[Pa]
\dot{Q}	: Heat release rate	[W]
r	: Radius	[m]
R	: Measurement function	
S	: Pool separation pool distance	[cm]
T	: Temperature	[°C], [K]
t	: Time	[s]

u, V	: Velocity	[m/s]
u	: Relative uncertainty	
\dot{v}	: Volumetric flow rate	[m ³ /s]
W	: Pool-wall distance	[cm]
X	: Molar fraction	
x	: Position	[m]
Z	: Species mass fraction	

Subscripts

A	: Air
b	: Boiling point, Black-body
B	: Blockage
c	: Convective, Combustion
$cond$: Conduction
$conv$: Convection
cr	: Critical
F	: Full scale
f	: Flame, flow
fu	: Fuel
g	: Gasification, gaseous state
i	: Initial state
M	: Model
rad	: Radiation
ref	: Reflective
s	: Surface, soot
T	: Tunnel
v	: Vaporization
Y	: Mass fraction
Z	: Mixture fraction

Superscripts

- A : Analyzer
- * : Dimensionless analysis symbol
- + : Non-dimensionalization symbol
- o : Standard condition symbol

Greek symbols

- ρ : Reflectivity, density [kg/m³]
- $\bar{\rho}$: Filtered density [kg/m³]
- ϕ : Oxygen depletion factor
- σ : Stefan-Boltzmann constant [W/m⁻²K⁻⁴]
- ε : Emissivity
- λ : Wavelength
- μ : Absolute viscosity [Pa.s]
- α : Specie
- θ : Slope grade
- κ : Absorption coefficient
- Δ : Numerical cell width [m]
- ∇ : Gradient operator
- γ : Excess temperature coefficient
- ω : Best-estimate uncertainty
- Π : Scaling Pi groups

Acronyms

- BR Blockage ratio
- CFAST Consolidation Model of Fire Growth and Smoke Transport
- CFD Computational Fluid Dynamics
- DNS Direct Numerical Simulation
- EDC Eddy Dissipation Concept

FDS	Fire Dynamics Simulator
Fr	Froude number
HGV	Heavy Good Vehicle
HRR	Heat Release Rate
LES	Large Eddy Simulation
NFPA	National Fire Protection Association
NIST	National Institute of Standards and Technology
NTHR	Normalized Total Heat Released
Pr	Prandtl number
Re	Reynolds number
TC	Thermocouple at Combustion zone
TCTree	Thermocouple Tree
TD	Thermocouple at Downstream
TU	Thermocouple at Upstream

CHAPTER I

INTRODUCTION

Modern society demand for efficient transportation has highlighted the importance of tunnels as means of alleviating traffic congestion and providing faster transit of goods. However, with ever-increasing rate of tunnel construction and heavier traffic, fire accidents started to pose a threat to the lives of passengers as well as damaging the tunnel structure. With the overwhelming cost of tunnel construction, extensive research attention was drawn to the safety issues associated with the design of tunnels and risk perception and management strategies. It is well-known that the enclosed nature of tunnel structure (or any compartmentalized space) results in a rapid temperature increase and oxygen depletion during a fire, making it difficult for rescue operations especially in crowded traffic conditions. Fire incidents in Mont-Blanc tunnel between France and Italy, Tauern tunnel in Austria, the Kaprun tunnel in Switzerland, the Channel tunnel between UK and France, the underground railway tunnel in Azerbaijan, and most recently, the Soma mine disaster in Turkey are among catastrophic examples with dire consequences [1,2].

The number of fatalities in tunnel fire accidents reported in the literature over the years and in recent history highlight the fact that there are still significant issues regarding tunnel fire safety that need to be addressed through experiments and/or modelling, especially in the case of fires in metro and underground tunnels. Apart from the fire heat load, suffocation due to smoke and toxic gas inhalation is known as another cause of death and injuries in a tunnel fire incident. The safety issue becomes even more pronounced as the length of the constructed tunnels is increasing in the modern day. A better understanding of fire characteristics in confined spaces and related phenomena in general, and specifically fires in tunnels, would enrich the current state of knowledge on the matter and add valuable information needed in

deploying safety measures in tunnel design. These have been the main incentive for conducting of this research work.

1.1 Aims of this research

Use of pool fires have proved a good approach in simulating tunnel fires of different magnitudes. Study of the corresponding literature shows that there are still issues that need to be covered in order to better understand tunnel fire behavior under certain circumstances. In this research, a series of experiments were conducted in an attempt to investigate tunnel fires and improve existing database on the matter. The output of this work will provide data that can be utilized in fire safety design, pool fire combustion research and validation of numerical models. Specific aims and associated hypotheses of the study is discussed in this section.

1.1.1 Effect of tunnel wall coating

The purpose of these experiments was to qualitatively investigate the effects of different tunnel wall coating type, i.e. reflective or emissive, on the burning rates of the fire as well as radiative heat feedback upstream of the pool which is a safety hazard. As part of the experiments, the flame tilt was recorded using a camera. The results of the experiment could be used as an approximation to assess fire spread to the upstream of the fire zone by measurement of radiative heat flux. Numerical simulations were performed to accompany experimental results.

1.1.2 Adjacent pool fire

Even though there is the possibility of multiple fires with close proximity in tunnels, there is no major report in the literature assessing such scenario and fire interactions in compartmented spaces. Adjacent secondary pool fires were studied in current

research. The behavior of fire due to a secondary source was believed to be different compared to a single fire case in terms of heat release rate (HRR), burning intensity and fire-induced turbulence. Hence, effect of fire size and separation distance from secondary fire on the burning rate, interactions between fires, HRR and flame characteristics were analyzed. The pool fires were positioned traverse to the flow direction.

1.1.3 Effect of tunnel blockage

Temperature distribution along the tunnel ceiling is of critical importance in designing fire-proofing materials and lining structures in a tunnel [1]. Majority of the studies in the literature have investigated this parameter by only considering fire scenarios without any blockage effect except a few [3]. However, in most tunnel fires, vehicles usually exist near fire source in upstream, which will act as blockage and influence the air and plume flow. In this study, the upstream obstruction of tunnel was investigated by use of vehicular blockage with different blockage ratios. Burning rates, HRR of fire as well as gas temperature distribution at varying ventilation conditions were measured. Numerical simulations accompanied parts of the experimental results.

1.1.4 Effect of tunnel inclination

Flow characteristics upstream and downstream of the combustion zone tend to change significantly at negative and positive inclinations due to fire-induced buoyancy effect [4–6]. Current research also aimed to investigate the effect of uphill and downhill inclination on smoke movement, ventilation requirements, and gas temperature distribution in tunnel through experiments. This case also had considerable importance because in practice, a great number of metro and road tunnels need to be constructed with slopes up to ± 10 percentage.

1.2 Thesis outline

This thesis is organized in the following manner. Chapter II presents the background information on recent history, safety factors, research on tunnel fires and explains the aims of current research which were identified based on the gaps in the related literature. In Chapter III, the equipment and experimental method are discussed followed by design factors. The numerical model which was used to accompany parts of the experimental results is discussed in Chapter IV. Results of the tunnel fire experiments are presented and discussed in separate sections in Chapter V and finally, conclusive remarks are made in Chapter VI in an attempt to associate the major findings of the work and provide a summary.

CHAPTER II

LITERATURE SURVEY

Over the years, tunnel fires have taken the lives of many people. Tables 1 and 2 give a brief summary of the fire incidents in some of the road and railroad tunnels of special interest, their possible causes and consequences [1,6]. The numbers highlight the fact that there are significant issues regarding tunnel fire safety that need to be addressed. It is reported that as well as fire heat load, smoke and toxic gas inhalation plays an important role in the consequent casualties of tunnel fire incidents.

Table 2.1. Major road tunnel fires from 1949 to 2007 [6]

Year	Tunnel name	Location	Probable cause	Causalities
1949	Holland	USA	Load explosion	66 Injured
1978	Velsen	Netherlands	Collision	5 dead, 5 injured
1982	Salang	Afghanistan	Collision	More than 400 dead
1986	L'Arme	France	High speed collision	3 dead, 5 injured
1995	Pfänder	Austria	Collision	3 dead, 4 injured
1999	Mont Blanc	France-Italy	Oil leakage	39 dead, 27 injured
1999	Tauern	Austria	Collision	12 dead
2001	Gotthard	Switzerland	Collision	11 dead
2005	Frejuse	France-Italy	Diesel leakage	2 dead, 21 smoke inhalation
2007	San Martino	Italy	Collision	2 dead, 10 injured

Explosion, fuel leakage, collision of cars, heavy good vehicles (HGVs) and electrical fault are among the reported possible causes of tunnel fires. It is also indicated that railway and underground tunnels have had the major share in casualties and damage compared to road tunnels, expressing the severity of the problem in this

case. The coal mine fire in Soma, Turkey which took the lives of 301 workers and left many other injured was caused by carbon monoxide poisoning due to rapid depletion of oxygen in the mine shaft which could have been prevented if refuge chambers were designed properly and enough oxygen sensors were mounted [2].

Table 2.2. Major railroad and underground fire incidents [1]

Year	Tunnel name	Location	Probable cause	Consequences
1921	Batignolles	France	Collision	> 28 dead
1971	Wranduk	Yugoslavia	Fire in engine	34 dead, 120 injured
1987	King Cross station	UK	Not available	31 dead, many injured
1995	Baku underground	Azerbaijan	Electrical fault	285 dead, 245 injured
1998	Gueizhu	China	Explosion	> 80 dead
2000	Kitzsteinhorn fanular	Austria	Oil leakage	155 dead
2003	Jungangno underground	South Korea	Explosion	198 dead, 146 injured
2007	San Martino	Italy	Collision	2 dead, 10 injured

2.1 Safety measures

Tunnels are enclosed facilities for transportation of motor vehicles and passengers all over the world. As the rate of construction of longer tunnels grows, fires in road and rail road tunnels become an inevitable problem on a global scale. Life threatening factors of fire such as Heat Release Rate (HRR), also termed heat load, rapid temperature increase and oxygen depletion, fire growth and spread, and asphyxiation by inhaling the smoke and fumes make it more difficult for an effective means of escape and rescue. In some cases, even the lining and fitting structure of the tunnel can

be compromised due to thermal shock resulting in concrete spalling, total devastation and massive losses [1]. According to the tunnel fire safety standards of National Fire Protection Association (NFPA) 502 and Association Mondiale de la Route (AIPCR), there are certain requirements for ensuring human safety during fire emergencies and evacuation and rescue phases as well as protection of tunnel structural components [7,8]. Regardless of length of the facility, factors such as heat loads ranging from minor incidents to major catastrophes, occurrence of secondary fires at one or more locations inside the tunnel, traffic congestion and control during emergencies, built-in fire protection features and emergency ventilation systems should be fully considered as part of an engineering analysis of the fire protection. As well as using water mist and sprinkler systems to suppress fire and reduce temperature, ventilation (natural and forced) is utilized in most cases.

According to the NFPA standard, mechanical ventilation in tunnels is considered to be one of the most effective methods in providing fresh airflow and disposal of contaminants during normal conditions and control of smoke movement to create a safe passage for motorists [7]. Establishing air requirements and capacity of the ventilation system as well as determining the amount of hazardous toxic gases and temperature distribution at different fire scenarios is a challenging issue due to the difficulty of controlling many variables and there is an indisputable need for research in this field. Typical tunnel ventilation systems are transverse and longitudinal.

In case of transversely ventilated tunnels, fresh air is supplied from ducts along the tunnel whereas in longitudinally ventilated tunnels, air is forced in to the tunnel usually by jet fans mounted either on the ceiling of the tunnel or at the vertical shafts. Installation and maintenance of longitudinal ventilation systems usually cost less than transverse ventilation which makes them a more common choice especially in Europe and eastern countries [9]. Other ventilation systems include partial traverse and combined ventilation. Chow et al. highlighted the advantages and disadvantages of each system given in table 2.3 [10].

In case of a fire in a confined space such as tunnels, the arising buoyant plume spreads to both directions after deflecting with ceiling. If the buoyancy force of the

plume dominates the inertial forces of the ventilation airflow, a stratified layer develops upstream of fire source against the longitudinal airflow. The phenomenon is termed “backlayering” [11]. Introduction of longitudinal ventilation results in impingement of the airflow with backlayering plume which stops the back flow, ultimately directing it downstream as shown in figure 2.1 [12].

Table 2.3. Comparison of ventilation systems [10]

Type of the ventilation system	Advantages	Disadvantages
Longitudinal	less space to install, simple installation and low cost	Not desirable for bi-directional traffic
Semi-traverse	Good smoke control, low maintenance cost	High investment cost, no directional smoke control
Traverse	Suitable for long tunnels, applicable for bi-directional traffic	Large ventilation ductwork required, ineffective in smoke management
Partial traverse	Intermediate characteristics between traverse and semi-traverse	Large ventilation building and ductwork required, ineffective in smoke management
Longitudinal and semi-traverse combination	Good smoke control, applicable for bi-directional traffic	Relatively complex and high initial cost, high maintenance cost

The term “critical velocity” is used in tunnel fire literature to define the minimum longitudinal ventilation velocity required to prevent the toxic smoke back flow, i.e. zero backlayering length in figure 2.1.

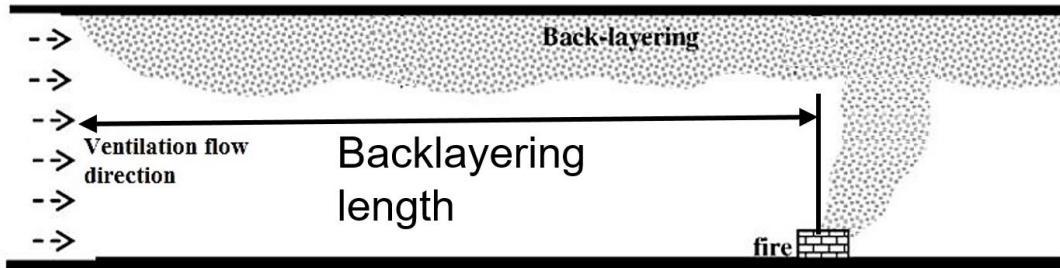


Figure 2.1. Formation of stagnation point in the backlayering flow due to longitudinal ventilation and the backlayering length

The confined fire exhibits five stages of ignition, growth, flashover, fully developed fire and decay as shown in figure 2.2. Following the ignition, in case of available fuel and oxygen supply, the fire will develop and reach later stages. The oxygen supply in fire growth stage is generally sufficient and the fire is referred to as “fuel-controlled” in this stage. In the flashover stage the radiation from hot combustion gases starts to dominate resulting in ignition of unburnt combustible materials. The peak HRR and burning rates are reached in fully developed stage. This stage is often referred to as oxygen (ventilation) controlled stage due to lower oxygen availability.

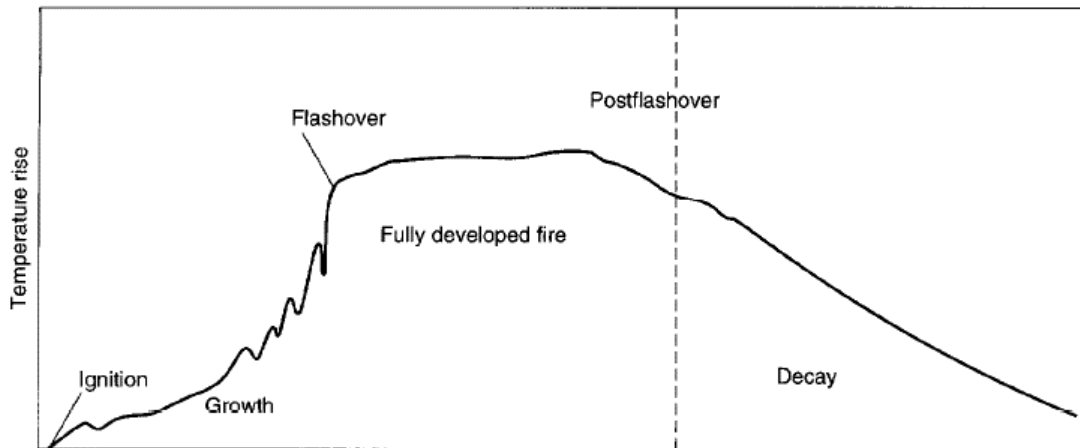


Figure 2.2. Evolution of compartment fire [13]

2.2 State of fire research

Fire is a complex phenomenon within which several physical and chemical processes take place that render combustion and fire research a challenging branch requiring knowledge of the flow field, heat transfer, mass transfer, and chemistry. Nevertheless, tunnel fires have been the topic of research since early 1960s when transport tunnels were being mass constructed [1]. Most of the fundamental data on tunnel fires have been achieved through large-scale fire tests conducted in abandoned or disused tunnels or in operational tunnels in smaller scales. However, the overwhelmingly high cost of large scale tunnel fire experiments turned the attention to reduced scale or model experiments which is also the topic of current work. The reduced scale experiments are often accompanied by numerical modeling to reproduce full-scale features. There are a number of distinct mathematical models that are being used in the fire research community. The zonal models such as Consolidation Model of Fire Growth and Smoke Transport (CFAST) are simplified thermodynamic models and highly dependent on empirical expressions which are not suitable for tunnel fire simulation [14]. However, in recent years, better numerical simulation of the tunnel fire phenomena is made possible using Computational Fluid Dynamics (CFD) models, including FDS [15] and OpenFOAM [16], as well as commercial software such as CFX, FLUENT, and FLOW3D that can provide detailed representation of the flow field domain. In the following sections, the common terminology in fire research, as well as scaled modelling is discussed followed by a literature survey on some of the most relevant large-scale, small scale and numerical studies available in the field. The specific aims of current research are also summarized at the back end of this chapter.

2.2.1 Scaling in fire research

In order to utilize data achieved from reduced scale experiments, a well-defined similarity should exist between the large scale and model. Due to the complex fire

dynamics, especially in the case of confined fire, it is impossible to achieve complete similarity. However, partial similarity can be achieved by preserving some of dimensionless groups of interest which is the fundamental of scaled fire modeling [17]. In this section, the procedure of establishing dimensionless Pi groups and suitable normalizing factors from conservation equations used in fire modeling are briefly discussed but the reader is encouraged to refer to the original document for a detailed study [17]. Density is assumed constant throughout these derivations and only the vertical momentum is examined explicitly. The mass and momentum conservation is applied to achieve normalizing factor for velocity under constant pressure conditions as in equation (2.1) [17];

$$u^* = \sqrt{gl} \quad (2.1)$$

which is a suitable normalizing factor for natural convection and maximum velocity due to buoyancy without forced velocity. Equating the momentum flux and stress terms in the momentum equation gives equation (2.2);

$$Re = \Pi_1 = \frac{\rho_\infty u^* l}{\mu} \quad (2.2)$$

which is the ratio of inertial forces to shear stress, also known as Reynolds number. The energy equation establishes multiple Pi groups due to inclusion of different phenomenon such as combustion and heat transfer which are inherent in the physics of the problem [17]. Below are the final forms of some of other pertaining normalizing factors and associated Pi groups that will be used throughout this study. Equation (2.3) commonly known as Zukoski number relates the fire power or heat load to the enthalpy flow term;

$$Q^* = \Pi_2 = \frac{\dot{Q}}{\rho_\infty c_p T_\infty^{5/2} g^{1/2}} \quad (2.3)$$

where \dot{Q} is the fire HRR, l is the length scale and denominator is the enthalpy flow. Normalized heat fluxes to the solid boundaries of an enclosure fire were derived in terms of Zukoski number for conduction, convection and radiation given in equation (2.4) through (2.6) [17].

$$Q_{Cond.}^* = \Pi_3 = \frac{(k \rho c)^{1/2}_w}{\rho_\infty c_p g^{1/4} l^{3/4}} \approx \frac{Conduction}{Enthalpy\ flow} \quad (2.4)$$

$$Q_{conv.}^* = \Pi_4 = \frac{h_c}{\rho_\infty c_p \sqrt{gl}} \approx \frac{Convection}{Enthalpy\ flow} \quad (2.5)$$

$$Q_{rad.}^* = \Pi_5 = \frac{\sigma T_\infty^3}{\rho_\infty c_p \sqrt{gl}} \approx \frac{radiation}{Enthalpy\ flow} \quad (2.6)$$

Other Pi groups exist for mass flow terms due to droplet evaporation and chemical energy of species present in the reacting mixture which are not in the scope of this context. It is impossible to preserve all the Pi groups discussed above, or any other Pi groups of interest not covered here at once. This is due to inherent inconsistencies in the heat loss terms once we attempt to preserve a specific Pi group, say Zukoski number. In fire correlations, the gas phase radiation, wall boundary thermal properties and the Reynolds number are therefore not generally preserved. Instead, partial scaling is maintained which requires a good understanding of the competing phenomena in the physics of the problem at hand. This is referred to as “the art of scaling” [17]. One of the most prominent applications of scale modelling is Froude scaling which is extensively used in reduced scale tunnel fire studies [18–26]. This scaling technique is principally achieved by maintaining the Zukoski number constant and requires that velocities scale as $(gl)^{1/2}$ given in equation (2.7).

$$Fr \approx \frac{u^2}{gl} \quad (2.7)$$

which represents the ratio of inertial forces to buoyancy forces [1]. Based on preservation of the Froude number, the relationships for HRR, velocity, and gas temperature between model tunnel and full scale can be expressed as follows [25,26].

$$\frac{\dot{Q}_M}{\dot{Q}_F} = \left(\frac{l_M}{l_F}\right)^{5/2} \quad (2.8)$$

$$\frac{V_M}{V_F} = \left(\frac{l_M}{l_F}\right)^{1/2} \quad (2.9)$$

$$T_M = T_F \quad (2.10)$$

in which \dot{Q} is the HRR of the fire, T is the gas temperature in Kelvin, V is the characteristic flow velocity (i.e. ventilation velocity), M stands for model and F stands for full scale. The relations mean that, for example, if the model length scale is half the full size tunnel, the measured HRR will be up-scaled with a factor of 5.65 in the full-scale fire calculations. Table 2.4 gives a quantitative idea as to what these scaling measures would correspond to in the full scale tunnel as well as the equivalent fire scenario.

Table 2.4. Full scale versus model HRR comparison

Model HRR (kW)	Equivalent full scale HRR (MW)	Equivalent tunnel fire scenario
3 – 14	1.5 – 8	Small cars
32 – 50	20 – 30	Truck or bus
21 – 328	13 – 202	Heavy good vehicle
12 – 70	7 – 43	Railroad vehicles

2.2.2 Heat release rate

HRR is a pivotal parameter in defining safety associated with tunnel fires since it relates to many factors including temperature, fire spread, heat transfer, and flame length. In fact, HRR is believed to be the most hazardous factor in evaluating fire safety and is of greater importance in tunnel fire research since heat feedback could intensify the problem [27]. There are two common methods for calculation of HRR from tunnel fire experiments, by measuring of the mass loss rate of the burning material and using oxygen consumption calorimetry method [28,29]. While the former method relies on using a balance to record mass loss rate during combustion and then doing calculation based on the mass loss rate and lower heating values of fuel, the latter calculates HRR based on oxygen depletion and combustion species concentrations variations.

The premise of the calorimetry method is to use constant heat of combustion per unit volume of oxygen consumed which is approximately the same for most of the organic materials [29]. The method has been extensively used in the literature [30–34]. The heat released due to oxygen calorimetry method can be calculated according to equation (2.11) and (2.12).

$$\dot{Q} = \left[\phi - \left(\frac{E'' - E'}{E'} \right) \left(\frac{1 - \phi}{2} \right) \frac{X_{CO}^A}{X_{O_2}^A} \right] E' X_{O_2}^o \dot{V}_A \quad (2.11)$$

$$\phi = \frac{X_{O_2}^o - X_{O_2}^A (1 - X_{CO_2}^o - X_{H_2O}^o) / (1 - X_{CO_2}^A - X_{CO}^A)}{X_{O_2}^o [1 - X_{O_2}^A / (1 - X_{CO_2}^A - X_{CO}^A)]} \quad (2.12)$$

in the above equations, the “o” superscript refers to standard conditions, X is the mole fraction of species measured by gas analyzer or at standard conditions, E' is the net heat release of combustion per unit volume of oxygen consumed equal to 17.2 MJ/m³, E'' is heat release per volume of oxygen consumed in the burning of CO equal to 23.1 MJ/m³ and ϕ is the oxygen depletion factor. The method has been

demonstrated at tunnel experiments in previous studies [35,36]. Detailed derivations of equation (2.11) and (2.12) are illustrated in [28].

2.2.3 Critical ventilation velocity

It was stated that the minimum ventilation velocity required for prevention of smoke movement in upstream direction, is known as the critical ventilation velocity. Empirical formulations for critical ventilation velocity based on Froude number could be found in the literature. One of the earlier correlations was given by Thomas [37] in which the inertial force of incoming fresh air and the smoke buoyancy force were compared. He suggested that the critical ventilation velocity is achieved when these forces are equal, i.e. critical Froude number of unity. The proposed equation for critical ventilation velocity by [37] is given in equation (2.13).

$$V_{cr} = \left(\frac{g \dot{Q}_c H}{\rho_o c_p T_f A} \right)^{\frac{1}{3}} \quad (2.13)$$

which estimates the critical ventilation velocity proportional to one-third power of convective HRR. In equation (2.13), V_{cr} is the critical ventilation velocity in m/s, H is the tunnel height, ρ_o is the ventilation flow density at standard conditions, c_p is the specific heat of ventilation flow, T_f is the measured ventilation flow temperature in Kelvin. Similar correlations have been proposed by others such as equation (2.14) and (2.15) by Kennedy [38].

$$V_{cr} = k_g \left(\frac{g \dot{Q}_c H}{\rho_o c_p T_f A F r_{cr}} \right)^{\frac{1}{3}} \quad (2.14)$$

$$T_f = T_0 + \frac{\dot{Q}_c}{\rho_o c_p A V_{cr}} \quad (2.15)$$

In equation (2.14), critical Froude number was proposed to be 4.5 and k_g is the grade correction factor to be applied when used for inclined tunnels. Wu and Bakar argued that the critical velocity is dependent on the hydraulic diameter of the tunnel rather than tunnel height through experiments on a small scale variable cross-sectional tunnel [39]. They introduced two regimes for critical velocity variations as given in equation (2.16), (2.17) and (2.18). They showed that at lower HRR, the critical velocity varies as the one-third power of the HRR; however, at higher rates of heat release, the critical velocity becomes independent of HRR.

$$V'_{cr} = 0.4(0.2)^{-\frac{1}{3}} Q^*, \quad Q^* \leq 0.2 \quad (2.16)$$

$$V'_{cr} = 0.4 \quad Q^* > 0.2 \quad (2.17)$$

$$V'_{cr} = \frac{V_{cr}}{\sqrt{gH}} \quad (2.18)$$

where Q^* is the Zukoski number based on tunnel hydraulic diameter as the length scale in equation (2.3).

2.3 Large scale experiments

One of the earliest large scale tunnel fire experiments was carried out in a disused railway tunnel in Glasgow in 1970 [1]. The tunnel was 620 m long, 7.6 m wide, and 5.2 m high and the fire source was kerosene pools of 1.44 m² area. It was found out that smoke layers of 1-2 m in thickness would form and thicken in time, reaching 4 m in 10 min. The smoke would advance at about 1-1.5 m/s. Some years later, 30 fire tests including large petrol and diesel pool fires and mixed load of wood, car tires and sawdust were performed in a 390 m long deserted railway tunnel in Austria [1]. The tunnel was modified to simulate longitudinal and traverse ventilation conditions.

Ceiling temperatures as high as 1200 °C were recorded. Table 2.5 summarizes some of the main large-scale tunnel fire experiments in tunnel fire research history and their respective results.

Table 2.5. Summary of large scale tunnel fire experiments in literature

Test title	Year	Tunnel	Fire source	Main result
Glasgow experiments	1970	Disused railway tunnel	Kerosene pools	Smoke layers of 1-2 m advancing at 1-1.5 m/s speed
Zwenberg experiments	1976	Disused railway tunnel	Petrol and diesel pools	Ceiling temperatures as high as 1200 °C
EUREKA EU-499 test series	1990-92	Abandoned mine tunnel in Hammerfest	Cars, trains, carriages, heptane pools, and heavy good vehicles (HGV)	- Temperature of 800-900 °C during car fires and 1300 °C for HGVs. - Fire growth and burning pattern considerably affected by ventilation.
Memorial Tunnel Fire Ventilation Program	1993-95	Two lane road tunnel	diesel pool fires ranging in size (10-100 MW)	Considerable reduction in visibility due to smoke which posed a greater threat than fire heat load
Benelux experiments	2001	Operational tunnel	Pool fires, cars, a van and covered truck loads	High ventilation rates retarded development of car fire by up to 30 min but enhanced burning of HGV fires by up to 20 MW

The fire test series under project EUREKA EU-499 ‘FIRETUN’ were the milestone of tunnel fire research [40]. A wide range of HRR data for different vehicles such as cars, trains, carriages, heptane pools, and HGVs were recorded. However, in the

EUREKA tests little attention was given to the risk of fire spread between vehicles (multiple fires) which had been the topic of more recent work [41]. It was found that fire tends to develop fast in the first 10-15 min since the start of fire. Fire growth and burning pattern was seen to considerably affected by ventilation conditions [1]. Another milestone in large-scale tunnel fire experiment was the Memorial Tunnel Fire Ventilation Program (MTFVTP) between 1993-95 [42]. During the tests, 98 Diesel fueled pool fires were burned in the 850 m long two-lane road tunnel near Charleston, West Virginia, USA. It was concluded that longitudinal ventilation velocity of 2.5-3 m/s was sufficient for smoke extraction of fires with HRR up to a maximum of 100 MW. A series of pool fire tests were carried out during construction of Shimizu tunnel in Japan in 2001 [1]. It was concluded that the three-lane tunnel provides faster evacuation than a two-lane tunnel and that longitudinal ventilation does not have great effect in the three-lane tunnel as it does in a two-lane one. Fire test series in the Benelux tunnel in Netherlands between 2000 and 2001 investigated the fire detection systems, mechanical ventilation and sprinklers [43]. Different combustion related parameters such as gas temperature and HRR were measured. Figure 2.3 shows the cross section of the tunnel with propagating smoke in a Benelux fire test.



Figure 2.3. Propagating smoke in Benelux experiments [43]

Figure 2.4 presents the HRR results of the experiment for a passenger car and small truck [43]. It was seen that for the car fire test, longitudinal ventilation delayed fire spread compared to test case without ventilation. As for the truck fire test, results showed that influence of ventilation was primarily noticeable by its effect on the fire development during the initial stages.

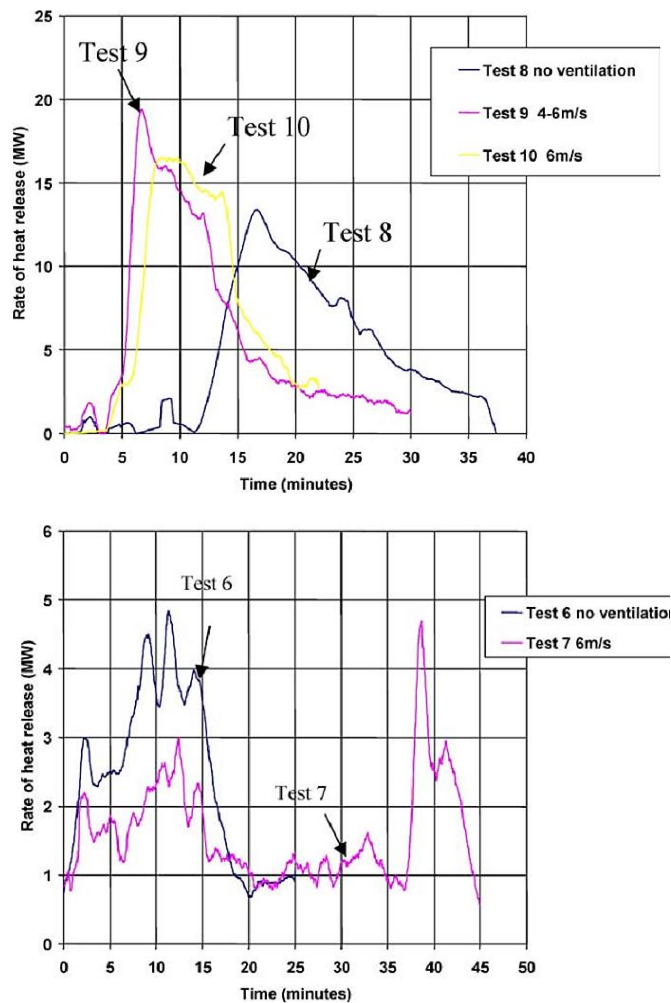


Figure 2.4. Fire development of a car and small truck fire [43]

Large scale tunnel fire tests were also conducted in the Runehammar tunnel in Sweden in 2003 [41,44–46]. In these experiments, mock-ups were prepared to simulate

HGV fire. Figure 2.5 shows the used mock-ups. In order to measure the HRR on the downstream side of the fire, longitudinal flow was generated mobile fans located outside the tunnel entrance and 50–60 m inside the tunnel. Thermocouples, oxygen sensors, CO and CO₂ sensors, and pressure tubes were located at a suitable distance downstream of fire source. The probes divided cross section of tunnel in to five virtual areas for each of which species concentration, temperature and flow velocity were calculated separately for more accurate estimation of HRR.



Figure 2.5. Test commodity used in large-scale tests of Runehamar tunnel [44]

The fire growth rate of all four tests were approximately linear as seen in linear regression results of table 2.6 for used materials which were wood and plastic pallets (T1), wood pallets and mattresses (T2), furniture and fixtures (T3), and cartons and plastic cups (T4). It was also observed that T2 test yielded the fastest fire development (26.3 MW/min).

Table 2.6. Peak HRR and fire growth rate from Runehamar tunnel tests [44]

Test no.	Time from ignition to peak HRR (min)	Linear fire growth rate from 5 MW up to 100 MW (R = linear regression coefficient) (MW/min)	Peak HRR (MW)
T1	18.5	20.1 (0.996)	201.9
T2	14.1	26.3 (0.992)	156.6
T3	10.0	16.4 (0.998)	118.6
T4	7.4	16.9 ^a (0.996)	66.4

^a5–66.4 MW.

As a result of the Runehamar fire tests new design criteria were adopted for tunnels and applied to NFPA standards in 2008 [7]. Ingason collected the HRR data from all the large-scale tests available in the literature before 2006 and normalized the maximum heat release to the exposed fuel surface area [41]. The fuel surface area was defined as the freely exposed area where release of gasified fuel can occur simultaneously. According to his results, HRR data could be divided into three different groups based on the fuel type. The data is summarized in table 2.7. It was concluded that that the heat release data per exposed area in a fuel controlled fire using different vehicles and solid materials is rather narrow.

Table 2.7. Summary of normalized HRR for fire tests in tunnels [41]

Type of fuel	Test series	Exposed fuel area (m ²)	Maximum heat release rate per square meter exposed fuel area MW/m ²
Liquid			
Gasoline	Ofenegg, Zwenberg, No.3 Shimizu	6.6, 47.5, 95	0.35 – 2.6
Kerosine	Glasgow	1.44	1.4
n-Heptane	Eureka	1, 3	3.5
n-60 % heptane/40% toluene	2nd Benelux	3.6, 7.2	1.1 – 1.6
Low-sulfur No 2 fuel oil	Memorial	4.5, 9, 22.2, 44.4	1.7 – 2.5

Table 2.8. Continued

Solid fuel			
Wood cribs	Eureka (test 8, 9 and 10)	140	0.07 – 0.09
Wood pallets	2nd Benelux (tests 8, 9, 10 and 14)	120 (36 pallets) 240 (72 pallets)	0.11- 0.16
82 % wood pallets and 18 % PE pallets	Runehamar (test 1)	1200	0.17
82 % wood pallets and 18 % PUR mattresses	Runehamar (test 2)	630	0.25
81 % wood pallets and cartons and 19 % plastic cups	Runehamar (test 4)	160	0.44
HGV- furniture	Runehamar (test 3)	240	0.5
HGV- furniture	Eureka (test 21)	300	0.4
Vehicles			
Medium sized passenger cars	Assuming a 5 MW fire in the car	12 - 18	0.3 – 0.4
Passenger car plastic	Test 20 in Eureka	17 (no ceiling)	0.35
Buss	Test 7 in Eureka	80	0.36
Train	Test 11 in Eureka	145	0.30
Subway coach	Test 14 in Eureka	130	0.27

* The heat of combustion of gasoline is assumed to be equal to 43.7 MJ/kg, 43.5 MJ/kg for kerosene, 44.6 MJ/kg for n-heptane.

2.4 Reduced scale experiments

Due to costly nature of large-scale experiments, research attention was turned to reduced scale experiments. In this section, some of the most cited experimental work in tunnel fire research literature are discussed. Roh et al. investigated the effect of longitudinal ventilation on burning rate of n-heptane pool fires at different pool sizes using a reduced scale tunnel [47]. In this work, a 1/20 reduced-scale model tunnel was used constructed based on Froude scaling to examine difference of backlayering between naturally ventilated HRR and longitudinally ventilated HRR of fire. Schematics of the model used in this work is given in figure 2.6. The experiments were performed with n-heptane pool fires with sizes of 4.5-8.5 cm and depth of 2 cm. Figure 2.7 shows plot of the non-dimensional burning rate against non-dimensional ventilation velocity which are defined as the values of ventilation velocity and burning rate per that of critical velocity for various pool sizes as defined in equation (2.19) and (2.20) [47]. It was concluded that non-dimensional burning rate of n-heptane pool fire

increase as the non-dimensional ventilation velocity is increased due to larger oxygen supply effect at higher ventilation velocities compared to its cooling effect.

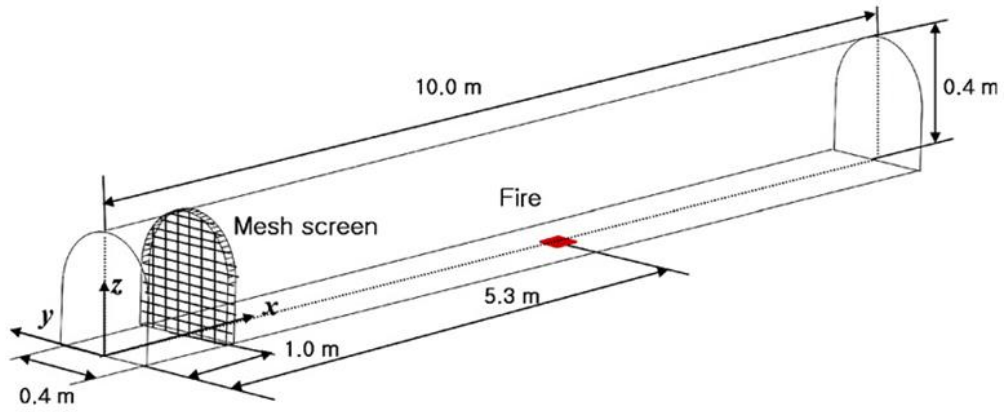


Figure 2.6. Configuration and dimensions of model tunnel used in [47]

$$V^+ = \frac{V}{V_{cr}} \quad (2.19)$$

$$m^{m^+} = \frac{m^m}{m_{cr}^m} \quad (2.20)$$

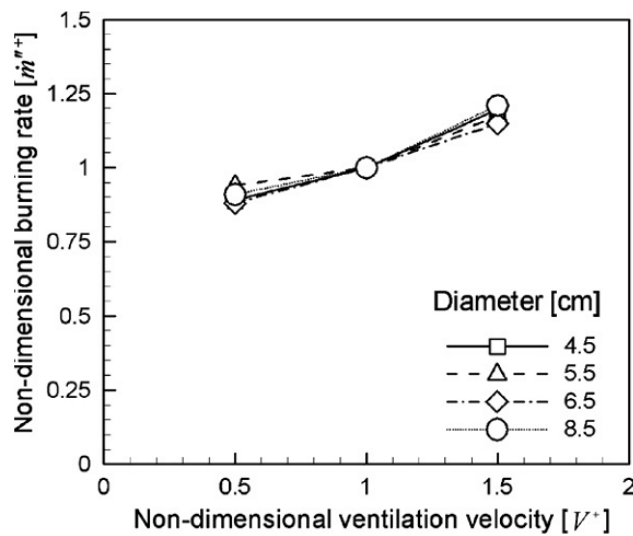


Figure 2.7. Non-dimensional burning rate vs. non-dimensional ventilation velocity for n-heptane pool fire [47]

A wind tunnel configuration was used to generate longitudinal air flow at the combustion section to compare flame characteristics and heat transfer mechanism associated with pool fire of a sooting (gasoline) and a non-sooting (methanol) fuel on square and rectangular pans as shown in figure 2.8 [48].

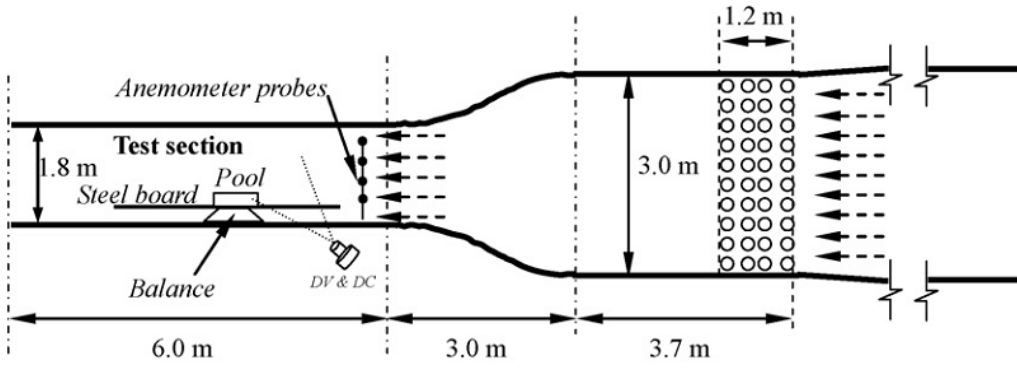


Figure 2.8. Schematics of wind tunnel used in experiments [48]

Figure 2.9 and 2.10 show the results of this experiment for stretching of rectangular gasoline pool fire with two kinds of orientations to the longitudinal airflow direction. It was shown that the flame tilted more largely for the rectangular pool fire with longer rim perpendicular to the longitudinal airflow of the same speed. The orientation effect seemed to be more remarkable for the gasoline pool fire than that for the methanol pool fire. Results also indicated that radiation from flame to the pool surface had a great impact on burn rate of gasoline fuel due to increased temperature of the fuel and tray rim.

Maximum temperature and its location is one of the important safety factors in tunnel fires. Li et al. proposed an empirical correlation for calculation of fire-induced flow temperature distribution along the tunnel ceiling under longitudinal ventilation condition as a function of ventilation velocity and fire HRR [49]. The correlation was validated using two sets of experimental data from past reduced scale experimental results of [47] and laboratory scale data from [50]. Results showed an agreement for maximum temperature trends between measurements and model along the tunnel.

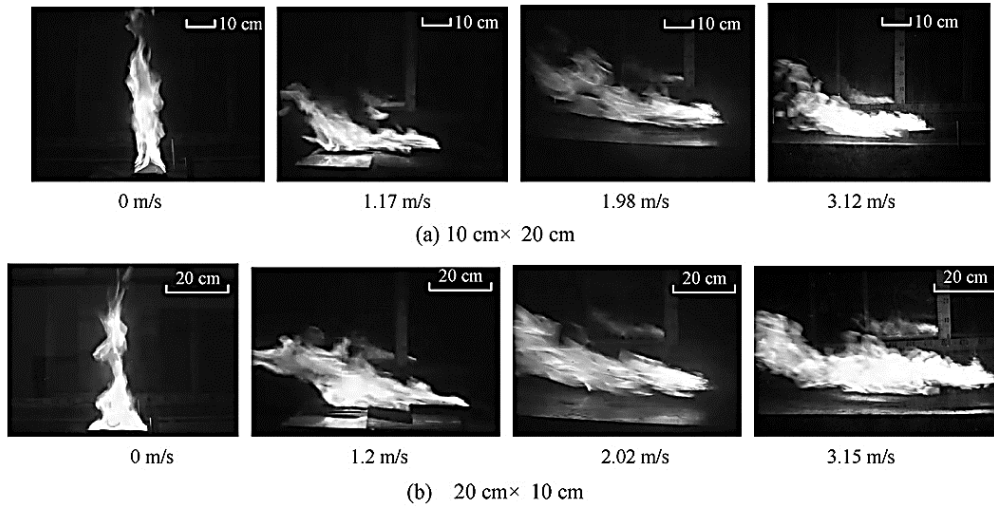


Figure 2.9. Flame stretching in 20 x 10 cm pool fires [48]

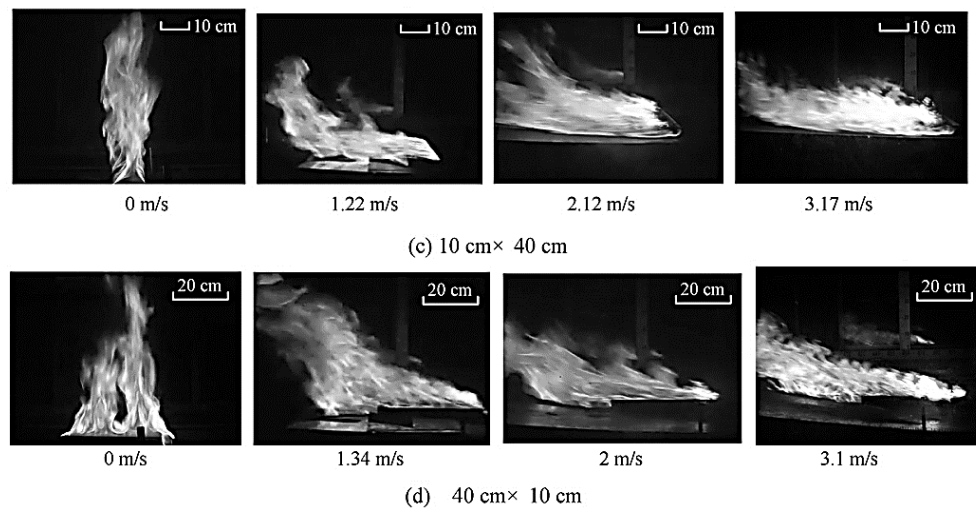


Figure 2.10. Flame stretching in 10 x 40 cm pool fires [48]

Atkinson and Wu investigated the effect of downhill inclination on critical ventilation velocity in tunnels [4]. A model tunnel was used with a height of 24 cm and colliery arch type cross-section. Propane was used as a fuel in the experiments feeding via a porous burner. The propane flow rate was varied to generate fire loads

of 15 and 75 MW in a tunnel of diameter of approximately 5 m. Results showed that for tunnels with a downhill slope the critical velocity was greater than for the corresponding horizontal tunnel with no slope as shown in figure 2.11.

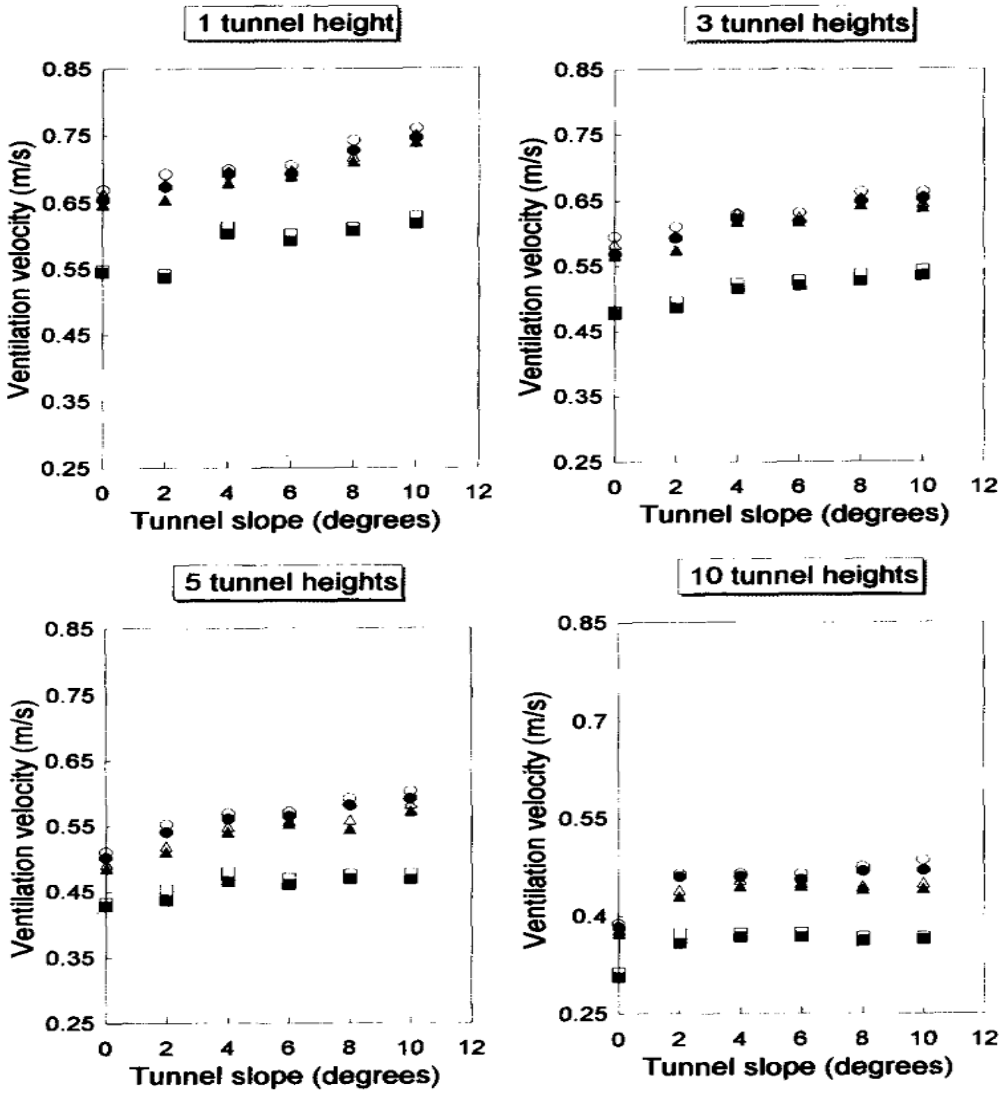


Figure 2.11. Effect of tunnel slope on ventilation velocity [4]

A 1/5 reduced scaled model tunnel was used to study the effect of a vehicular blockage at the upstream of the fire source on the buoyancy driven back-layering

length and critical velocity in a longitudinal ventilated tunnel [23]. Figure 2.12 shows the schematics of the setup with fire source and blockage configuration. The experiments were conducted on various fire-blockage distance. Three different longitudinal ventilation velocities, 0.5 m/s, 0.75 m/s and 1 m/s were considered in the experiments.

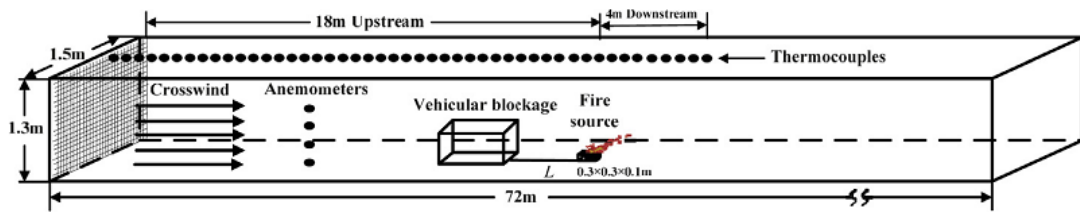


Figure 2.12. Schematics of the experimental setup [23]

The local ventilation velocity was defined due to existence of blockage upstream of fire as given in equation (2.21). In this equation, A_1 and A_2 are the cross-sectional area of the tunnel and the vehicular blockage respectively and V_{local} is the local ventilation air flow velocity imposed on the fire region.

$$V_{local} = \frac{A_1 - A_2}{A_1} V = \alpha V \quad (2.21)$$

According to the results of the experiments with a range of HRR between 50 – 100 kW, global correlations were derived for backlayering length as well as critical ventilation velocities for blocked tunnels, which are given in table 2.8. It was found that with increase in blockage-fire distance, both the back-layering length and critical velocity first decrease then maintain to be constant (similar to the situation with no blockage).

Table 2.9. Global non-dimensional correlations for blocked fire [23]

Non-dimensional backlayering length	
$L_{\text{blockage}(L)}^* = \begin{cases} 18.5 \ln \left\{ 0.81 Q^{*1/3} / \left(\left[\frac{A_1 - A_2}{A_1} + \frac{A_2}{A_1} (0.3L/\bar{H}) \right] V^* \right) \right\} & L/\bar{H} \leq 3.3, Q^* \leq 0.15 \\ 18.5 \ln(0.81 Q^{*1/3} / V^*) & L/\bar{H} > 3.3, Q^* \leq 0.15 \\ 18.5 \ln \left\{ 0.43 / \left(\left[\frac{A_1 - A_2}{A_1} + \frac{A_2}{A_1} (0.3L/\bar{H}) \right] V^* \right) \right\} & L/\bar{H} \leq 3.3, Q^* > 0.15 \\ 18.5 \ln(0.43 / V^*) & L/\bar{H} > 3.3, Q^* > 0.15 \end{cases}$	
Non-dimensional critical ventilation velocity	
$V_{\text{blockage}(L)}^* = \begin{cases} \frac{0.4}{\left[\frac{A_1 - A_2}{A_1} + \frac{A_2}{A_1} (0.3L/\bar{H}) \right]} \left(\frac{Q'}{0.2} \right)^{1/3} & Q' \leq 0.2, L \leq 3.3\bar{H} \\ 0.4 \left(\frac{Q'}{0.2} \right)^{1/3} & Q' \leq 0.2, L > 3\bar{H} \\ \frac{0.4}{\left[\frac{A_1 - A_2}{A_1} + \frac{A_2}{A_1} (0.3L/\bar{H}) \right]} & Q' > 0.2, L \leq 3.3\bar{H} \\ 0.4 & Q' > 0.2, L > 3\bar{H} \end{cases}$	
Q^* : dimensionless heat release rate (Zukoski number) based on tunnel height Q' : dimensionless heat release rate (Zukoski number) based on hydraulic tunnel diameter L^* : dimensionless backlayering length	

The 1/13 scaled model tunnel which was modified for use in current research was previously used to conduct a series of experiments on the blockage effect of vehicle mock-ups prepared by wood cribs on the HRR inside the tunnel with longitudinal ventilation velocities ranging from 0.5 m/s to 3 m/s [25,26]. In this work, the ratio of the cross sectional area of the wooden objects to the tunnel cross sectional ratio was defined as the blockage ratio (BR). The variation of maximum HRR with ventilation velocity for different BR values are shown in figure 2.13. It was shown that as the BR increases at constant air velocity, the HRR also increases. In addition, it was seen that as the air velocity is increased after some point, the cooling effect of the ventilation becomes dominant and the HRR starts decreasing at constant BR. It was concluded that temperature values along the tunnel increased as the BR increased and that the

maximum temperature location was shifted to downstream at higher ventilation velocities. The temperature variations along the tunnel could be seen in figure 2.14.

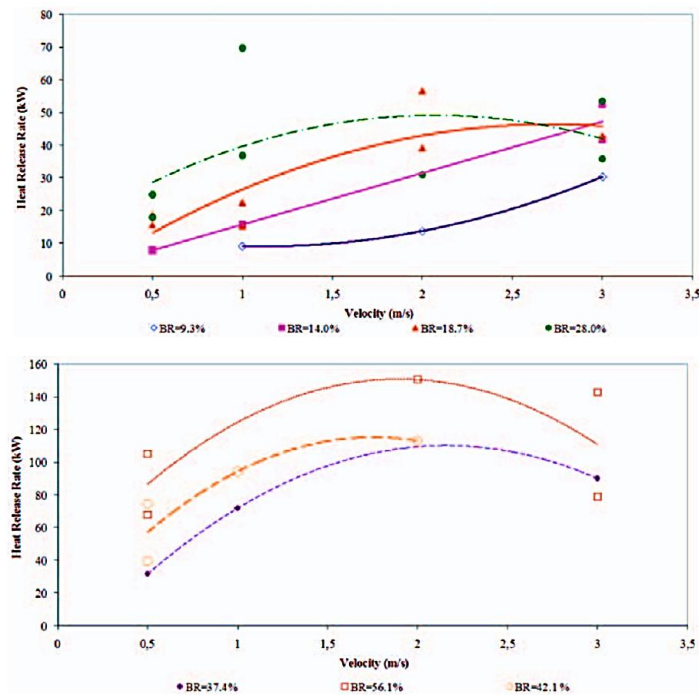


Figure 2.13. HRR as a function of blockage ratio [26]

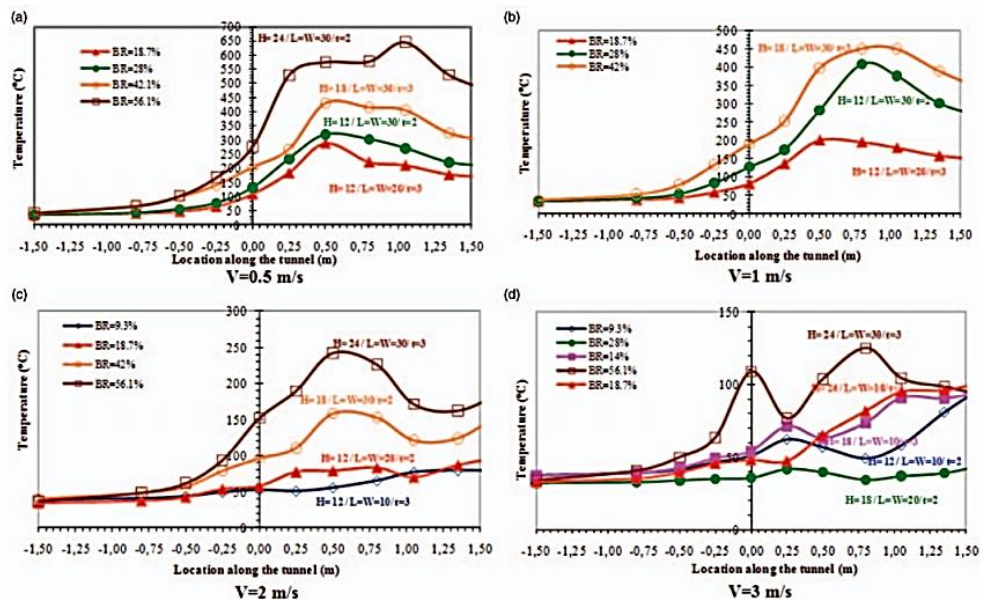


Figure 2.14. Temperature distribution at different longitudinal ventilations [26]

Pool fires where the fuel level is not kept constant are termed as batch pools. Burning rates and pool temperature variations of circular 0.2 m batch pool with an initial fuel layer of 6.5 and 13 mm were studied under quiescent conditions in [51]. The results indicated a two-stage increase in burning rates of n-heptane pool fires in which fuel bulk boiling occurs in second plateau. It was shown that the burning rates as well as flame height was increased at 13 mm pool fires. Figure 2.15 shows the temperature profiles inside the fuel layer measured by mounted thermocouples in the fuel vessel for (a) 6.5 mm and (b) 13 mm pool fires tested in this study. Wang et al. examined the merging behavior of unconfined jet fuel (JP5) pool fires in specially designed hollow square trays under quiescent and airflow conditions in a wind tunnel with airflow velocities ranging between 2 and 7.5 m/s [52]. The experimental setup was very similar to that of ref. [48]. Two hollow trays as well as an ordinary fuel tray were used which all had the same area of 0.16 m². Results showed that merging increases the pool fire burning rate and flame height up to 100 % given constant fuel surface area. According to the results, two correlations were proposed to estimate the critical burning rate for fire merging on the hollow tray in quasi-quiescent and windy conditions. Airflow was shown to decrease burning rates as the wind speed ranged up to 2 m/s due to its cooling effect and then increase the burning rate due to competing effects of cooling and combustion enhancement.

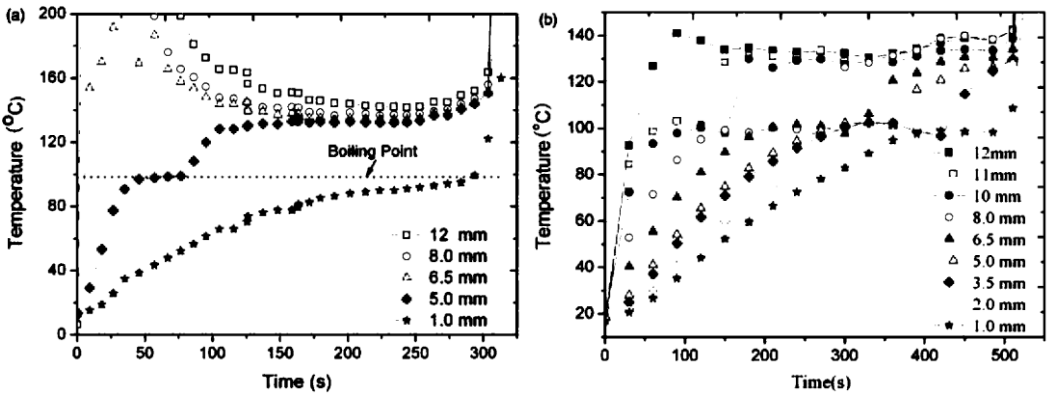


Figure 2.15. Fuel layer temperature profiles [51]

Effect of side wall on burning rates and flame characteristics of batch n-heptane pool fires with 225 cm² area and varying length to width ratios were studied in a 1/6 scaled channel with length of 6 m, width of 2 m and height of 0.86 m [53]. It was shown that the pool-wall distance affects the burning rates in several positive and negative ways, such as increasing heat feedback from the walls and restriction of air entrainment, the contribution of which results in peak burning rates to occur at 0.2 m pool-wall distance. Burning rate results of this study as a function of distance from the wall are given in figure 2.16. The effect of vessel material and freeboard height was investigated using glass, copper and steel on steady state burning rates of small scale ethanol pool fires [54]. It was reported that lip height could be a controversial aspect of pool fires, which is dependent on vessel material and pool size.

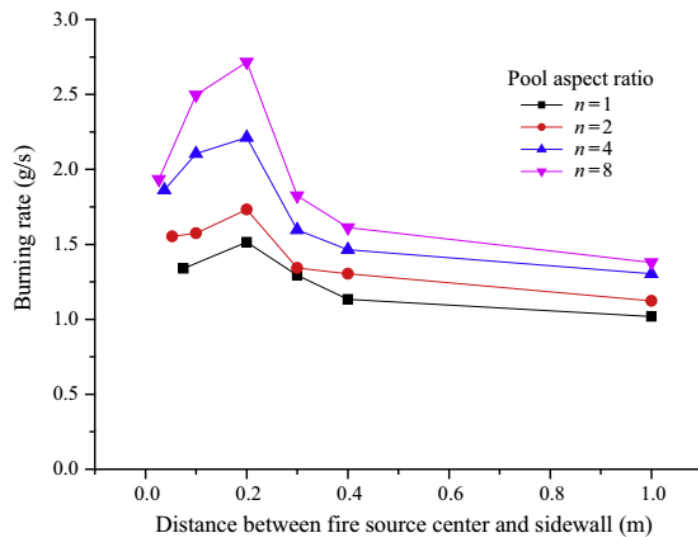


Figure 2.16. Average burning rates as a function of distance to wall and pool aspect ratio [53]

Results showed that as the lip height increased past a critical value, fuel started to boil in copper and steel vessels and the burning rate decreased monotonously for glass vessels. Square ethanol pool fires ranging from 10 to 25 cm were burnt in unconfined condition with 0-2.5 m/s cross airflow [55]. Burning rates showed progressive increase

with airflow velocities in this range, however, this enhancing effect was more pronounced at smaller pools. Flame length showed similar trends.

2.5 Numerical studies

Miloua and Azzi implemented two combustion models in FDS code to investigate the effect of different ventilation velocities and fuel pan geometry on the flame shape and smoke plume temperature of octane pool fire [56]. Model results were verified using experimental data from a full-scale tunnel. In the numerical model, flow field was resolved using the Large Eddy Simulation (LES) solver in the FDS code. For turbulent combustion process modeling, the Eddy Dissipation Concept (EDC) and the mixture fraction methods were used. The heat transfer through walls of tunnel was modeled with adiabatic and non-adiabatic wall boundary conditions. It was noted that the critical velocity was considerably affected by wall conditions meaning that for a good prediction of temperature, accounting for the heat loss through walls was important as shown in figure 2.17. The EDC model was believed to give more quantitatively correct values.

In the work by Nilsen and Log, several full-scale fire tests data for both small and large fires were gathered and three numerical models including a simple spreadsheet model, the and two CFD models implemented in order to find out which model has better compliance with the experimental fire tests and how far the results could be trusted [57]. The recorded temperatures from tests which were used to compare with the simulation results were taken at 10 m downstream of the fire zone. In order to gain insight into the back-layering length, blockage effect and flame length of the tunnel fire, Wang [58] used FDS code with implemented EDC combustion model. It was hypothesized that the empirically based correlations on propagation of smoke and the flame length ignore dynamic fire development and heat losses which was overcome in a numerical simulation. The dimensions of the large scale tunnel was similar to experimental data used by [56].

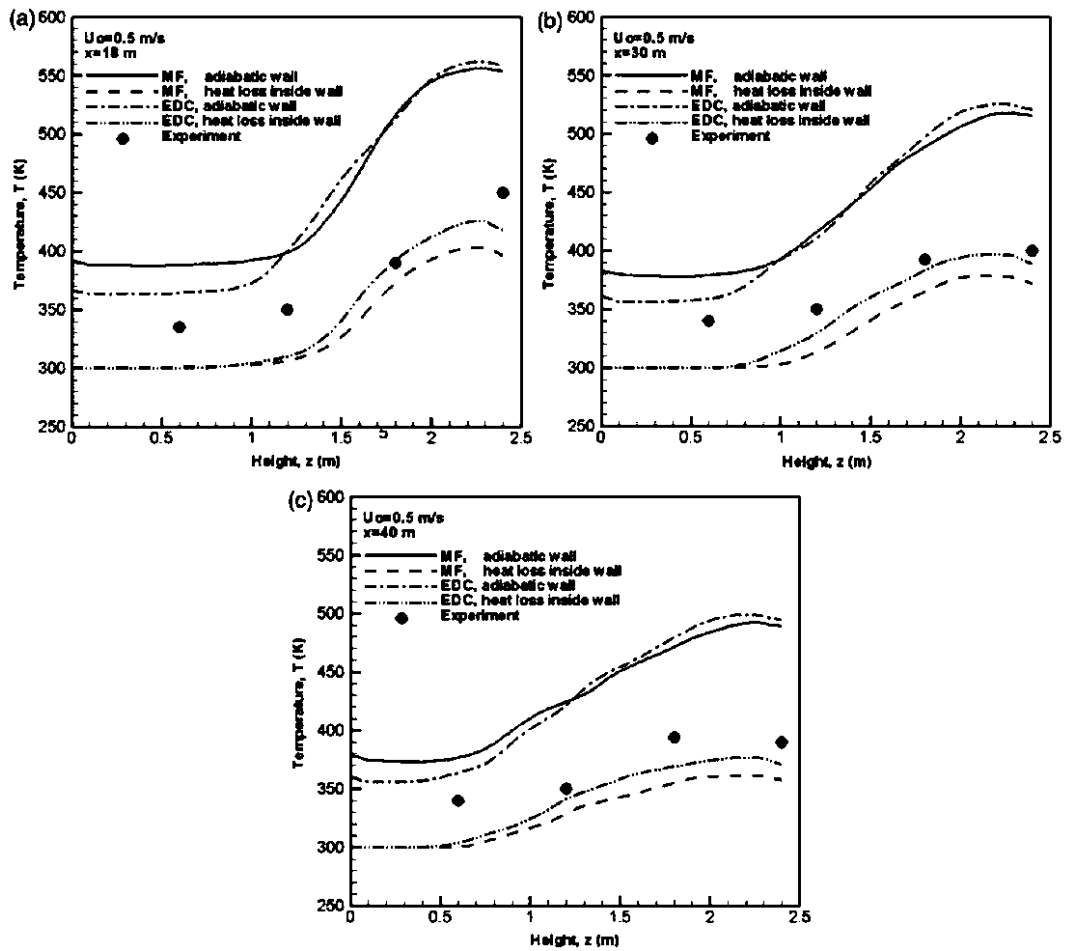


Figure 2.17. Comparison of the calculated temperature to the experimental data downstream the fire using different combustion models and boundary conditions at a low ventilation rate of 0.5 m/s (a) at $x = 18$ m, (b) at $x = 30$ m, (c) at $x = 40$ m boundary condition: (a) at a ventilation rate of 0.85 m/s, (b) at a ventilation rate of 2.0 m/s [56]

The fire source was octane pool fire at central position in the tunnel with a cylindrical blockage in the upstream of fire and ventilation velocities ranging between 0.5, 0.85 and 2 m/s. The verification of numerical model was achieved by comparing results for smoke temperature and backlayering length with experiments. Figure 2.18 shows results of the model which match the experimental data to a good degree. As for the effect of blockage on fire behavior, it was shown that due to a large recirculation behind the blockage, the gas temperature over fire source and also flame length was increased as shown in figure 2.17.

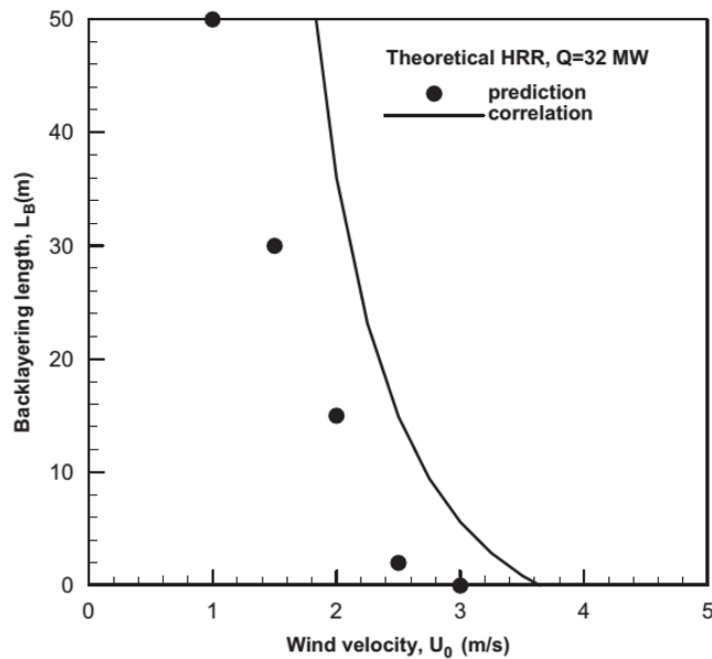


Figure 2.18. Evolutions of the backlayering length obtained from prediction and correlation as a function of the wind velocity [58]

Shorab et al., [59] compared two types of numerical models to study flow temperature and velocity profiles in a case of wood crib fire inside a naturally ventilated tunnel. CFAST was used as a popular zonal model along with CFX. The zonal models are one-dimensional models which divide the compartment into small number of volumes with uniform properties. Heat and mass transfer among the zones were processed through smoke plume. In such models, conservation equations are solved numerically together with empirical equations from experiment such as radiation and combustion models. Using the CFX model, detailed resolution of flow field and temperature profile was achieved. In the CFX simulations, volumetric heat source model was used which doesn't take the combustion chemistry into account. The results of the paper showed that the maximum smoke temperature achieved in the fire room is approximately 400 K in 24 min from start of combustion. The CFX simulations also captured flame tilt in the flow direction.

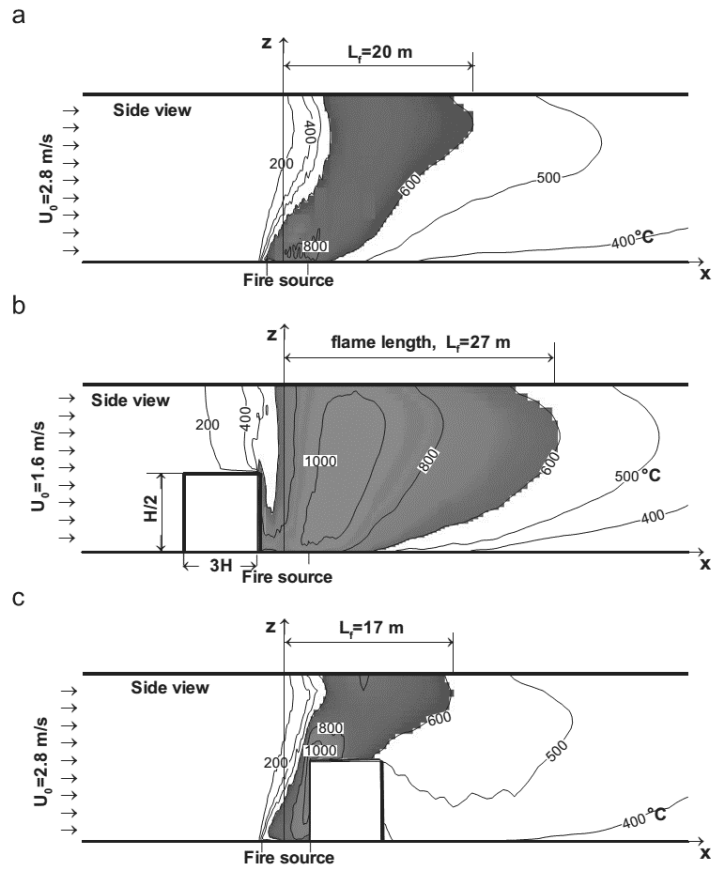


Figure 2.19. Blockage effect on iso-temperatures under a critical velocity condition, (a) smooth tunnel, (b) blockage upstream the fire source, and (c) blockage downstream the fire source [58]

CHAPTER III

EXPERIMENTAL SETUP AND METHODS

The scaled model used in this study was constructed based on Froude scaling. The model represents a bored underground metro tunnel in Istanbul, Turkey. The real scale tunnel has a diameter of 5.2 m and cross-sectional area of 20.75 m² [25,26]. The cross-section of model is composed of a rectangular base and an arched roof. Figure 3.1 shows the schematics of the real tunnel and model cross section. The model is 9 m long, 0.4 m wide and the height is 0.36 m. The structure is made of steel and is insulated on the outside using rock wool of 0.05 m thickness. There is a 2.5 m “upstream section” where flow straightener is used to rectify the airflow. The next 1.5 m is defined as the “combustion zone” where pool fire tests are conducted. There are openings on both sides of this combustion zone, with one providing access to the inside of tunnel for placement of fuel and the other as an observation pane. The remaining 5 m was termed “downstream section”. The airflow was supplied by an axial compressor which takes in the air at laboratory temperature, which is for the most part, almost constant throughout the experiment seasons at 24±2 °C.

The entrance of the tunnel was connected to a plenum that was used to dampen the airflow from the compressor. The incoming air passed through the flow straightener in the entrance compartment of tunnel. Figure 3.2 shows the experimental setup. Airflow velocity was measured and its uniformity ensured by hot-wire anemometer in both downstream of the flow straightener and in the combustion zone, upstream of fire. The measurements were conducted at 5 cm height intervals at the center of the tunnel cross section by traversing anemometer probe. The readings of anemometer were obtained with 0.2 Hz frequency over 600 s period while the compressor was operated at a specified speed to maintain ventilation range between 0.5 and 2.5 m/s. The maximum non-uniformity of airflow was found to be around 5 %.

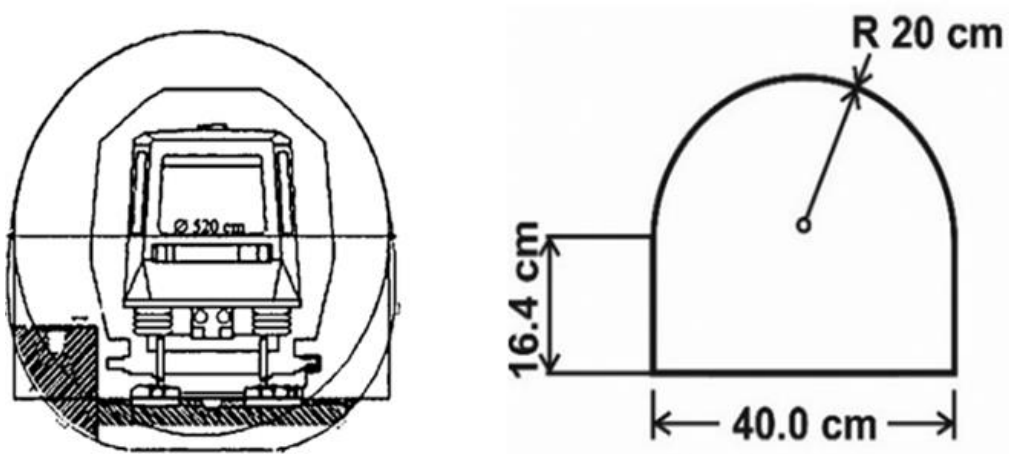


Figure 3.1. Schematics of the real tunnel and model cross section

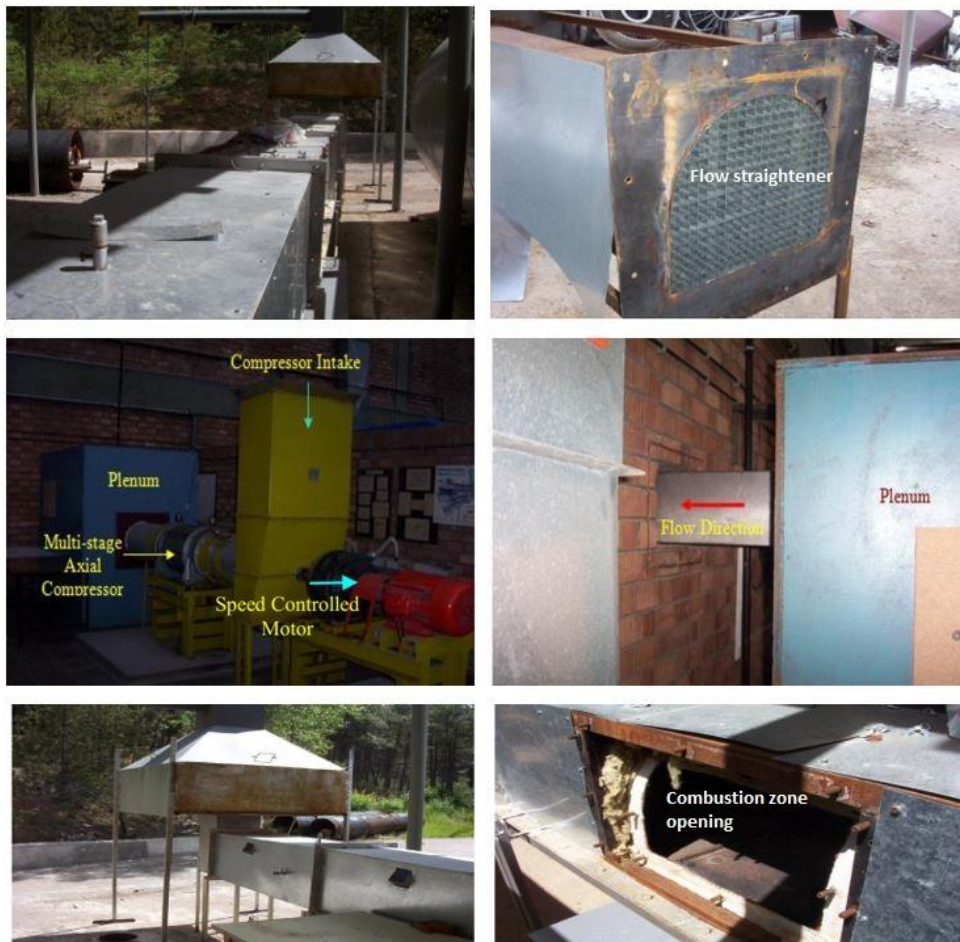


Figure 3.2. Experimental setup

3.1 Instruments

3.1.1 Gas temperature

K-type thermocouples with wire diameter of 0.5 mm were implemented along the model tunnel to measure the gas temperature. Figure 3.3 shows thermocouple and tree configuration and dimensions. For ease of data logging and saving, thermocouple location, connection series number and distance from ceiling were designated using indicators. For instance, TU200/30 means thermocouple is in the upstream section connected to port number 200 and is at 30 cm distance from ceiling. Apart from the tree configurations shown separately, other thermocouples were fixed 4 cm below the ceiling to measure smoke layer temperature. Thermocouples were Nickel and Nickel-Chromium alloy and could measure temperatures up to 1200 °C with a readability of $\pm 2.2^\circ\text{C}$.

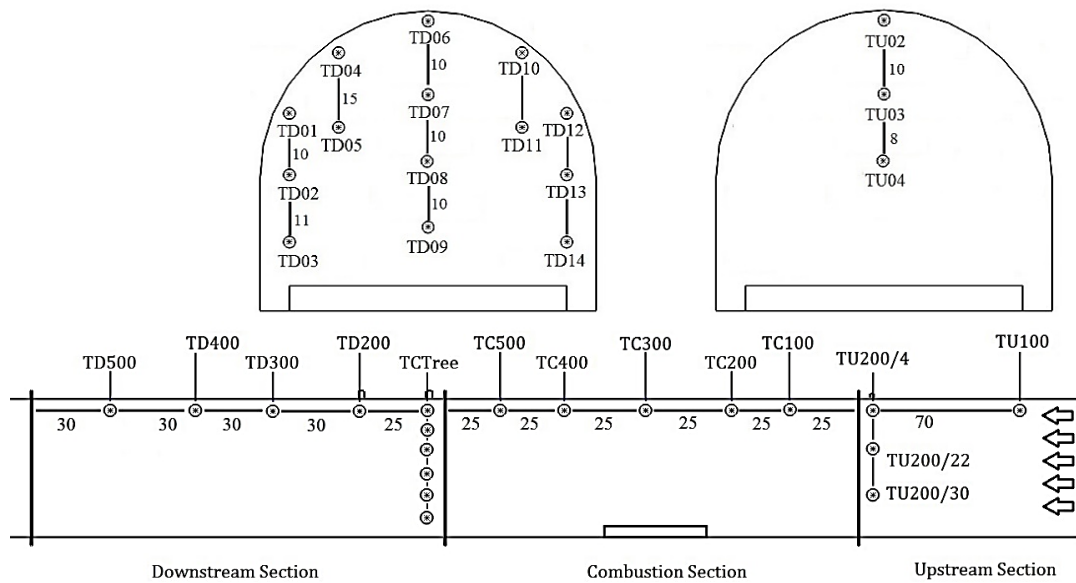


Figure 3.3. Thermocouple configuration along the tunnel (dimensions are in cm)

Temperature data were logged using an Omega OMB-DAQ-3005 data acquisition system with an expansion module connected to a computer. The data acquisition system was grounded using a wire connecting the device to a pipeline as suggested by the instrument manual. DaqView software was used to record the data with a 1 Hz frequency over the course of experiments. The temperature data acquisition pack can be seen in figure 3.4.



Figure 3.4. Data acquisition pack with connected thermocouple

Figure 3.5 shows a typical temporal history for recorded tunnel ceiling temperature during experiments. As can be seen, gas temperatures started to rise after a short period of time and almost reached a steady value during the steady state burning phase of fire, and decreased in fire decay period (also refer to figure 2.2). Enough time was allowed before the fire tests according to the thermocouple response times to ensure accurate quasi-steady temperature measurements.

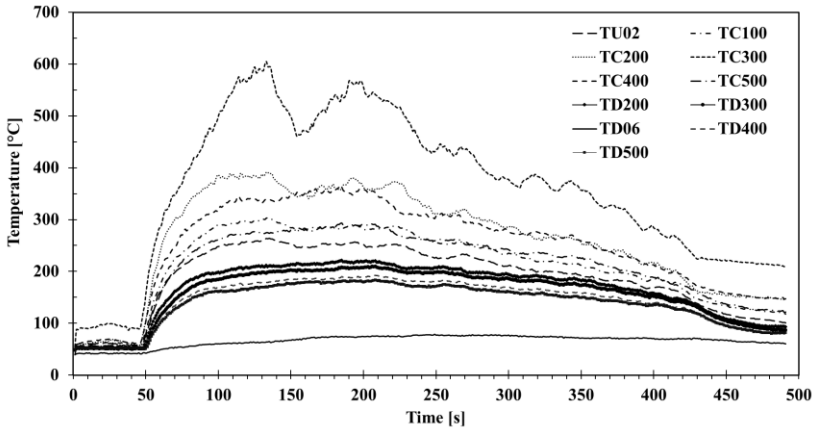


Figure 3.5. Typical temporal evolution of ceiling temperature

3.1.2 Burning rate

Mass loss histories during experiments were measured using A&D GX-K and RADWAG 25-R2 load cells with internal stability feature and a readability of 0.1 g at a sampling frequency of 5 Hz. Air tightness around the balances was ensured to avoid draft effect on devices. The balances were connected to a computer and measurements were recorded using specific software for each device. The devices can be seen in figure 3.6.



Figure 3.6. A&D GX-K and RADWAG APP-R.2 precision load cells

The derivative of mass loss history was used to obtain the mass loss rates. The burning rates of the fuel was then defined as the mass loss rate per unit area of the pool as in equation (3.1) and (3.2). The burning rates could be reproduced to within $\pm 0.0015\text{-}0.002 \text{ kg/m}^2\text{s}$. Figure 3.7 shows a typical mass and burning rate history taken from experiments.

$$m'' = \frac{dm_{fu} / dt}{A_{Burned}} \quad (3.1)$$

$$-\left(\frac{dm_{fu}}{dt}\right)_i = \frac{-m_{i-2} + 8m_{i-1} - 8m_{i+1} + m_{i+2}}{12\Delta t} \quad \text{and} \quad i : \text{data scan number} \quad (3.2)$$

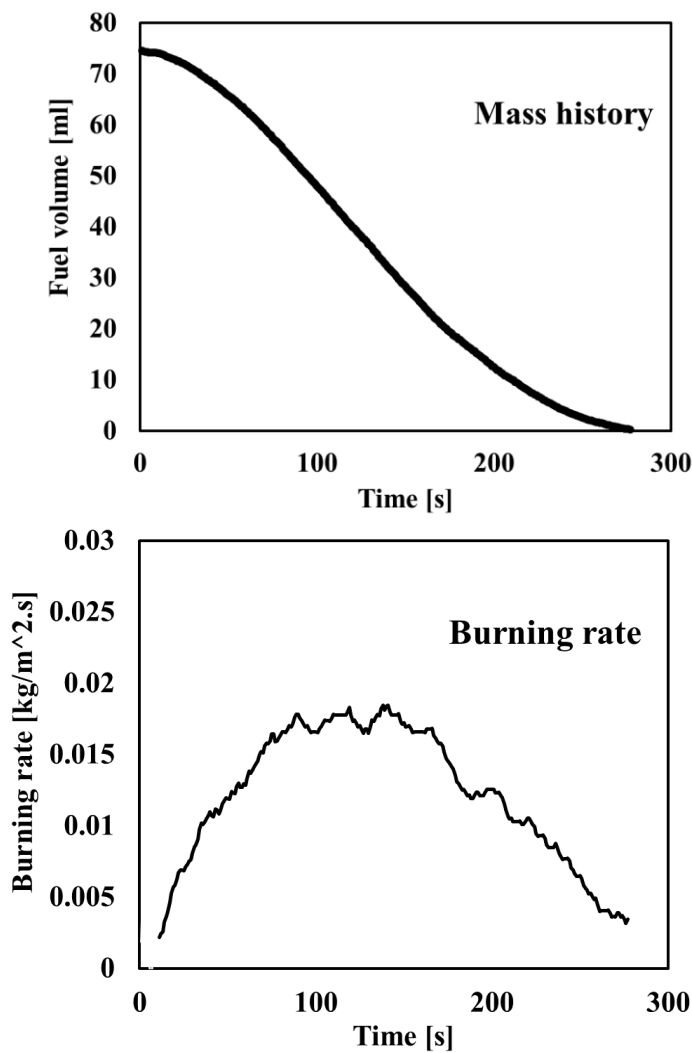


Figure 3.7. Typical mass history and calculated burning rate curves taken from experiments

3.1.3 Species concentration

Species concentration data was used to estimate the chemical HRR of the fire due to oxygen consumption calorimetry method discussed in section 2.2.2. The flue gas analyzer probe used in the experiments was a TESTO 350-S with O₂, CO and CO₂ modules as well as temperature and pressure gauges, which was mounted downstream of the fire. The device is shown in figure 3.8.



Figure 3.8. TESTO 350-S gas analyzer

3.1.4 Radiative heat flux

In order to measure radiative heat flux to upstream of the fire source during part one of the experiments, HUKSEFLUX SBG-01 water cooled heat flux sensor was mounted in the tunnel at two different orientations. The device is shown in figure 3.9. Water cooling was maintained as prescribed by device operation guide, to ensure that errors related to conductive heat transfer on the sensor measurements were minimized.

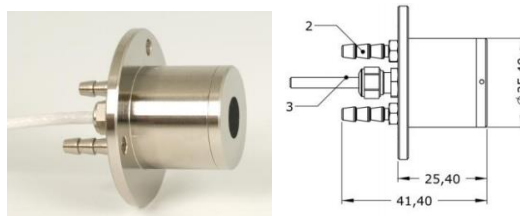


Figure 3.9. Hukseflux SBG-01 radiative heat flux sensor

3.1.5 Visualization

Flame images were captured using a high speed camera with Ethernet connectivity and a Nikon camera. The images were used in some of the experiments to investigate flame tilting and interactions between flames in case of dual pool fire cases.

3.2 Pool fires

Liquid pools as a fire source are one of the most commonly used methods in the literature to simulate fire scenarios of different magnitudes [20,47,48,60]. The frequency of their use is due to their easier handling and also the fact that liquid fuel spillage is also one of the causes of tunnel fires [1]. A vast range of liquid fuels have been used as the pool fire source in literature such as heptane, ethanol and Diesel fuel among others. Pool fire research has been around for decades, with pioneering work by Blinov and Khudiakov [61] and Rasbash [62] followed by more recent experimental studies on combustion and burning properties of pool fires that classify different phenomenon associated with hydrocarbon fuel, pool type, pool size, heat transfer regime and flame characteristics [63–66]. An informative summary of relevant studies is given in [67]. There are various physical and chemical phenomena taking place during pool fire including conductive, convective and radiative heat transfer, fuel heating and evaporation and diffusion of species and flame which all make study of the pool fires even more complex. Analysis by Hottel indicated that generally speaking, there are two distinct regimes associated with pool fires; a radiation dominated burning regime for large pools and a convectively dominated one for smaller pool fires [64].

Studies suggest that at small pool diameters, i.e. 0.1 m, the conduction effects are more dominant. Between diameters of 0.1 and 0.2 m the effects of conduction reach a minimum and mass transfer is dominated by convective heat transfer from the flame. At larger diameters due to increasing flame radiation, the effect of convective heat transfer also decreases. Finally, a maximum burning rate is reached for large enough pools due to radiation blockage at the center of the pool [67]. Figure 3.10 shows the major heat transfer regimes in a typical pool fire. There is usually an evaporation layer where fuel temperature is at its boiling point. Below this layer a preheating layer exists where fuel temperature varies exponentially and below that, the fuel temperature is almost constant.

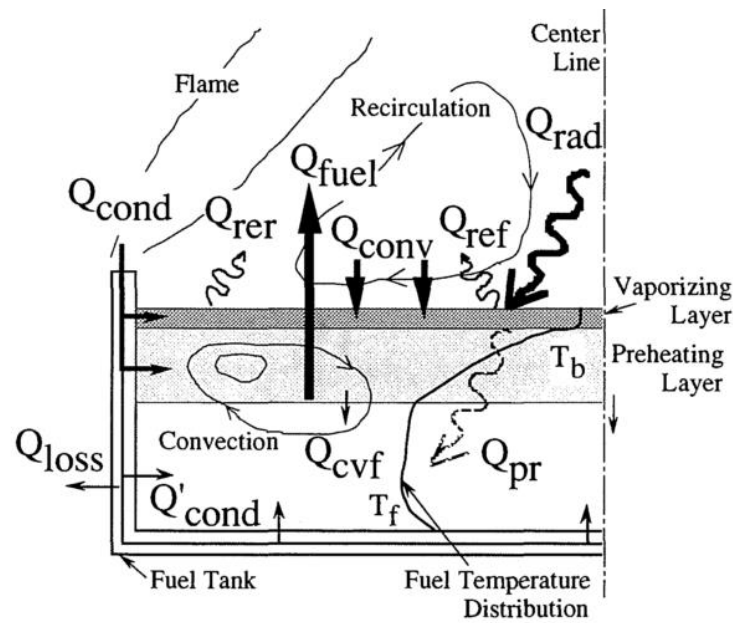


Figure 3.10. Main heat transfer regimes in a pool fire [68]

In this study, square pools were used due to their easier construction and maintenance. Considering the width of the model tunnel which is 40 cm, three pan sizes were used having inner edge length of 10, 15 and 31 cm. keeping in mind the geometry of the pans, the inner edge length can be defined as the side length inside the square fuel tray, which has an approximate wall thickness of 8 mm. This puts them into small (10 cm), medium (15 cm) and medium/large (31 cm) categories considering definitions by Hottel and Ditch, adding versatility to the ranges of the experiments in the research [64,67]. In terms of the flow regime, according to Drysdale [69], the pool sizes in this study can be categorized under “transitional flow” at quiescent conditions, however, due to the confined conditions of the tunnel as well as existence of airflow, the pool fire combustion of this study can be considered as turbulent. The pool fires were burned in either single or dual (in part two of experiments) pool orientations placed centric in the combustion zone along the longitudinal axis of tunnel. The inner height of the steel pool vessels was approximately 2 cm for 10 and 15 cm pools and 1 cm for 31 cm pool. Thermal conductivity of the vessel was approximated as 50 W/m.K at 20°C and its density as 7.85 g/cm³. Heat loss through the bottom side of the vessels

were minimized using insulation. The fuel level was not kept constant during these experiments; thus, the lip height (freeboard height) varied according to the amount of initial fuel layer (i.e. pool depth). Ethanol was used as the fire source throughout the experiments with thermos-physical properties given in table 3.1.

Table 3.1. Ethanol fuel properties

Molar mass (g/mol)	Density (g/cm³)	Boiling point (°C)	Specific heat (J/mol.K)	Heat of combustion (kJ/mol)
46.07	0.79	78.4	112.4	1365

3.3 Experiment procedure and selection of parameters

The experiments were designed and conducted after carefully examining the corresponding literature and identifying the gaps. Experiments were more or less conducted in similar ambient conditions during the two consecutive late spring/summer periods. Due to the nature of the experiments, the airflow supply properties and heat transfer from tunnel structure to surrounding could become an important factor affecting repeatability of the results. However, since the airflow was supplied from the compressor placed indoors, making it less prone to outside conditions, and the tunnel was properly insulated, it was believed that such effects would not be considerable. The experiments were conducted at least two times. Randomly selected experiments were performed three times. The results for HRR and burning rates were then given based on the average from the repeated experiments. Liquid fuel storage, preparation and use in the tunnel was carefully handled to avoid unwanted disturbances. Before the pool fire experiments, a warm up test was done with some amount of fuel to ensure uniform pan and tunnel ambient temperature conditions in the succeeding experiments. The pan temperature for instance, was

monitored during the consecutive experiments using a pyrometer. In this section, the experiment design parameters as well as variables are discussed for each part of the research. The limitations that were imposed to different parts of the experiments are also discussed.

3.3.1 Effect of tunnel wall coating material

Radiation from compartment fires is among the topics for which only a limited number of work is available in the literature. Besides, fire spread due to thermal radiation to the upstream is also known to be a safety hazard in tunnels. According to NFPA standards, the threshold water saturated temperature human respiratory tract burnout is 60°C and radiative heat flux with maximum of 30 min exposure for skin burns is 2.5 kW/m^2 [7]. As discussed in section 2.4.1, simultaneous effects of tunnel wall coating type and pool depth variations on the radiative heat loss from the ventilated pool fire as well as the burning characteristics were investigated as the first part of the research. Ethanol was used as the pool fuel due to its non-sooting flame characteristics which reduced the complexity of interpreting the results of measured radiation fluxes. Figure 3.11 shows the modified experimental setup used in these experiments. The wsnhole length of the model is not depicted in this figure.

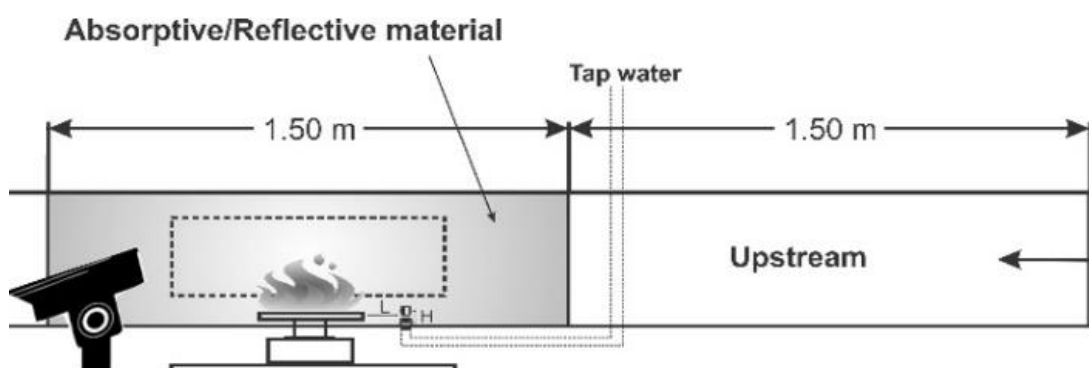


Figure 3.11. Modified experimental setup due to wall coating tests

In order to evaluate the effect of wall coating, two types of isolation material having opposite emissivity characteristics were applied to the combustion zone as seen in figure 3.11. A highly emissive black-painted anodized aluminum coating with an emissivity of approximately $\epsilon = 0.85$ and a highly polished steel with reflectivity of $\rho = 0.9$ at 300 K were used. Grey diffusive opaque surface was approximated for the coating materials. Table 3.2 lists the parameters and variables for these series of experiments. The pool sizes used in this study span the range of small to medium/large pool fires as discussed in section 3.2. In this part of the experiments, since the effect of upstream radiation was to be analyzed, the large pan was used. The ventilation velocity was varied between 0 up to 2.5 m/s, which was selected as the upper limit for longitudinal ventilation during the experiments of this study firstly due to intense turbulence induced at velocities higher than 2.5 m/s which start to affect the mass loss rate readings and secondly due to the fact that this value corresponds to approximately 8.9 m/s in the real scale tunnel which is above the common average longitudinal ventilation velocity. The increment interval of ventilation velocity was because of difficulty in establishing the desired airflow velocity from the providing compressor which operated at a fixed range of speeds. Pool depth was varied between 0.1 and 0.3 cm. This range of pool depth put the pool fire partly in the spill fire or thin-layered pool fire category, for which limited data was available in the literature.

The maximum pool depth (measured from pan bottom to fuel surface) was 0.3 cm corresponding to approximately 300 ml of fuel. The reason for selection of this range was to 1) compare different behavior of thin layered pool fire 2) minimize fuel usage due to large pan size in this part of the experiment since increased pool depth case studies would also be investigated at other sections of the research and 3) due to the geometry of the pan, the effect of freeboard height was thought not to be significant at this pool depth range (less than 1 cm). The radiative heat flux was measured in the upstream of fire using the water-cooled radiometer. The two radiometer configurations used in the experiments are shown in figure 3.12. The horizontal radiometer orientation was flush with the fuel pan aiming to obtain a good view factor on the flame body.

Table 3.2. Experiment variables due to tunnel wall coating tests

Pool size [cm]	31
Pan inner height [cm]	1
Pool depth, D [cm]	0.1, 0.2, 0.3 (equal to 100, 200 and 300 ml)
Wall coating	Reflective ($\rho = 0.9$) Emissive ($\varepsilon = 0.83$)
Ventilation velocity [m/s]	0, 0.5, 1, 1.5, 2.5
Ventilation temperature [°C]	24±2

In case of the vertical orientation, the aim was to achieve a qualitative idea of the effect of different wall coating by measuring the back-radiation which will be majorly from the walls.

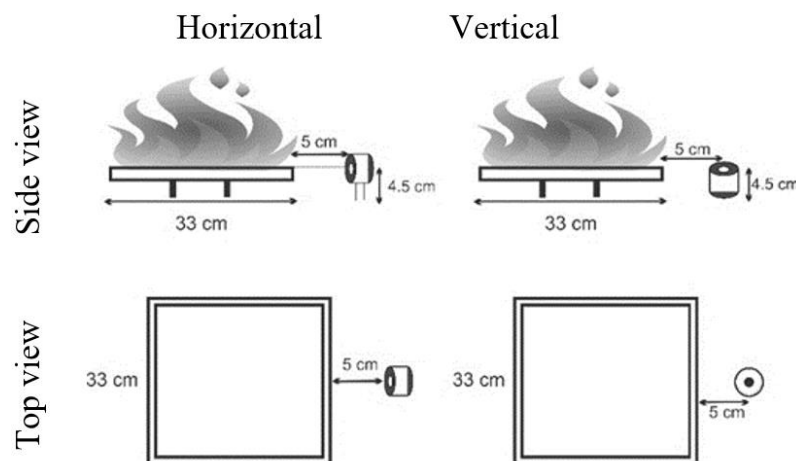


Figure 3.12. Horizontal and vertical radiometer orientations used in wall coating experiments

3.3.2 Adjacent pool fires

In an attempt to address effect of interacting confined pool fires on their burning rates, a series of experiments were conducted with varying pool size, depth and airflow

velocities. Schematics of the combustion zone and the pool orientations in this part of the experiments is shown in figure 3.13 with the arrow showing the ventilation direction. Details regarding experiment variables shown in this figure as well as other test conditions are given in table 3.3. Due to physical restrictions imposed by tunnel width, only 10 and 15 cm pool sizes were used in single or dual pool configurations as seen in figure 3.13. The pools were assigned as P1 and P2 in dual pool fire tests and rim edges of pools are flush with each other. The maximum ventilation velocity was limited to 1.5 m/s in these series of experiments due to intense turbulence induced by secondary fire which affected the balance readings at higher ventilation velocities.

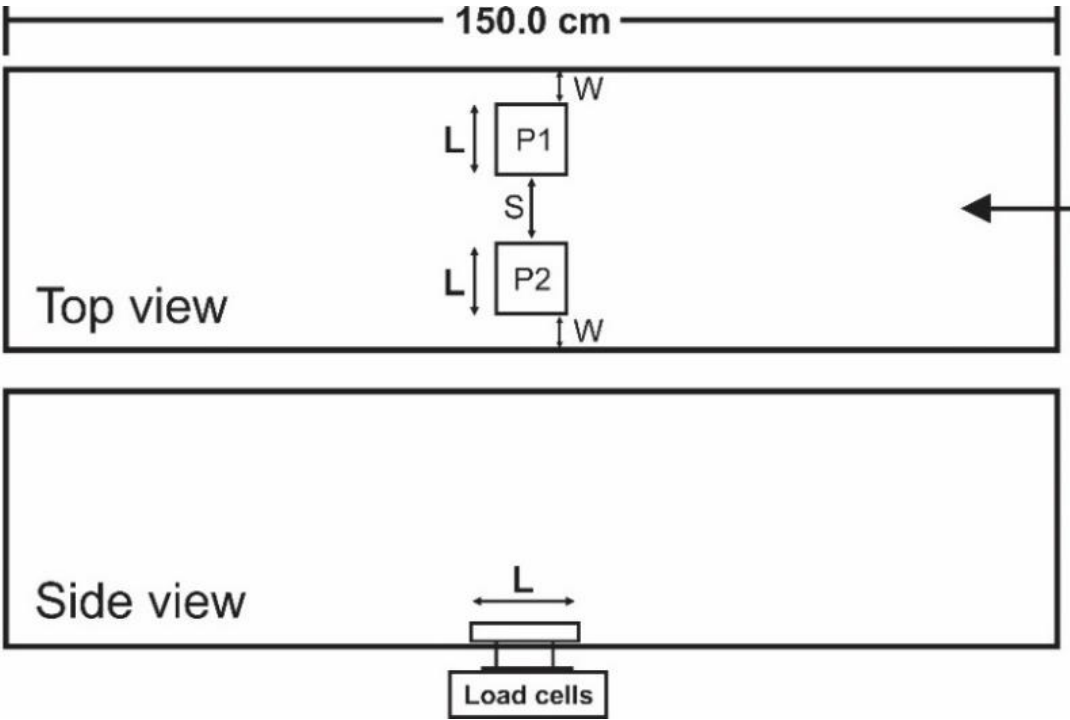


Figure 3.13. Model cross section and pool orientation in the combustion zone

Considering the pool sizes and geometry, initial fuel mass of 40 g and 80 g was used for 10 cm pool cases which corresponded to 0.5 and 1 cm pool depth. As for the 15 cm pool cases, 40, 80 and 178 g fuel was used which corresponded to an extended 0.22, 0.45 and 1 cm pool depth range. Affected by tunnel width and pool sizes, the

separation distance was varied between 4 and a maximum value of 8 cm for the 10 cm pool and was kept constant at 4 cm for 15 cm pools. Separation distance below 4 cm was not considered since the induced flame from the adjacent pool resulted in unstable balance readings. Airflow humidity was around 60 ± 5 % throughout the experiments.

Table 3.3. Experiment variables due to multiple pool fire experiments

Pool dimension, L [cm]	10 and 15
Initial fuel mass [g]	40, 80 and 178
Initial fuel temperature [°C]	24±2
Pool depth, D [cm]	0.22 - 1
Airflow velocity [m/s]	0, 0.5, 1 and 1.5
Pool separation distance, S [cm]	4 and 8
Pool-wall distance, W [cm]	3 - 8
Airflow temperature [°C]	24±2

3.3.3 Effect of tunnel blockage

The effect of obscured flow on changes of critical ventilation velocity, HRR and tunnel ceiling temperature in case of blocked tunnel fire were investigated in these series of experiments. Table 3.4 shows the experimental variables for tunnel blockage experiments. By this point in the experiments, the effect of pool size and pool depth on burning characteristics of fire had been investigated and due to this reason, only 15 cm pool fires were used in the blocked fire and tunnel inclination tests in section 3.3.4. Also it should be noted that as discussed earlier, the 15 cm pan falls in the medium pool size category which is less dependent on a dominant heat transfer regime [67]. The pool depth was fixed at an average value of 0.45 cm deducted from previous

experiments and the ventilation velocity ranged as in section 3.3.2. The blockage fire separation distance was defined as the edge-to-edge length from the mock up at the upstream to the inside edge of the pan rim (fire). It was believed that at increased separation distance, the effect of the blockage on the burning rates would decrease [24]. Also, again due to physical restrictions of the tunnel, the length of the upstream section of tunnel between the entrance and combustion zone is limited which confines the movability of the mock up further upstream due to possible effects on the entering flow (especially in case of metro mock up).

Table 3.4. Experiment variables due to tunnel blockage tests

Pool size, L (cm)	15	
Pool depth, D (cm)	0.45	
Ventilation velocity (m/s)	0, 0.5, 1, and 1.5	
Blockage-fire distance, S (cm)	5, 15 and 30	
L/S	3, 1 and 0.5	
Blockage dimensions, L1 x L2 x L3 (cm)	No Blockage	0 (L/S = 0)
	Car mock-up	30 x 15 x 12
	Subway car mock-up	70 x 30 x 24
Blockage ratio (%)	No blockage	0 (L/S = 0)
	Car mock-up	$\frac{A_B}{A_T} = 14$
	Metro wagon mock-up	$\frac{A_B}{A_T} = 56$

Thus, a maximum separation distance of 30 cm was used in the experiments. The factor L/S was also defined as the ratio of pool size (15 cm) to the blockage fire separation distance (S) which varied between 0 for no blockage case and 3 for the case of 5 cm separation distance. In order to simplify the production of mock ups, rectangular obstruction in form of a typical road sedan car dimensions and a metro wagon were constructed using metal sheets and placed upstream of pool fires at varying separation distances. Figure 3.14 shows the modified experimental setup, i.e. the combustion zone, used throughout this part of the experiments.

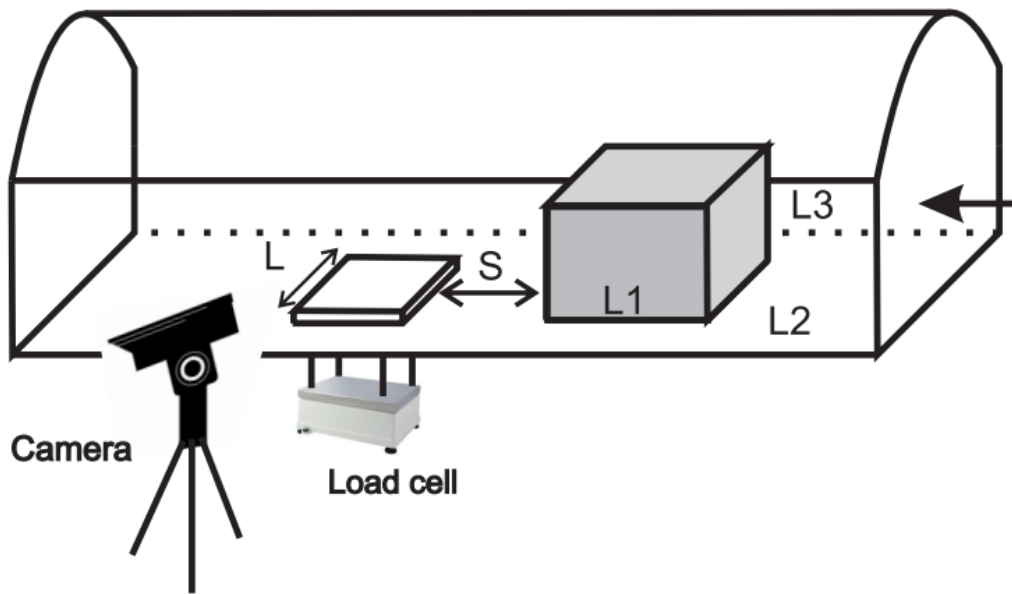


Figure 3.14. Schematics of modified combustion zone at tunnel blockage experiments

3.3.4 Effect of tunnel inclination

The effect of uphill and downhill inclination on smoke movement, backlayering length, critical ventilation velocity, and gas temperature distribution was investigated by generating slopes up to 6 % according to table 3.5. Ventilation velocity to the tunnel was varied from quiescent condition up to 1.5 m/s. The pool depth was fixed at an average value of 0.45 cm and the ventilation velocity ranged as in sections 3.3.2 and

3.3.3, albeit, with refined increments of 0.25 m/s to better capture smoke movement at different ventilation velocities due to inclination effect of tunnel.

Table 3.5. Experiment variables due to inclination tests

Pool size, L (cm)	15
Pool depth, D (cm)	0.45
Ventilation velocity (m/s)	0, 0.5, 1, and 1.5
Inclination grade (%)	0, ± 3 , +6
Inclination angle (deg)	0, ± 1.72 , +3.43

Schematics of the experimental setup can be seen in figure 3.15. Steel supports were used to hold the tunnel model while the tunnel grade was adjusted using a lift (for downhill inclination) and a crane (for uphill inclination) mounted on the model during the experiments. Due to physical restrictions, a maximum of +6 % grade was applied in the uphill (positive) inclination case study while the negative slopes were only performed at -3 %.

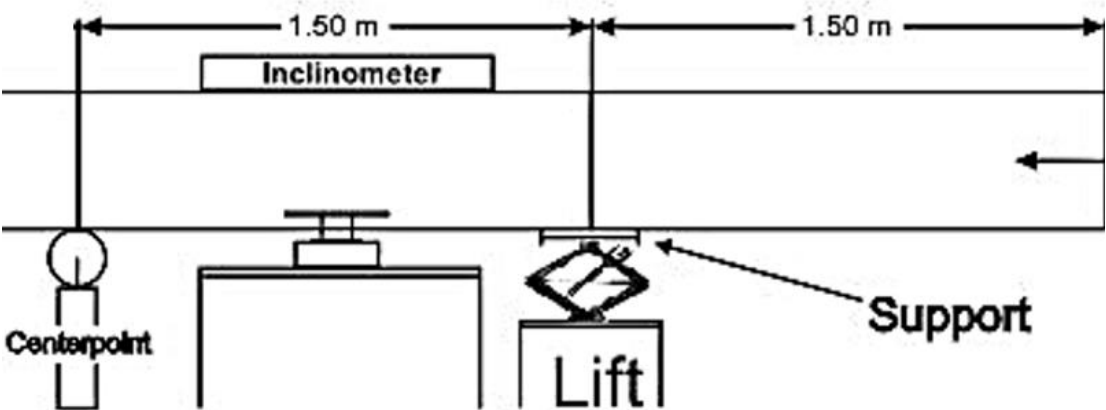


Figure 3.15. Modified model for tunnel inclination experiments

3.3.5 Uncertainty of calculations

The HRRs and burning rates of different fire scenarios investigated within the range of this research were calculated based on measured oxygen depletion values according to equations (2.11) and (2.12) and derivation of the mass loss history according to equations (3.1) and (3.2) based on load cell measurements, respectively. Such experimental measurements are prone to an uncertainty due to inaccuracy of equipment, random variation in measured quantities, and approximations which reflect in a combined uncertainty of the final result [70]. The following equation is suggested for calculation of the “best-estimate uncertainty” of R which is a function of n measured variables x_1, x_2, \dots, x_n as below [70].

$$\omega_R = \left(\sum_{i=1}^n \left[\omega_{x_i} \frac{\partial R}{\partial x_i} \right]^2 \right)^{1/2}; R = f(x_1, x_2, \dots, x_n) \quad (3.3)$$

in which ω_{x_i} is the uncertainty estimate of measured variable x_i . Equation (3.4) gives the combined relative uncertainty as a function of estimate uncertainty [71].

$$u_R = \pm \left(\sum_{i=1}^n \left[\frac{x_i}{R} \frac{\partial R}{\partial x_i} u_i \right]^2 \right)^{1/2} = \frac{\omega_R}{R} \quad (3.4)$$

3.3.5.1 Uncertainty of burning rate calculations

Due to inherent measurement uncertainties in their calculations, it is good practice to calculate the uncertainty related to the HRR and burning rates reported in the research. The burning rate is a function of mass loss rate and pool area. From equation (3.1), with slight modification of scan number notion, one can write;

$$m^m = \frac{dm_{fu} / dt}{A_{Burned}} = \frac{m_{j+1} - m_j}{(\Delta t)(A_{pool})} = f(\Delta m_{fu}, \Delta t, A_{pool}) \quad (3.5)$$

Critical operating conditions were selected based on the previous discussions in this section regarding the pool depth and ventilation velocity. In doing so, limiting cases of 31 cm pool fire with 0.1 cm pool depth at 2.5 m/s ventilation velocity and 10 cm dual pool fire case with 1 cm pool depth at 1.5 m/s ventilation velocity were selected and the fuel mass data from the quasi-steady state burning phase, the refresh rate of the balance and the resolution of ruler were used derive the relative uncertainties. The maximum refresh rate of the load cell used in the study was 10 Hz. The relative uncertainties of measured pool surface area for the 31 and 10 cm pool sizes were estimated to be 0.3 % and 0.7 % respectively considering the probable measurement error of the ruler (± 0.5 mm) and by applying equation (3.4). The relative uncertainty of the time interval was calculated based on the sampling rate of the measurements. Table 3.6 gives the calculated relative and combined uncertainties for burning rate calculations. Maximum combined uncertainty was found to be 1.5 %.

Table 3.6. Relative and combined uncertainties associated with burning rate measurements

	1 cm pool depth			0.1 cm pool depth		
	Mass (g)	u_i	u_{m^m}	Mass (g)	u_i	u_{m^m}
m_{t1}	47 ± 0.2	± 0.0042	0.015	64.1 ± 0.2	± 0.0031	0.008
m_{t2}	27 ± 0.2	± 0.0074		40.8 ± 0.2	± 0.005	

The combined uncertainty for burning rate calculations given in table 3.6 was calculated as a function of relative uncertainty of measured net mass, time interval and pool area from equations (3.4) and (3.5) as;

$$u_{m'''} = \pm \left(\left[\frac{\Delta m}{m'''} \frac{\partial m'''}{\partial \Delta m} u_{\Delta m} \right]^2 + \left[\frac{\Delta t}{m'''} \frac{\partial m'''}{\partial \Delta t} u_{\Delta t} \right]^2 + \left[\frac{A}{m'''} \frac{\partial m'''}{\partial A} u_A \right]^2 \right)^{1/2} \quad (3.6)$$

in which the relative uncertainty of mass variation in the steady-state interval was calculated due to equation (3.7).

$$u_{\Delta m} = \pm \left(\left[\frac{m_2}{\Delta m} \frac{\partial \Delta m}{\partial m_2} u_{m_2} \right]^2 + \left[\frac{m_1}{\Delta m} \frac{\partial \Delta m}{\partial m_1} u_{m_1} \right]^2 \right)^{1/2} \quad (3.7)$$

3.3.5.2 Uncertainty of HRR measurements

The uncertainty of HRR measurements was calculated by applying the same method as in section 3.3.5.1 using equations (3.3) and (3.4) to equations (2.11) and (2.12). From these equations, HRR can be deduced as a function of several variables and combustion constants. In order to simplify the calculation of the derivative terms in the estimated uncertainty equations, , the relative uncertainties of heat release of combustion per unit volume of oxygen and CO, i.e. the E', E'' terms, $X_{O_2}^0$ (assumed constant) and X_{CO}^A terms were neglected. The HRR can then be written as a function of oxygen concentration and the volumetric flow rate whereas the oxygen depletion factor is substituted by a simplified term as a function of measured oxygen concentration as seen in equation (3.8).

$$\begin{aligned} \dot{Q} &= f(E', E'', \phi, \dot{V}_A, X_{CO}^A, X_{O_2}^A, X_{O_2}^0) \rightarrow \dot{Q} \approx f(\dot{V}_A, X_{O_2}^A) \\ \phi &= f(X_{O_2}^o, X_{O_2}^A, X_{CO_2}^o, X_{CO_2}^A, X_{CO}^o, X_{CO}^A, X_{H_2O}^o) \rightarrow \phi \approx f(X_{O_2}^A) \end{aligned} \quad (3.8)$$

This assumption is valid as documented elsewhere, which states that the uncertainty of oxygen measurement is the dominant factor in calculation of expanded uncertainty for the HRR according to oxygen consumption calorimetry method [72]. With that in mind, the combined uncertainty for the heat release rate was calculated

according to equations (3.9). by neglecting the effect of CO, CO₂ and H₂O concentrations which was assumed to be a correct assumption given the data in the literature [72,73]. The estimated uncertainty for volumetric airflow rate was 5 %.

$$u_{\dot{Q}} = \pm \left(\left[\frac{\dot{V}_A}{\dot{Q}} \frac{\partial \dot{Q}}{\partial \dot{V}_A} u_{\dot{V}_A} \right]^2 + \left[\frac{X_{O_2}^A}{\dot{Q}} \frac{\partial \dot{Q}}{\partial X_{O_2}^A} u_{X_{O_2}^A} \right]^2 \right) + \left(\left[\frac{X_{CO}^A}{\dot{Q}} \frac{\partial \dot{Q}}{\partial X_{CO}^A} u_{X_{CO}^A} \right]^2 \right)^{1/2} \pm \left(\left[\frac{\dot{V}_A}{\dot{Q}} \frac{\partial \dot{Q}}{\partial \dot{V}_A} u_{\dot{V}_A} \right]^2 + \left[\frac{X_{O_2}^A}{\dot{Q}} \frac{\partial \dot{Q}}{\partial X_{O_2}^A} u_{X_{O_2}^A} \right]^2 \right)^{1/2} \quad (3.9)$$

in which the $\partial \dot{Q} / \partial X_{O_2}^A$ derivative term was calculated by below assumption for oxygen depletion factor;

$$\phi \approx \frac{X_{O_2}^o - X_{O_2}^A}{X_{O_2}^o - X_{O_2}^o X_{O_2}^A} \quad (3.10)$$

The derivatives were calculated as below,

$$\left\{ \begin{array}{l} \frac{\partial \dot{Q}}{\partial \dot{V}_A} = \left[\frac{X_{O_2}^o - X_{O_2}^A}{X_{O_2}^o - X_{O_2}^o X_{O_2}^A} - \left(\frac{E'' - E'}{E'} \right) \left[\frac{1 - \frac{X_{O_2}^o - X_{O_2}^A}{X_{O_2}^o - X_{O_2}^o X_{O_2}^A}}{2} \right] \frac{X_{CO}^A}{X_{O_2}^A} \right] E' X_{O_2}^o \\ \frac{\partial \dot{Q}}{\partial X_{O_2}^A} = \frac{E' X_{O_2}^o \dot{V}_A (X_{O_2}^o - 1) (X_{CO}^A \left(\frac{E'' - E'}{E'} \right) + 2)}{2 X_{O_2}^o (1 - X_{O_2}^A)^2} \end{array} \right. \quad (3.11)$$

Critical operating conditions were selected as the minimum and maximum limits of HRR achieved throughout the experiments, which corresponded to maximum and minimum oxygen concentration in the equations. Table 3.7 gives the calculated relative and combined uncertainties for HRR calculations. The accuracies regarding

mole fraction measurements were taken from the producer catalogue of flue gas analyzer device and other parameters were plugged in from measured data corresponding to the maximum HRR obtained in the selected experiments to equations (3.11) and (3.9). Results indicated that the maximum contribution to the combined uncertainty was more than 80 % due to oxygen measurement (second term on the RHS of equation (3.9) and to a much lesser degree due to uncertainty corresponding to airflow measurement. Also it was seen that the expanded uncertainty tends to increase at lower HRR values associated with lower oxygen depletion factor which was in agreement with the literature [72]. According to the results, the average estimated combined uncertainty of the experiments was 16 % which tends to decrease to 9.4 % at increased HRR values.

Table 3.7. Relative and combined uncertainties associated with HRR measurements

Case 1: HRR = 7 kW		Case 2: HRR = 85 kW	
$u_{X_{O_2}^A}$	$u_{\dot{Q}}$	$u_{X_{O_2}^A}$	$u_{\dot{Q}}$
0.0065	0.226	0.0063	0.094

CHAPTER IV

NUMERICAL MODEL

Numerical simulations using a model developed based on the FDS code accompanied parts of the experiments. The FDS is a Fortran based model that solves a form of the Navier-Stokes equations appropriate for low-speed, thermally-driven flow using a finite difference solver with an emphasis on smoke and heat transport from fires developed by National Institute of Standards and Technology (NIST) [15]. The general procedure for simulation of a test case in FDS was as follows; An input file was generated that contained information about the mesh size and dimensions, the geometry of the domain, material properties, ambient conditions, combustion model, solver type and desired output data. The materials for instance, were defined by their thermos-physical properties such as conductivity, specific heat, and burning characteristics. The input file was then read after initiation of the FDS solver. Solver parameters were also assigned prior to run. After obtaining the results, output files were post-processed using SmokeView software. In this chapter, a review of this model and the corresponding conservation equations are discussed which are generally based on FDS user guide and technical reference guide documents [15,74].

4.1.1 Fundamental governing equations

The conservation equations for mass, momentum and energy employed in FDS are summarized as given in equations (4.1) through (4.4) with the assumption the fluid is treated as perfect gas and stress [74]. It should be noted that these fundamental equations are practically similar to their counterparts used in other CFD models with specific approximation and simplifications applied according to the type of problem and the code.

The mass conservation equation in general form is as follows;

$$\frac{\partial \rho}{\partial t} + \nabla \cdot \rho \mathbf{u} = m_b''' \quad (4.1)$$

And in terms of mass fractions for individual gas species, Y_α , it can be re-written as;

$$\frac{\partial}{\partial t} (\rho Y_\alpha) + \nabla \cdot \rho Y_\alpha \mathbf{u} = \nabla \cdot (\rho D_\alpha \nabla Y_\alpha) + m_\alpha''' + m_{b,\alpha}''' \quad (4.2)$$

The momentum and energy equations are as follows;

$$\frac{\partial}{\partial t} (\rho \mathbf{u}) + \nabla \cdot (\rho \mathbf{u} \mathbf{u}) + \nabla p = \rho \mathbf{g} + \mathbf{f}_b + \nabla \cdot \boldsymbol{\tau}_{ij} \quad (4.3)$$

$$\frac{\partial}{\partial t} (\rho h) + \nabla \cdot \rho h \mathbf{u} = \frac{Dp}{Dt} + \dot{q}''' - \dot{q}_b''' - \nabla \cdot \dot{q}_b'' - \nabla \cdot \mathbf{q}'' + \varepsilon \quad (4.4)$$

in which the bold quantities represent vectors and τ_{ij} is the stress tensor in three dimensional form, \mathbf{f}_b is the external force vector excluding gravitational forces, \dot{q}''' is the volumetric heat release rate due to chemical reactions, \dot{q}_b''' is the energy flux to evaporating fuel droplets, \mathbf{q}'' represents the radiative and conductive heat flux vector and ε is the energy dissipation factor due to viscosity of the fluid which is modelled in FDS as in equation (4.5) with \mathbf{s}_{ij} as the strain tensor and μ as the dynamic viscosity of fluid;

$$\varepsilon \equiv \boldsymbol{\tau}_{ij} \cdot \nabla \mathbf{u} = \mu (2\mathbf{S}_{ij} \cdot \mathbf{S}_{ij} - \frac{2}{3} (\nabla \cdot \mathbf{u})^2) \quad (4.5)$$

This is a crucial part in distinguishing between different CFD codes as they model this term differently. Simulation of turbulent flows by numerically solving the Navier–Stokes equations requires resolving a very wide range of time and length scales that can be achieved via Direct Numerical Simulation (DNS). However, DNS is computationally heavy and impractical in engineering systems with complex geometry or flow configurations. This has led to development of alternative turbulence models such as the k-epsilon or k-omega models that include additional transport equations to represent the turbulence properties of the flow by satisfying the momentum equation closure. These models have the advantage of simplicity and cost effectiveness. However, due to the fact that the root of these models are from time-averaged approximation of the conservation equations of fluid dynamics and would not be able to account for the evolution of large-eddy structures characteristic of fire plumes and the transient nature of it, their application to fire simulations are limited [75]. LES technique, on the other hand, is a viable alternative to the computation heavy DNS methods and could be applied to model the turbulence in fire applications. In a LES model, the larger eddies which account for most of the mixing process are calculated on the numerical grid while the smaller scaled eddies are modelled using subgrid closure models. Therefore, the equations for LES are derived by applying a filter, parameterized by a width Δ , to the mass, momentum and energy equations and solved for the large eddies. For instance, the filtered density for a cell of width Δ in one dimension is as equation (4.6) below.

$$\bar{\rho}(x,t) = \frac{1}{\Delta} \int_{x-\Delta/2}^{x+\Delta/2} \rho(r,t) dr \quad (4.6)$$

In default mode, FDS uses the Smagorinsky subgrid closure model to account for the thermophysical and transport parameters, such as viscosity in equation (4.5), thermal conductivity and diffusivity, in modelling of the smaller eddies, as follows:

$$\mu_{LES} = \rho (C_s \Delta)^2 (2\overline{\mathbf{S}}_{ij} \overline{\mathbf{S}}_{ij} - \frac{2}{3} (\nabla \cdot \overline{\mathbf{u}})^2)^{1/2} \quad (4.7)$$

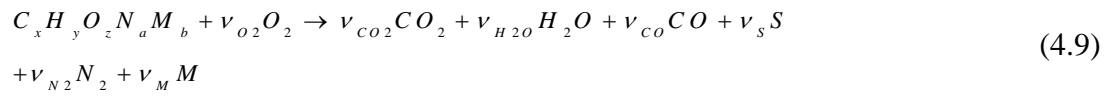
$$k_{LES} = \frac{\mu_{LES} C_p}{Pr_t}; (\rho D)_{i,LES} = \frac{\mu_{LES}}{Sc_t} \quad (4.8)$$

in which C_s is an empirical constant set to a default value in FDS to provide numerical stability, Δ is the length on the order of the grid size and turbulent Prandtl and Schmidt number are constants defined in the FDS for a fire modeling scenario. The equations give the subgrid values for dissipative terms as a function of the computed resolved quantities (denoted with bars above the quantities, i.e. the strain terms) to be used in closure of the momentum transport equation. All spatial derivatives in the governing equations are approximated by second-order finite differences and the flow variables are marched in time by utilization of “explicit second-order predictor-corrector scheme” which is a well-known method in the CFD and numerical research community. Details of this updating method along with the details of decomposition of governing equations in the numerical model can be found elsewhere [74,76].

4.1.2 The combustion model

Two types of combustion models can be applied in FDS. In default mode, FDS uses mixture fraction model, which will be discussed in this section, and a more detailed-model which accounts for individual gas species reaction according to specified Arrhenius reaction parameters only available in a DNS simulation. In combustion applications, “the mixture fraction is a conserved quantity traditionally defined as the (mass) fraction of the gas mixture that originates in the fuel stream” and is a function of space and time, denoted by $Z(\mathbf{x}, t)$ [74]. The rate of the infinitely fast reactions of species in a given grid cell are determined by a characteristic mixing time. If the reaction between fuel and oxidizer can be assumed fast and complete, then the

combustion can be called “mixing controlled”. This would imply that species fractions included in the reaction can be represented by the mixture fraction and, in a simple form, can be calculated through utilizing a single transport equation for the mixture fraction. In order to reduce computational time on solving species transport equations, FDS limits the number of species. This simplified approach usually involves six gas species of fuel, O₂, CO₂, H₂O, CO and N₂ plus particulate matter. Considering the single-step reaction of fuel and oxidizer as equation (4.9) below;



in which S is the soot which is assumed a mixture of carbon and hydrogen, M is the additional product species lumped into a single term, ν_S and ν_{CO} are the stoichiometric coefficients of soot and CO calculated based on default values given in the FDS model for the soot and CO yield. The mixture fraction can then be defined as equation (4.10);

$$Z = Y_{fu} + \frac{M W_{fu}}{x M W_{CO_2}} Y_{CO_2} + \frac{M W_{fu}}{x M W_{CO}} Y_{CO} + \frac{M W_{fu}}{x M W_S} Y_S \quad (4.10)$$

which satisfies the conservation equation;

$$\rho \frac{DZ}{Dt} = \nabla \cdot \rho D \nabla Z \quad (4.11)$$

The mixture fraction (Z) is then decomposed in two partitions as below such that the sum would be equal to (Z). In this model, the fuel is a single gas species, and air and products are assumed as lumped species having a single set of transport properties (Z₂).

$$Z_1 = Y_{fu}$$

$$Z_2 = \frac{M W_{fu}}{x M W_{CO_2}} Y_{CO_2} + \frac{M W_{fu}}{x M W_{CO}} Y_{CO} + \frac{M W_{fu}}{x M W_S} Y_S \quad (4.12)$$

Transport equations are then solved for Z components separately and as the ultimate result, the mass fraction of species present in the combustion are then recovered as a function of these components (i.e. $Y_i(Z_1, Z_2)$) by matrix manipulation after each time-step [74]. The HRR of fire is calculated based on rate of the fuel consumption in each grid cell obtained directly from the solution of the mixture fraction (Z) and the heat of combustion of the fuel. Also, in a more simplified method, the HRR of the fire known from experimental measurements or estimated through empirical formula is directly input to the code. The transport equation for each of the lumped species Z_1 and Z_2 has the same form as equation (4.13).

$$\frac{\partial}{\partial t}(\rho Z_\alpha) + \nabla \cdot (\rho Z_\alpha \alpha \mathbf{u}) = \nabla \cdot (\rho D_\alpha \nabla Z_\alpha) + m''' + m'''_{b,\alpha} \quad (4.13)$$

in which Z_α is the species mass fraction, $m'''_{b,\alpha}$ is the production rate of species by evaporating droplets or particles. The diffusion coefficients (D_α) of implicit species are chosen so that the sum of diffusive fluxes ($\sum \rho D_\alpha \nabla Z_\alpha$) is zero. The code advances the flow velocity in time by estimating the thermodynamic variables at the next time step, computing the divergence term, and then by solving an equation for the pressure ensures the divergence of the updated velocity is identical to that computed from the thermodynamic variables.

4.1.2 Radiative transport equation

The radiative transport equation for a non-scattering medium is defined in FDS as in equation (4.14) [74].

$$\mathbf{s} \cdot \nabla I_{\lambda}(\mathbf{x}, \mathbf{s}) = \kappa(\mathbf{x}, \lambda) [I_b(\mathbf{x}) - I_{\lambda}(\mathbf{x}, \mathbf{s})] \quad (4.14)$$

in which $I_b(\mathbf{x})$ is the source term due to Planck equation as a fraction of the blackbody radiation, $I_{\lambda}(\mathbf{x}, \mathbf{s})$ is the radiation intensity at wavelength λ for which \mathbf{s} is the direction vector and $\kappa(\mathbf{x}, \lambda)$ is the local absorption coefficient. Since in practice the spectral (λ) dependence cannot be solved accurately, the radiation spectrum in FDS solutions is divided into a relatively small number of bands and a separate radiative transport equation is derived for each band. Also, due to soot being the most important source of thermal radiation in fire, and the fact that radiation spectrum of soot is continuous, the gray medium assumption can stand. The spectral dependence can then be lumped into one absorption coefficient and the source term $I_b(\mathbf{x})$ will be calculated by equation (4.15).

$$I_b(\mathbf{x}) = \sigma T(\mathbf{x})^4 / \pi \quad (4.15)$$

In a FDS simulation, the absorption coefficient is calculated based on tabulated data as a function of mixture fraction and temperature. In calculations where mesh cells are in order of a centimeters or larger, the temperature near the flame surface cannot be approximated, so the source term is modeled as a specified fraction of the energy generated (X_{rad}) which is assumed to be emitted as thermal radiation. This value is estimated in the model according to the data in the literature. In the outside the flame region, there is more confidence in the temperature field, the source term can be computed according to equation (4.15).

4.1.2 Numerical grid

The FDS calculations are performed within a rectilinear mesh domain. This is a limitation posed by the FDS code which requires the input mesh to be structured.

However, it is possible to run a simulation based on multiple meshes in FDS with different grid sizes each assigned to a separate CPU. In this work, the computational grid was constructed according to the geometry of the tunnel model. The domain accounted for 6 m of the length of the tunnel, including upstream, combustion zone and a part of downstream section, as modeling the rest of the downstream was not relevant to required results and also helped save computational time. The roof of the constructed tunnel is arch type which was simulated in the numerical model using solid blocks. The mesh was consisted of three resolutions considering the computational intensity of simulations. The mesh size was calculated based on characteristic diameter of fire using equation (4.16).

$$D^* = \left(\frac{\dot{Q}}{\rho_{\infty} c_p T_{\infty} g^{1/2}} \right)^{2/5} \quad (4.16)$$

A value of D^* divided by cell size ranging from 4 to 16 was suggested in the FDS guides to be adequate for the LES solver as well as fine enough to capture fire dynamics [74]. In order to test the mesh sensitivity of the model, two types of mesh resolutions with cell sizes within the limits of $4 < D^* / dx < 16$ were generated which differentiated in the grid sizes for the combustion section. The average grid sizes for both meshes were approximately 4 cm in x, y and z directions in the downstream section and 2 cm in the upstream. The cell size for the combustion zone section in “mesh 1” was 1 cm while the same value for “mesh 2” was a refined 0.5 in spatial directions. Therefore the total number of cells for mesh 1 was 285,120 and 2,049,000 for mesh 2. Figure 4.1 compares the HRR values obtained by experiments and simulation results using mesh 1 and mesh 2 for a sample test case from experiments at 0.1 and 0.2 cm ethanol pool depth at different ventilation velocities.

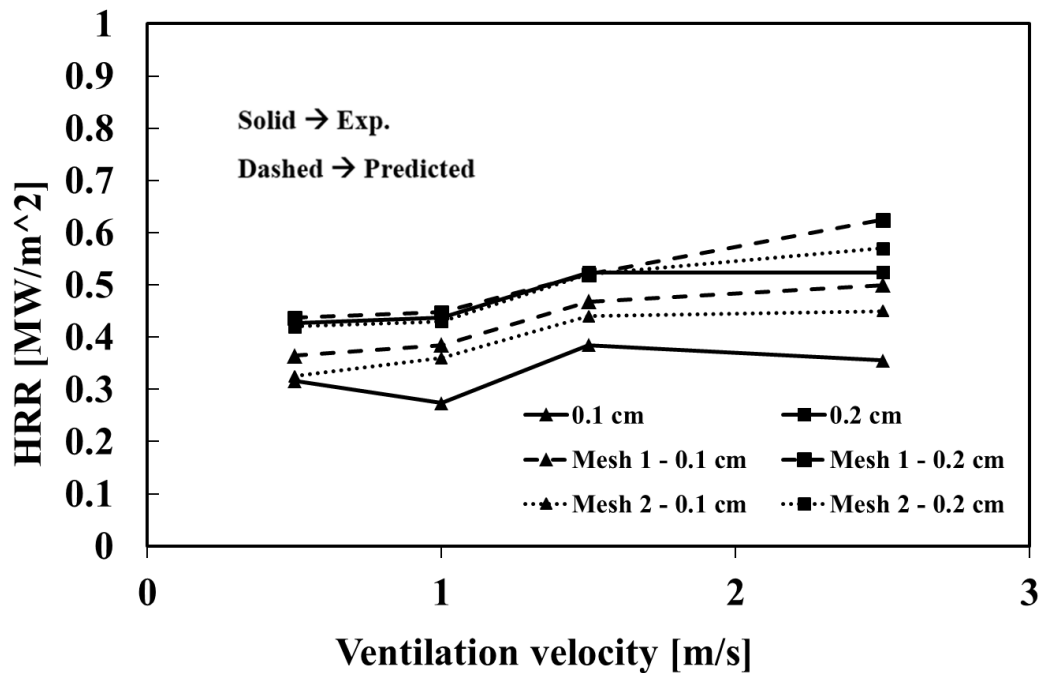


Figure 4.1. HRR comparison between experiments and numerical simulations using different mesh sizes

Given the fact that the results of simulations did not show considerable variation, but a slight decrease in over prediction of HRR from FDS, it was decided to use mesh 1 in the simulations which resulted in the immensely improved run times, while still taking 20-25 hours to complete in an Intel-core-i5 personal computer with sufficient memory. Figure 4.2 shows the grid based on mesh 1 and assigned thermocouple locations. There are some general limitations to the FDS code as following: (1) It is only valid for low speed flow with an emphasis on smoke and heat transport from fires which means that it cannot be applied to model detonations and jet fires (2) The mesh should be structured and rectilinear. Unstructured mesh cannot be used which limits the geometry definition of model (3) The uncertainty of the model is higher when the HRR is predicted rather than specified as an input to the code, this was also observed in the predicted results presented in this study (4) The mixture fraction combustion model assumes that combustion is mixing controlled, and that the reaction of fuel and oxygen is infinitely fast which limits model predictions in under ventilated

compartment fires and (5) The model is less reliable when modelling small pool fires as opposed to large ones which limited the applicability of the model in heat release rate predictions of 10 and 15 cm pool fires in this study as is reported in later chapters.

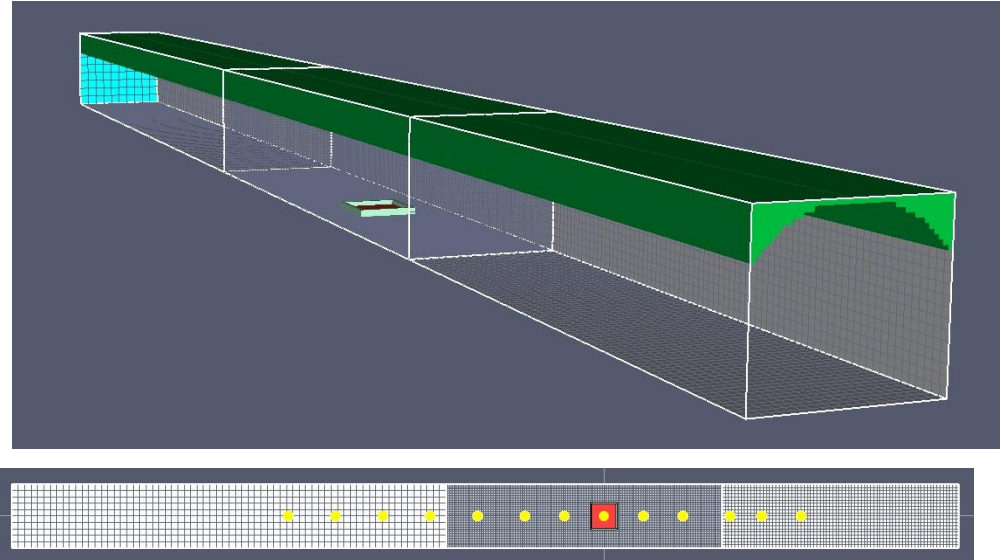


Figure 4.2. The numerical grid and thermocouple locations

CHAPTER V

RESULTS AND DISCUSSION

In this chapter, the results of pool fire experiments on the reduced scale tunnel model are presented and analyzed in separate parts for the case studies explained in section 2.6. Each section is categorized into subsections in which an important control parameter is discussed and analyzed.

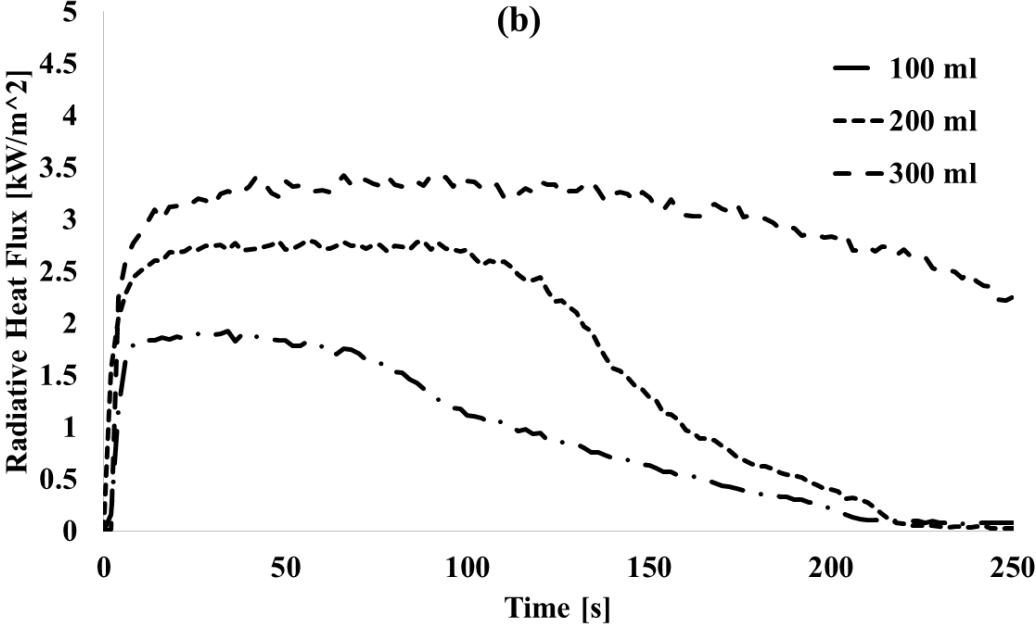
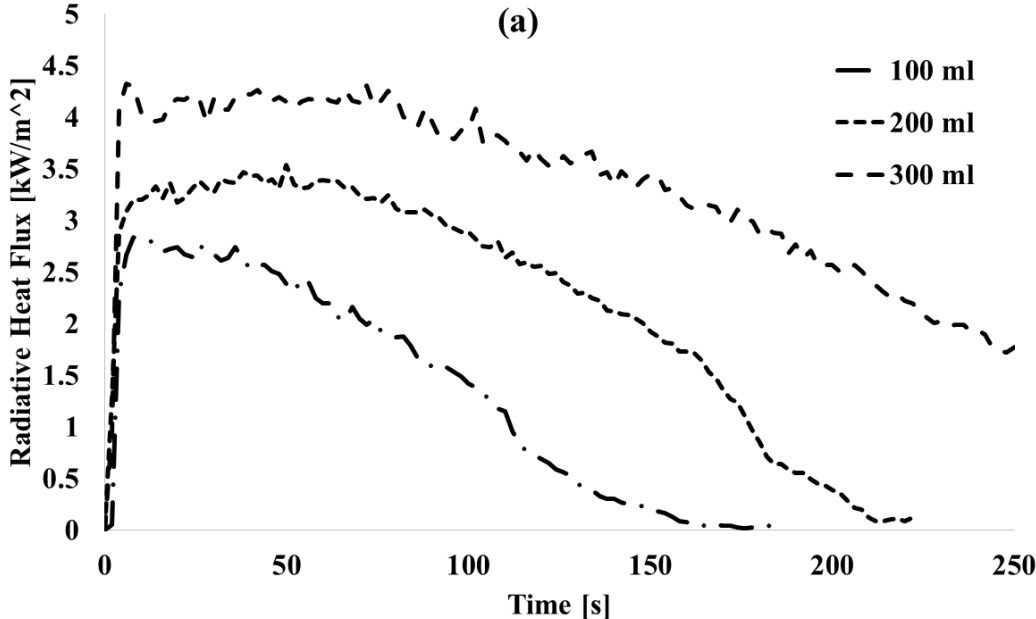
5.1 Effects of tunnel wall coating

In section 5.1.1, the effect of pool depth on the radiative heat flux and burning characteristics of the 31 cm ethanol pool fires are presented at different ventilation velocities using reflective tunnel wall coating. In section 5.1.2, the pool depth was maintained constant at 0.2 cm (average among considered cases) and effect of tunnel wall coating on upstream thermal radiation, HRR and temperature distributions were investigated. The experimental conditions as well as design criteria were discussed in section 3.3.1 but details are repeated within this section for ease of access.

5.1.1 Effect of pool depth and ventilation velocity

Figures 5.1 and 5.2 show measured incident radiation as a function of pool depth and ventilation velocity. The radiometer was horizontally oriented as described in figure 3.10 and the sensor was flush with the fuel pan lip. It was seen that increasing the ventilation velocity to the tunnel resulted in decreasing of the incident radiation due to more fire spread at tilted angles. This trend was more pronounced in case of 300 ml pool fire where prolonged quasi-steady burning phase of fuel was associated with

longer combustion duration. The heat flux trend was proportional to pool depth in the sense that, as the pool depth was increased, the combustion was steadier which was reflected in the radiation curves of 200 ml and 300 ml pools. At ventilation velocities above 1 m/s, the effect of pool depth became less dominant which was signified by peak values occurring in range of 2.5-3 kW/m² for 1.5 m/s and 2.5 m/s cases.



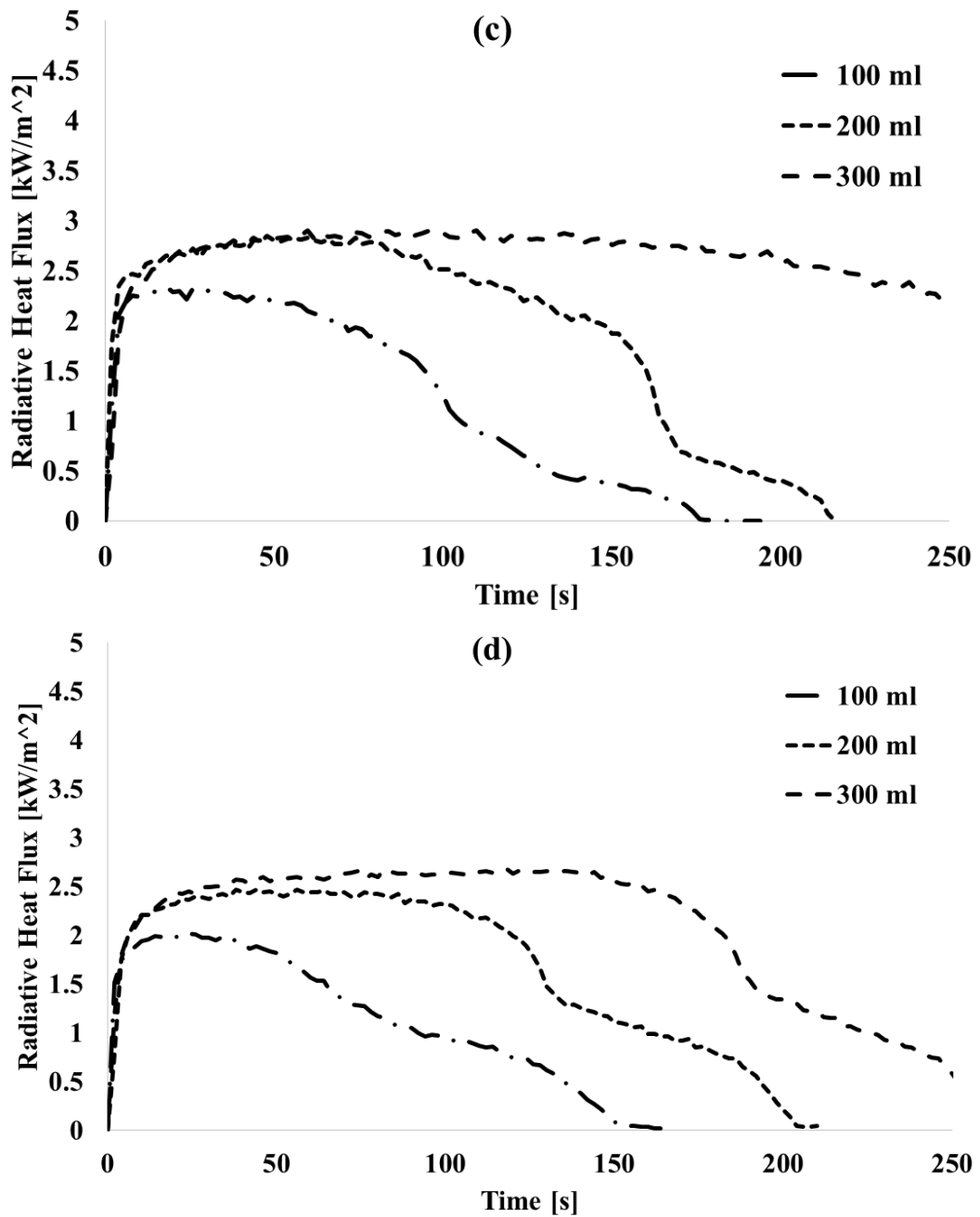


Figure 5.1. Effect of pool depth on incident radiation upstream of fire for (a) 0.5 m/s (b) 1 m/s (c) 1.5 m/s (d) 2.5 m/s ventilation velocity

Flame tilting also approached a steady value at this point, as seen in figure 5.3 where images of ethanol flame in 10 cm leading edge (in flow direction) of pool fire are given at 30 s after pool ignition.

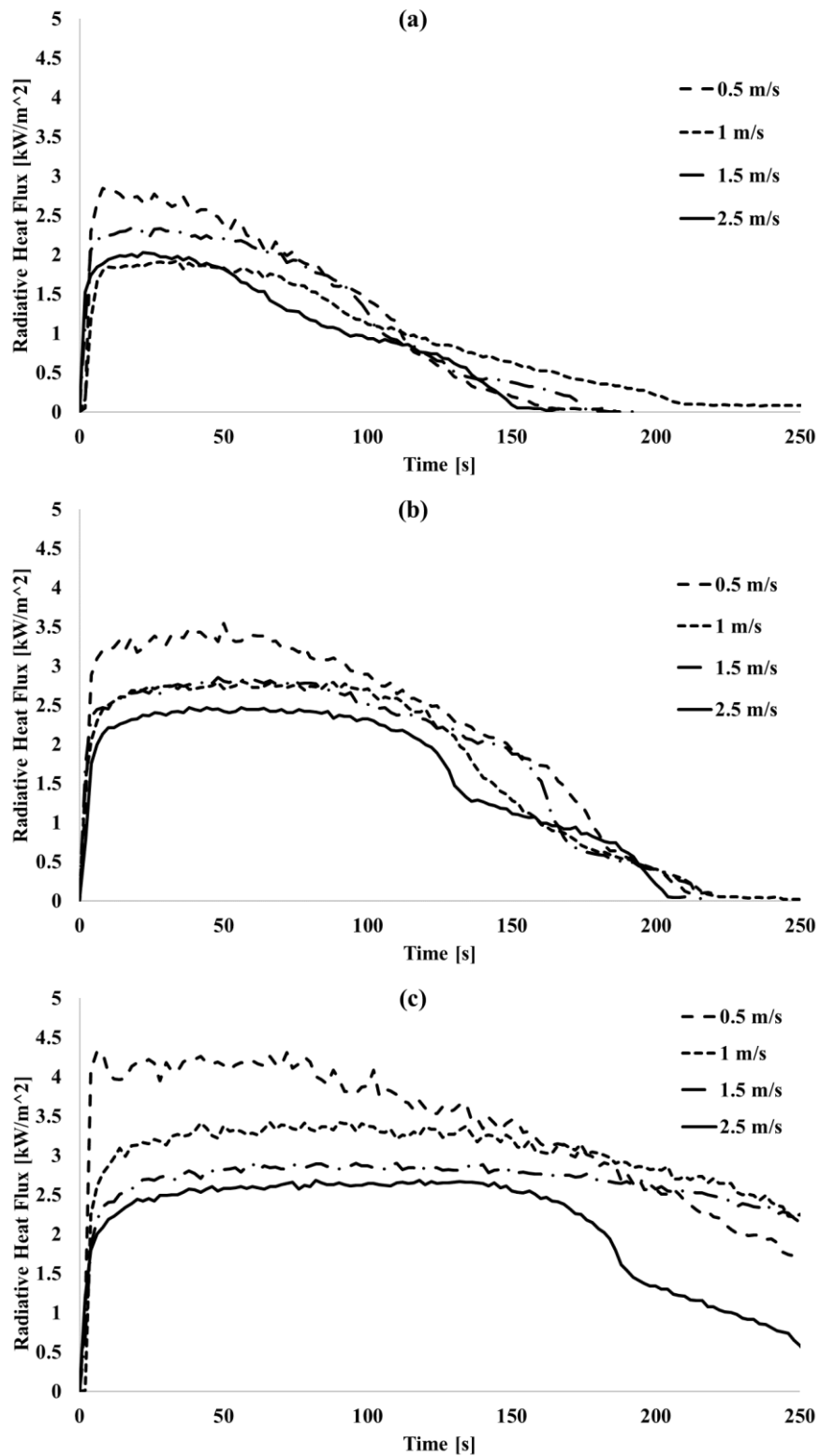


Figure 5.2. Effect of ventilation velocity on incident radiation upstream of fire for (a) 100 ml (b) 200 ml (c) 300 ml fuel

The camera used in the experiments captured 300 frames per second and the images were selected randomly at during the quasi-steady state burning phase for all test cases. The main conclusion was that as the ventilation velocity was increased, the fire tilt angle increased as well as flame height decreased. This was also reflected in the results presented in figure 5.2. The HRR flux (HRR per unit area of the pool) and burning rates of pool fire are given as a function of ventilation velocity and pool depth in figure 5.4. Error bars are given for the measured values in terms of standard error calculated based on repeated experiments. Assuming the pool fires heat transfer being more dominated by the convection regime, under forced ventilation conditions of this study, it can be shown that the burning rate is directly proportional to the Spalding transfer number and the airflow velocity as shown by equation (5.1) which is given by Glassman [77] as an exact solution to the forced convective burning of liquid fuel saturated over a flat plate.

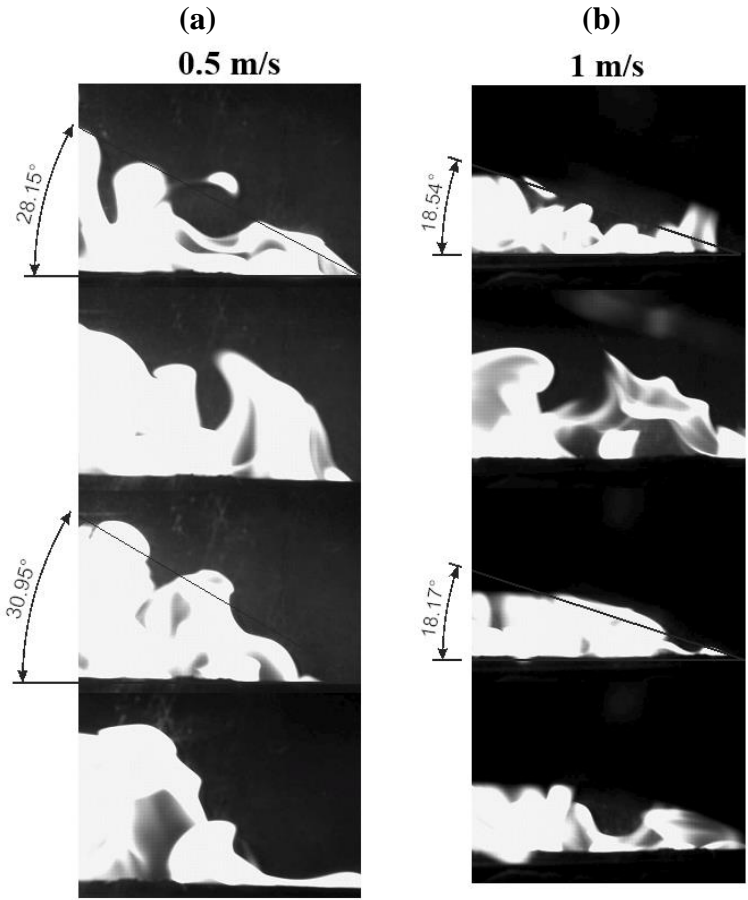
$$\dot{m}''' \propto \frac{C U_{\infty}^{1/2}}{x^{1/2}} \text{Pr} \frac{\ln(1+B)}{B^{0.15}} \quad (5.1)$$

in which C is a constant and the Spalding number can be given as [78];

$$B = \frac{H_c}{H_v} \frac{m_{O_2g}}{r} + c \frac{T_g - T_s}{H_v}$$

The Spalding number contains both environmental and fuel property factors. According to the burning rate results, there seems to always be a competition between the enhancing effect of increased ventilation on the burning rate promoting factors of oxygen availability and mass transfer coefficient and the cooling effect of ventilation. This shows itself in as an overall result of decrease in burning rate for pool fire in 1 m/s due to cooling effect dominating the pool fire combustion. Increase of ventilation velocity from 1 m/s to 1.5 m/s enhances the burning rate by increasing the mass transfer coefficient and oxygen availability (thus increasing the HRR). This description also justifies the burning rate behavior results in other section of the results as well. The results indicate that the pool depth has a considerable increasing effect on

the heat load as well as the burning rates. The maximum heat release rate tends to occur at 1.5 m/s ventilation velocity except for 300 ml case which peaks at 2.5 m/s. The numerical model's limitations regarding liquid fuel combustion resulted in a discrepancy of predicted burning rates compared to measurements, which was seen in this figure. The model predicted a constant increasing trend for the burning rates and HRR with increasing pool depth and ventilation velocity. HRR predictions agreed better with experimental measurements for 200 ml and 300 ml ethanol test cases. It could be said that the model over-predicted the burning rates due to thin pool depth which was identified as a shortcoming of the FDS model. The best results were obtained for 200 ml and 300 ml pool fire cases and low ventilation velocities. It could be said that the 100 ml pool cases were classified as very thin-layered spill fires, which showed a distinctive trend to increased ventilation.



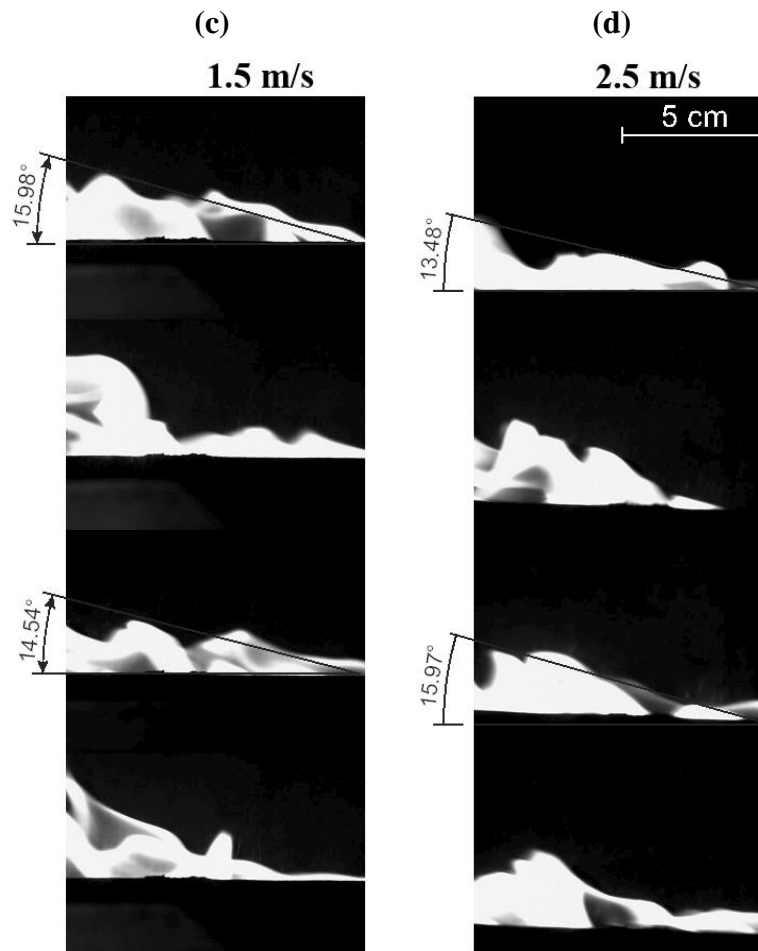
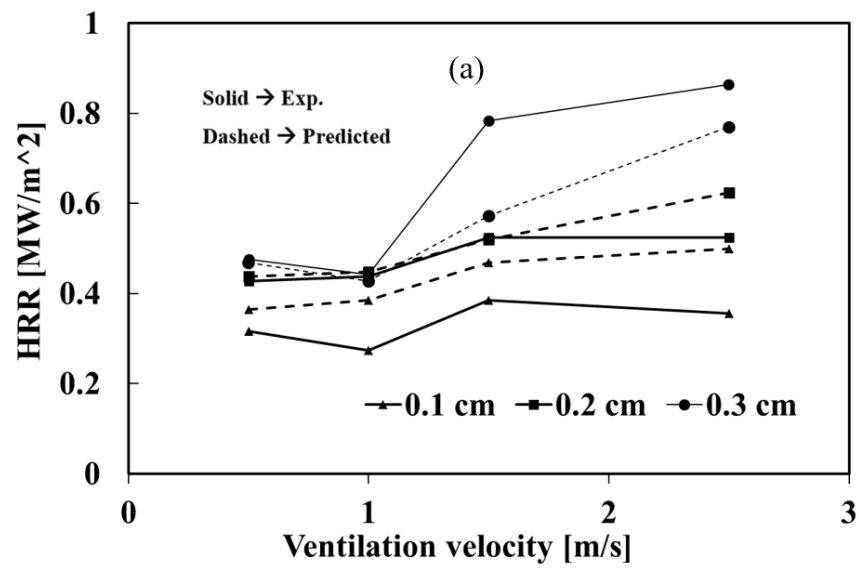


Figure 5.3. Ethanol flames at 10 cm leading edge of pool fire 30 s after ignition



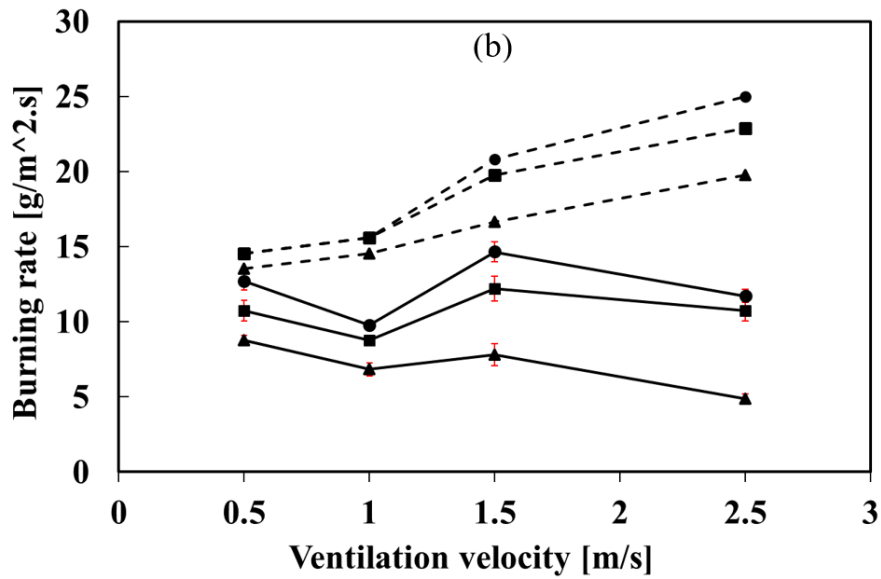
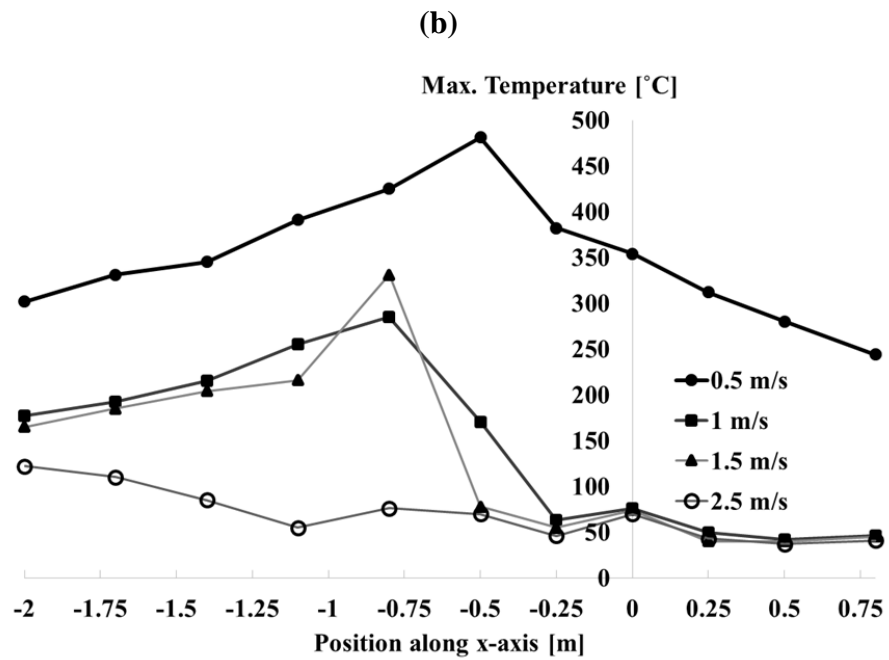
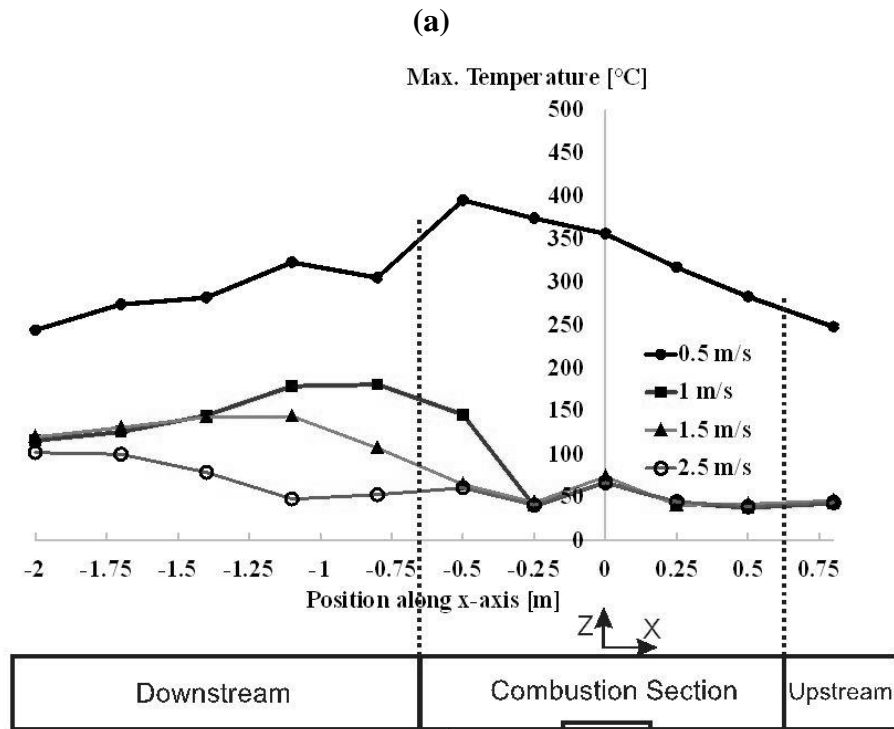


Figure 5.4. Variation of (a) HRR flux and (b) burning rate of ethanol pool fires as a function of pool depth and ventilation velocity – Experiments versus FDS predictions

Tunnel ceiling temperature distribution along the horizontal axis was recorded during the experiments and the results are presented in figure 5.5 as a function of pool depth and ventilation conditions. Results indicated existence of a back layering flow at 0.5 m/s case in which ceiling temperatures as high as 250-350°C were reached in upstream and combustion sections. The backlayering length extended to at least 0.8 m upstream of combustion in this case. At 1 m/s, the critical ventilation velocity was achieved for all cases as indicated by considerable gas temperature drop along the tunnel. Increasing the ventilation velocity to 2.5 m/s resulted in increased fire tilt angle and retarded smoke plume rising to the tunnel ceiling further downstream of fire. At 1 m/s and above, the maximum temperatures tend to occur further downstream of the pool fire due to stretching of the flame. The model predictions for maximum ceiling temperature for limiting cases of ventilation (0.5 m/s and 2.5 m/s) also showed a good agreement in trend and magnitude as seen in in the figure.



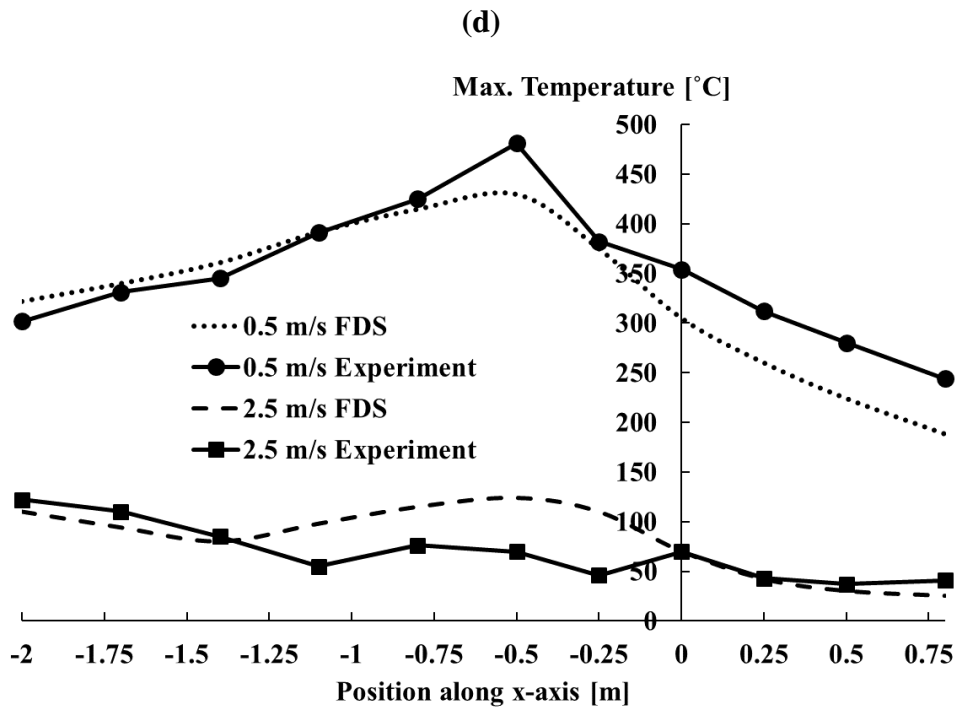
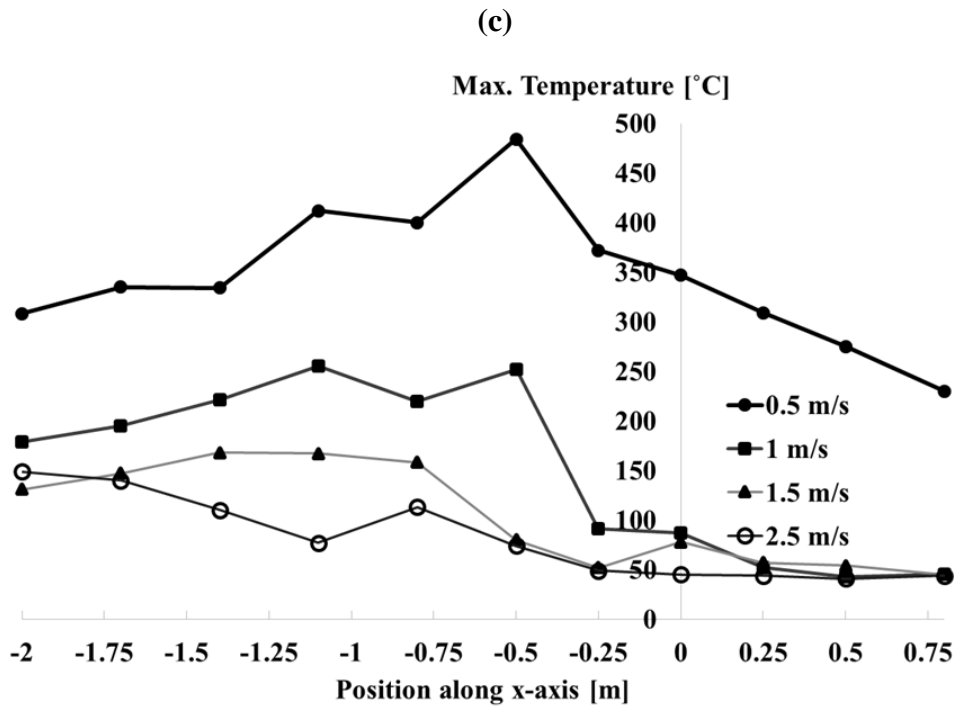


Figure 5.5. Maximum ceiling temperature along the tunnel axis for (a) 0.1 cm (b) 0.2 cm and (c) 0.3 cm pool depth (d) FDS simulations vs. experiment (0.2 cm pool depth case)

5.1.2 Effect of tunnel wall coating material

Figure 5.6 shows the effect of wall coating type on the radiative heat flux in the upstream of the pool fire. The radiometer was vertically oriented in order to achieve an enhanced view factor between the walls and radiometer. Using the highly emissive black-painted anodized wall coating resulted a considerable decrease in the incident radiative flux which was more pronounced in the quiescent case (no ventilation) where a 45 % drop could be measured. At increased ventilation velocities, the gap was reduced due to increased fire spread to downstream. The amount of thermal radiation exposure from tunnel fire is an important safety factor that needs to be considered.

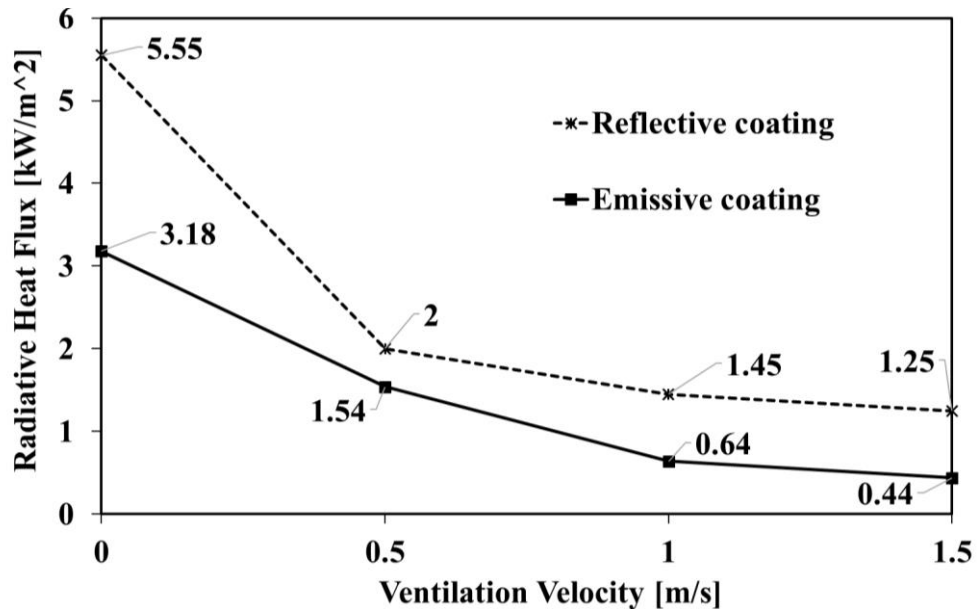


Figure 5.6. Effect of wall coating type on the radiative heat flux upstream of the pool

Effect of wall coating type on maximum temperature distribution along the tunnel is shown on figure 5.7. Results indicated a general increasing trend in the ceiling temperature across different ventilation velocities for the case of emissive coating material, especially in the combustion section. It was also seen that coating type had

no apparent effect on the critical ventilation velocity as both cases reached the critical ventilation at 1 m/s.

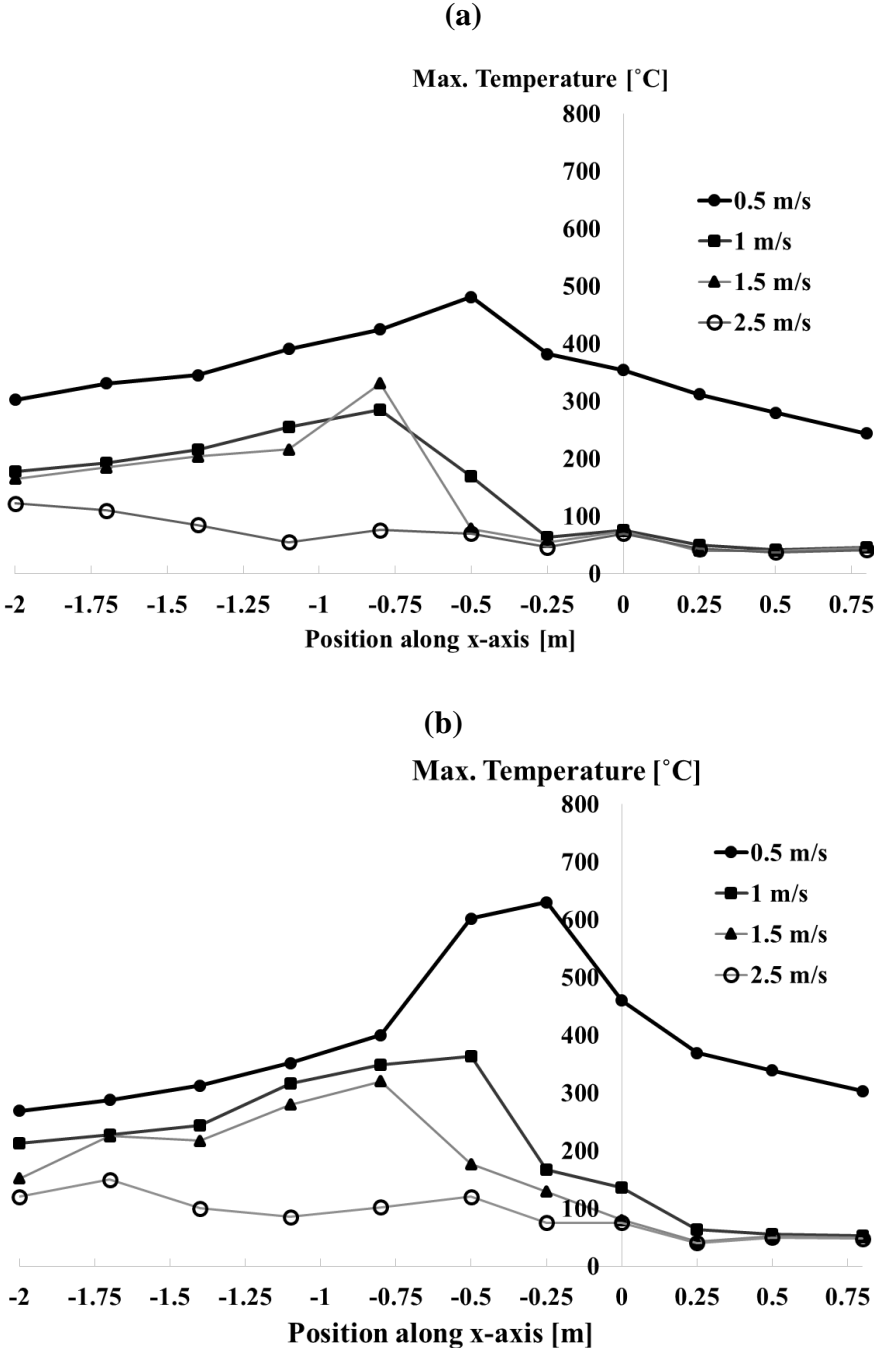


Figure 5.7. Effect of wall coating type on maximum ceiling temperature along the tunnel axis for (a) reflective coating and (b) emissive coating material

Figure 5.8 compares the total heat release from the pool fire normalized by unit volume of the fuel (200 ml) which was abbreviated as Normalized Total Heat Released (NTHR). The NTHR was calculated the time integral of HRR over period of combustion. It could be seen that while using the emissive wall coating material, there was a slight increase of heat release especially at 2.5 m/s ventilation velocity which could be attributed to increased gas temperature inside the combustion section as discussed in figure 5.6.

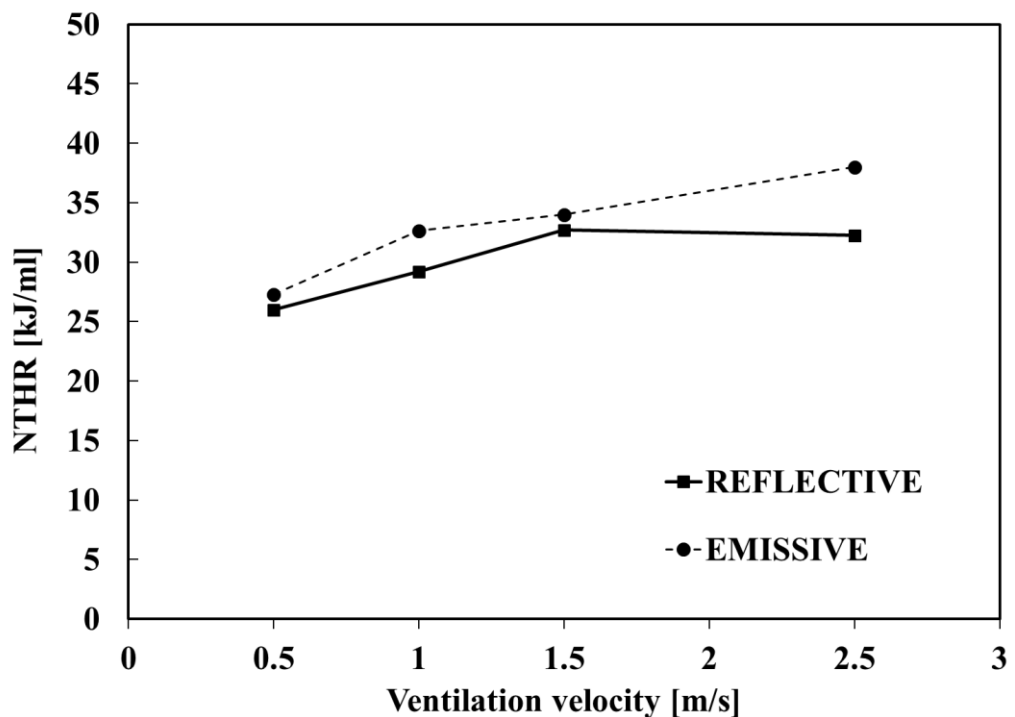


Figure 5.8. Effect of wall coating type on NTHR (0.2 cm pool depth)

5.2 Adjacent pool fires

This part of experiments aimed to contribute to the knowledge of hydrocarbon pool fires in confined conditions under effect of adjacent fire sources. As discussed before, the topic was of special interest since there are very few reports in the literature

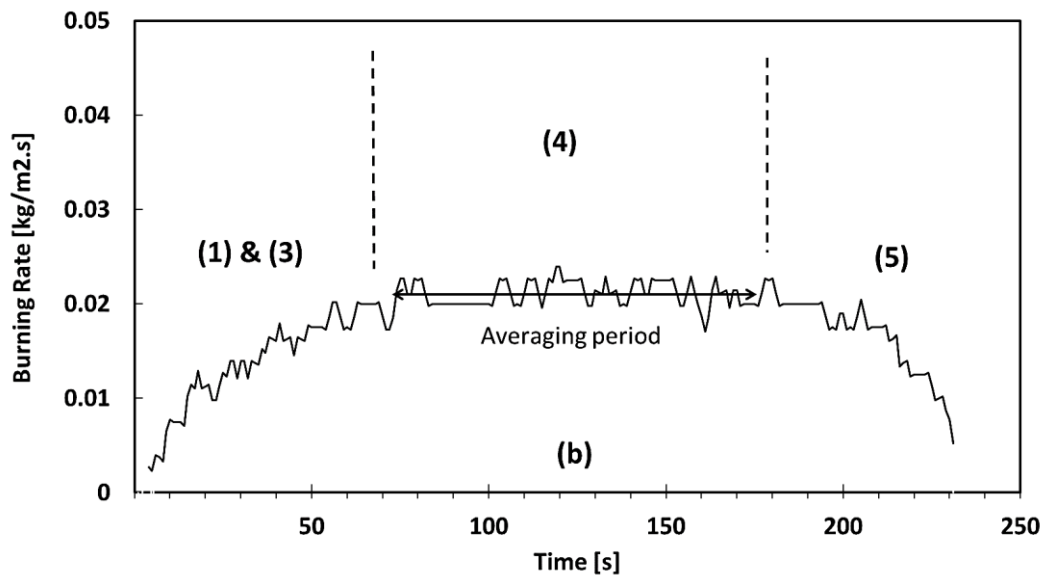
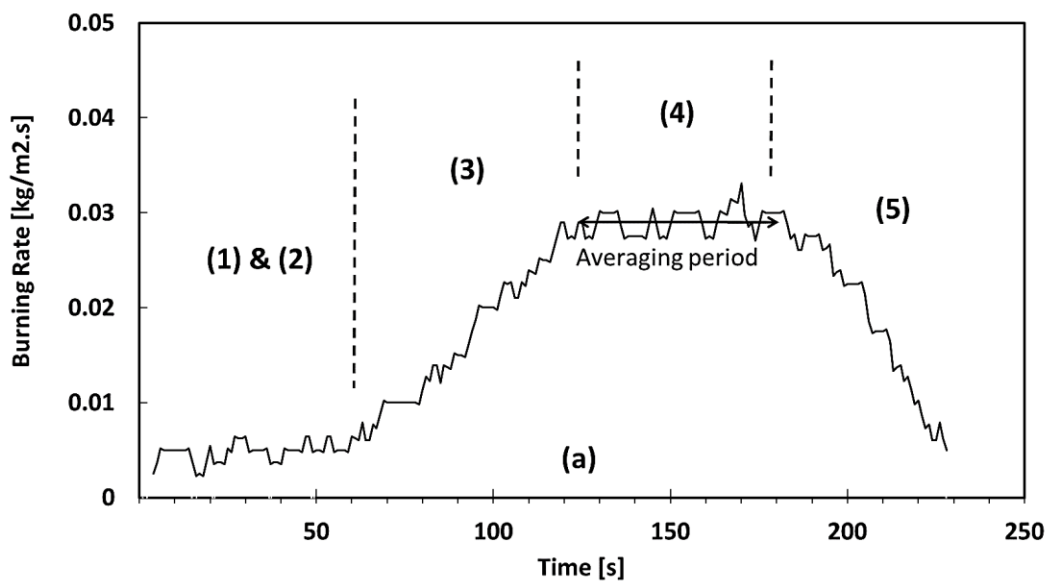
investigating such a scenario inside confined spaces as well as it covered the potential safety issues associated with occurrence of secondary fires in tunnel fire accidents. The results of current experiments conducted with varying pool size, depth and airflow velocities were used to address these issues. The design criteria as well as experiment specifications were given in section 3.3.2. The burning rate of pool fires is considered as one of the most prominent parameters in considering pertinent fire hazards [79]. Interaction between multiple fire sources may result in fire merging and significant alterations of burning rate behavior and flame heat feedback to fuel surface as also shown in work by Wang et. al [52].

5.2.1 Burning rate behavior

There are five distinct stages in development of batch pool fires [51,68,79] that occur in this order: (1) initial fire growth (2) quasi-steady burning with surface boiling (3) transition phase (4) bulk boiling where bubbles form in the bulk of fuel with increased flame height and (5) decay to extinction. Studies show that under specific conditions, duration of some of these phases might increase or decrease depending on factors such as pool size, pool depth and fuel temperature. In some cases a fire merging stage is also shown to exist [52]. In this section, the burning rate characteristics of confined ethanol pool fire was investigated as a function of pool depth, pool size and interactions of dual pool fires. Based on the observations and magnitude-wise, the burning rate curves could be categorized in four types.

Figure 5.9 shows the temporal evolution of burning rates for single and dual pool fires. The numbers in parenthesis indicate burning rate stage. Different staging phases of burning rates can be clearly identified in these results. In case of dual pool fires, the interaction between pool fires led to occurrence of fire merging which was associated to stage 4 on the burning rate curves. The quasi-steady state phase in figure 5.9 (a) did not occur in most of the test cases which will be discussed. According to the results and observations, the flame was attached to the windward tray rim and tilted stream-wise over the pool surface in initial growth and quasi-steady state stages. In following

phases, due to fuel boiling and dual fire interactions, the burning rate was enhanced and flame height increases substantially. Fuel boiling was also more pronounced in 10 cm pools compared to 15 cm pools. At this stage, flame is detached from leeward rim and extended outward downstream. Increased intermittency of the flame was observed in this phase, in case of dual pool fires, due to competing effect of air entrainment resulting in flames leaning inward and enhanced burning rates.



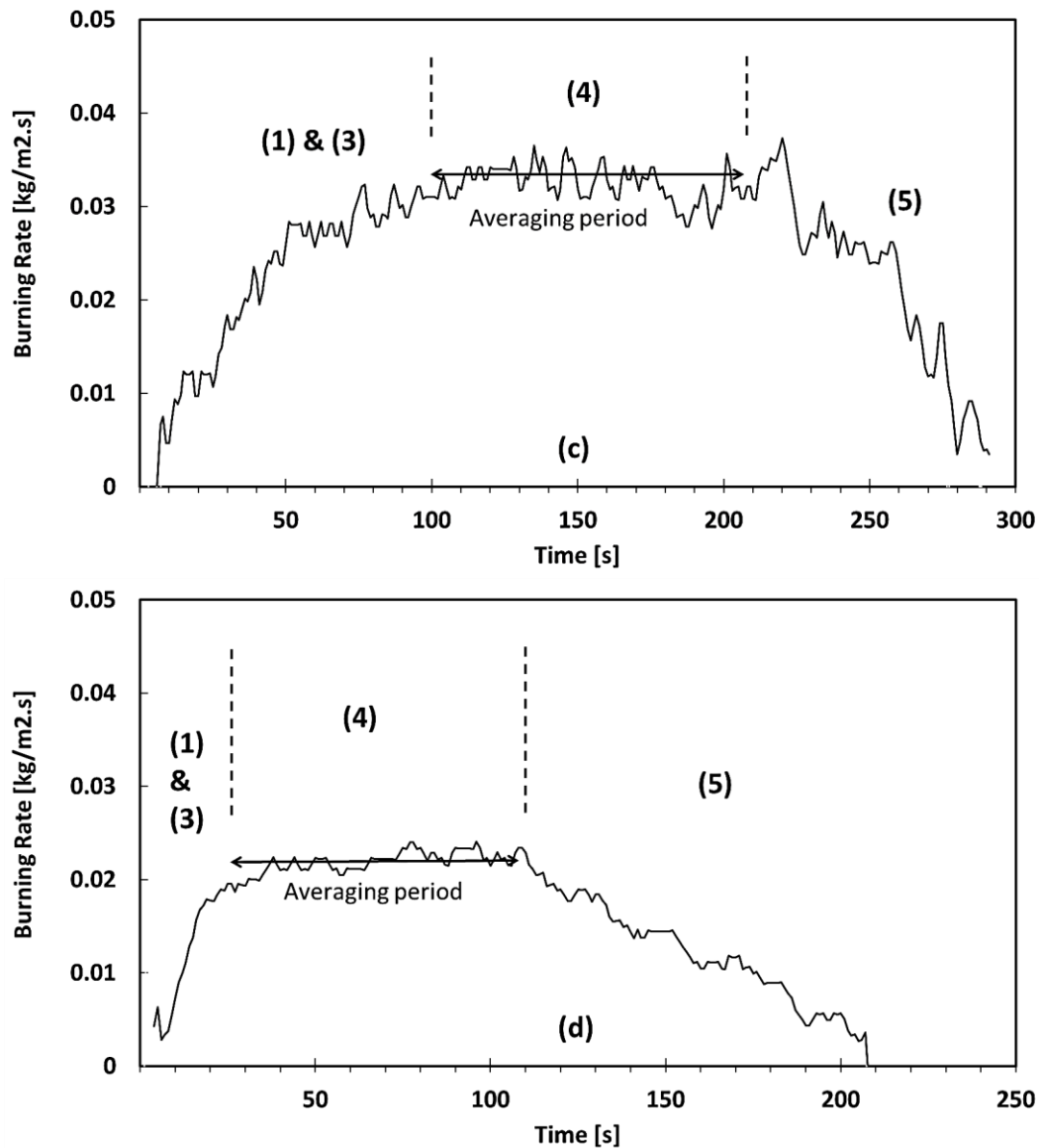


Figure 5.9. Observed temporal evolution of burning rates under tested conditions **(a)** single 10 cm pool, 1.5 m/s airflow, 40 g fuel **(b)** dual 10 cm pools, 0.5 m/s airflow, 40 g fuel **(c)** dual 10 cm pools, 1.5 m/s, 80 g fuel **(d)** dual 15 cm pools, 0.5 m/s airflow, 80 g fuel

To be on the safe side, tests were not conducted at airflow speeds above 1.5 m/s where flame interactions could cause ineligible fluctuations in load cell measurements. The burning rate then decreased in stage five, as the fuel was exhausted in the tray and freeboard height is passed a threshold. Overall, increased airflow velocity, pool size

and pool count, enhances the burning rate and shortened onset of transition to stage 4 as seen in figure 5.9 (c) and (d). The single 10 cm pool fires exhibit 5 stage burning behavior with two distinct peaks across tested airflow velocities, with the ratio being as high as 6.4 in case of single 10 cm pool with 40 g fuel and 1.5 m/s. However, the quasi-steady state phase did not occur in dual 10 cm pools nor in single or dual 15 cm pools. Figure 5.9 (c) typifies the burning rate curves with a single peak magnitude of 0.03 kg/m²s or higher, where intense burning and bulk boiling of the fuel occurred. Figure 5.9 (d) typifies the 15 cm pool fires in which the onset of transition to stage (4) occurred earlier compared to 10 cm pool fires which shows itself in the burn duration results to be discussed in later sections. In order to better explain different heat transfer phenomena and associated effects on the burning rates, conservation of energy for evaporating fuel could be established similar to other work elsewhere [68,80,81];

$$\dot{Q}_{fu} = \frac{dm_{fu}}{dt} h_g \quad (5.1)$$

$$h_g = h_v + \int_{T_{fu,i}}^{T_{fu,b}} c_{p,fu} dT \quad (5.2)$$

where \dot{Q}_{fu} is the heat exchange to the bulk of the fuel and h_g is the heat of gasification of fuel which includes the latent heat of evaporation, h_v , and sensible heat of fuel warming up from initial temperature to boiling temperature.

$$\dot{Q}_{fu} = (\dot{Q}_{f-rad} - \dot{Q}_{re-rad}) + \dot{Q}_{f-conv} + \dot{Q}_{cond} - \dot{Q}_{loss} \quad (5.3)$$

$$\dot{Q}_{f-conv} = Ah(T_{gas} - T_{fu,s}) \quad (5.4)$$

$$\dot{Q}_{f-rad} = F\sigma A(T_f^4 - T_{fu,s}^4) \quad (5.5)$$

where \dot{Q}_{loss} is the lumped heat loss from the fuel through conduction and convection, \dot{Q}_{cond} is conductive heat exchange between fuel and tray, T_{gas} is the gas temperature

above the fuel surface. The re-radiation from fuel is usually negligible at conditions similar to present work [64,68]. Constant specific heat may be assumed for the evaporating fuel. The burning rate can then be arranged as below.

$$m'' = \frac{dm_{fu}/dt}{A} = \frac{F\sigma(T_f^4 - T_{fu,s}^4) + h(T_{gas} - T_{fu,s}) + (\dot{Q}_{cond} - \dot{Q}_{loss})/A}{h_g} \quad (5.6)$$

in which m'' is the burning rate. Unlike works by [51,54,68,80] which considered pool fires in quiescent conditions, the effect of convective heat exchange to the fuel could not be neglected in this work. It was suggested that convective heat transfer can have major effect on the total HRR in confined ventilated conditions such as present work [21,64]. Equation (5.6) implied that, assuming a constant heat of gasification for ethanol, the burning rate depends on several influential factors. According to results of [51], the term $(T_{gas} - T_{fu,s})$ could be assumed nearly constant and the $h(T_{gas} - T_{fu,s})$ term is fairly small in quiescent conditions. If the airflow was accounted for, the convective term could then be approximated as a function of the coefficient of convection (h) only. The flame temperature was also almost constant during the quasi-steady burning stage, whereas it increased in later stages. The view factor of the flame would have changed with airflow velocity due to flame stretching as well as effect of pool count. Neglecting heat loss from the bottom of the vessel, major heat exchange between the tray and surroundings could be assumed to take place in the windward side where it was affected by airflow.

It is also said that at small pool sizes similar to ones used in this study, \dot{Q}_{cond} term is the dominant heat transfer regime which initially is from fuel to the tray and then from tray to the fuel in later stages [51,64]. Due to this effect, the rate of change of burning rate was slow in early stages of fire development and accelerated in later stages (see also figure 5.9 (a)). In the early stages of medium and large pool fires however, radiation from the flame to the fuel surface and convective terms in equation (5.6) were the dominant regimes which can be attributed to the 15 cm pool size in this study [79].

It can be concluded that it is very complex to quantify each term in this equation, however, for practical applications, above discussions could be utilized in qualitative analysis of burning rate behavior. Figures 5.10 and 5.11 present burning rate of 10 and 15 cm single pool fires as a function of initial depth and airflow velocity, respectively. Standard error bars calculated based on repeated experiments are given in figure 5.10 (a) as an example indicating the confidence level of experiments. Single 10 and 15 cm pools were denoted as SP 10 and SP 15 and dual 10 and 15 cm pools were denoted as DP 10 and DP 15. The burning rates were the measured time averaged peak values as assigned in figure 5.9.

In case of single 10 cm pools where two peaks were reached, the average of the two plateau values were assigned as the mean burning rate. Separation distance between the pools was 4 cm for both 10 and 15 cm pool cases for given results in figure 5.10 but corresponding values was marked for the case of 8 cm. Several observations could be made based on the results. The burning rates of dual pool fires was increased substantially if compared to corresponding single pool cases which was more pronounced for 10 cm pool cases. The result was a direct effect of pool fire interactions and enhanced convective heat transfer in the confined conditions due to more turbulent flow field. The increased view factor from the flame in equation (5.6) due to secondary fire source was also affecting the burning rates of adjacent pool.

The heat feedback from tunnel walls increased in dual pool cases, all of which enhanced the burning rate. The ratio between the two burn rates (m_{DP}''' / m_{SP}''') ranged between 1.375 - 2.25 for 10 cm pools and 1.06 - 1.73 for 15 cm pools with peak values occurring at quiescent conditions for 10 cm pool and at 0.5 m/s airflow for 15 cm pool fire. Under constant airflow, air entrainment factor was reduced in case of confined dual pool fires. It has been documented that air entrainment can have considerable impact on the burning rate of the pool fire [53]. Therefore, it might be said that a trade-off existed between reduced air entrainment and increased fire interactions and heat feedback to pool surface with overall effect being an enhanced burning rate.

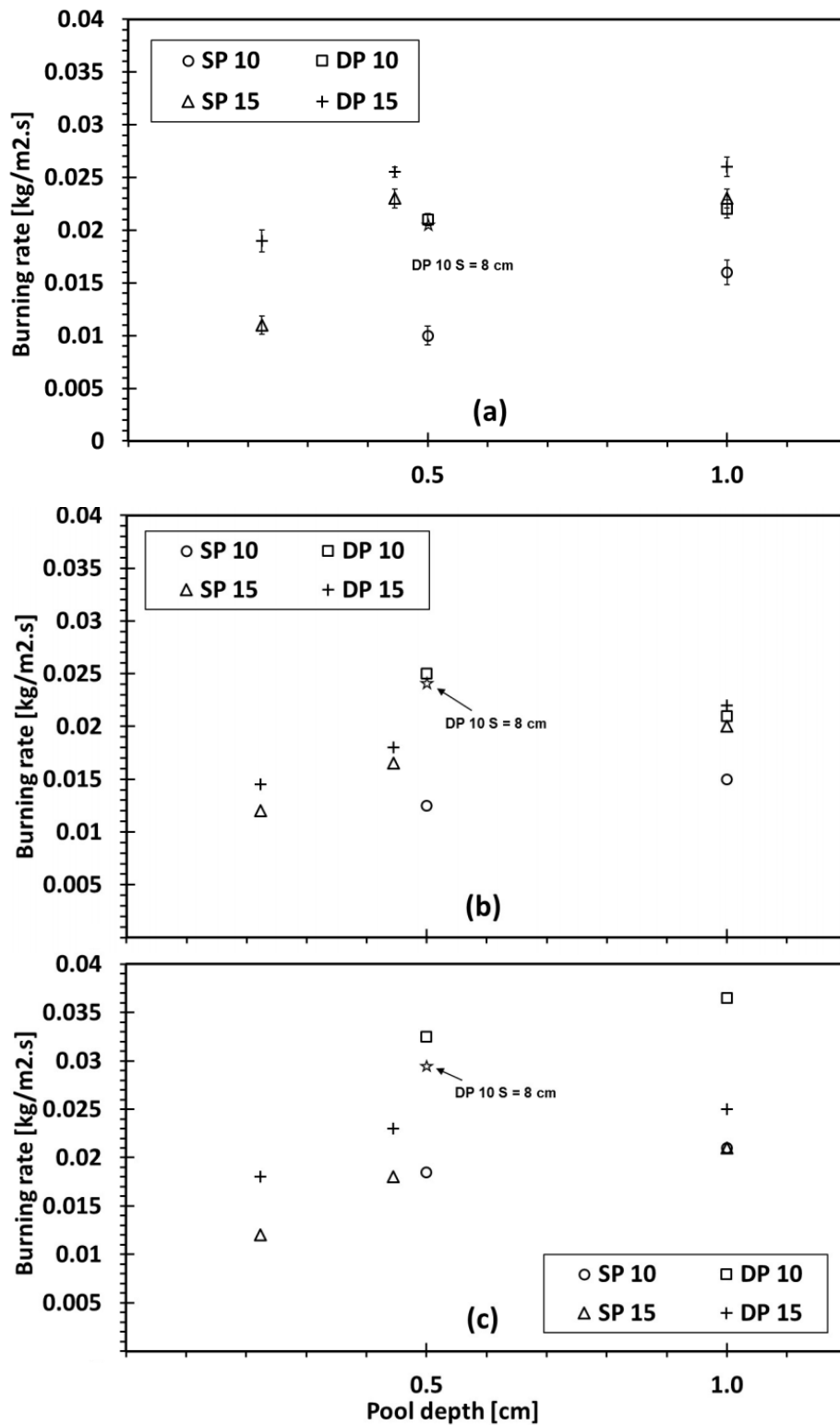


Figure 5.10. Burning rates of single and dual pool fires as a function of pool depth (a) 0.5 m/s (b) 1 m/s (c) 1.5 m/s

The claim was backed up by an observed increase in the burning rates of the single pool fires centrally positioned in the combustion zone compared to results of single pool fires configured as in figure 3.11. The flame length in merged fires was considerably increased at airflow conditions compared to single pool fires across all tested cases. For instance, it was observed that flame was stretched to 4 times size of the pool size in dual 10 cm pool fire case at 1 m/s airflow whereas flames extended 30–40 % shorter in single 10 cm pools at the same airflow conditions. It could be held that there was a monotonous increase in burning rates with increasing pool depth across range of tested airflow velocities. This increase was steeper for 15 cm pool cases and at 0.45 cm depth. The slope is changed moving from 0.45 to 1 cm depth. As for single 10 cm pools, the burning rate at 1.5 cm initial depth was 22 g/m²s (not reported on figure) which was not increased compared to 1 cm depth. It could be said that decreasing initial freeboard height in this range was not as influential as perceived. It was observed that bulk boiling of fuel tends to occur more intensely with increasing pool depth especially at 1 cm, resulting in increased burning rates as seen in figure 5.10. However, more fuel could form a cold layer at bottom of the tray resulting in a change in fuel layer temperature profile. These could both affect the rate of change of burning rates at increased pool depth.

There appeared to be a different trend to burning rate behavior with increasing airflow for the case of 10 and 15 cm pool fires as seen in figure 5.10. The 10 cm pool cases showed a progressive enhancement of burning rates from 0.008 kg/m²s to 0.019 kg/m²s for single and from 0.018 kg/m²s to 0.033 kg/m²s for dual pool cases at 0.5 cm depth. Similar trends were observed for the case of 1 cm depth but the burning rate enhancement was not as accelerated except at 1.5 m/s where there was a steep rise in burning rate. As for 15 cm pool cases, the burning rates first increased from quiescent to 0.5 m/s, then decreased at 1 m/s airflow and intensify again at 1.5 m/s. This was more pronounced in figure 5.10 (b) for 80 g fuel. This could be explained by competing effects of cooling, oxygen availability due to increased airflow [25,47,52] as well as variation of the combustion mass transfer coefficient with respect to the convective airflow as discussed earlier in section 5.1, figure 5.4.

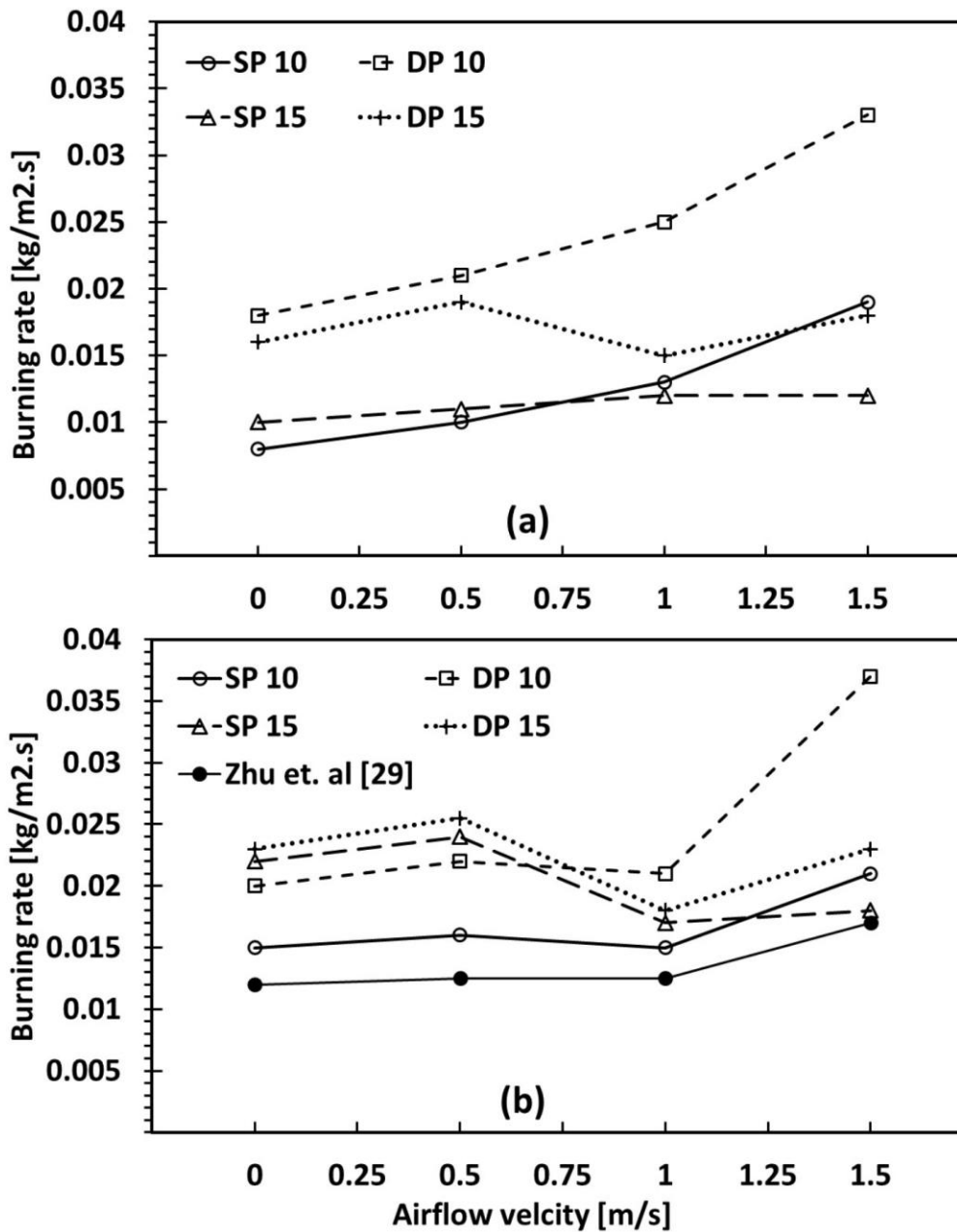
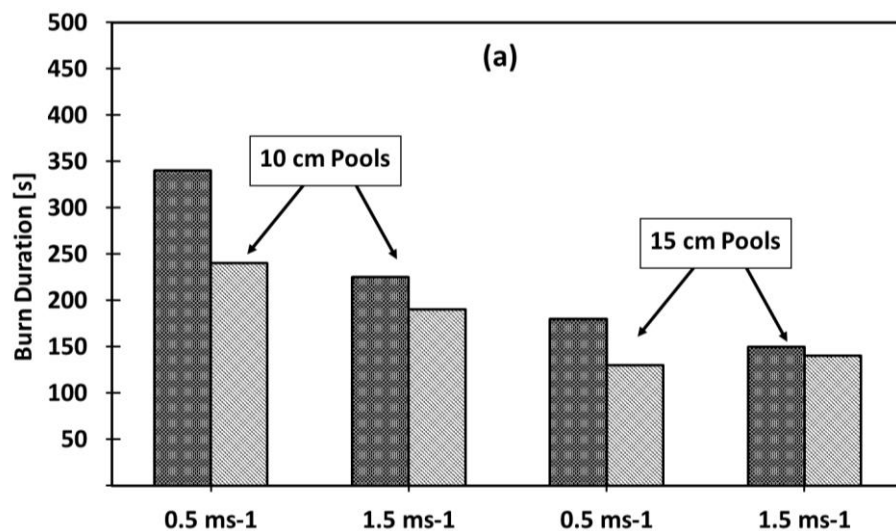


Figure 5.11. Burning rates of single and dual pool fires as a function of airflow velocity (a) 40 g initial fuel (b) 80 g initial fuel

It could also be inferred that there was a maximum threshold for burning rates of single and dual 15 cm pool fires at approximately 0.025 kg/m²s after which cooling effects dominated under tested conditions. This could be attributed to 50 % larger pool

edge that resulted in increased cooling in windward rim of 15 cm pool cases. It could also be said that increasing the separation distance to 8 cm had a slight decreasing effect on the burning rates of 10 cm pool fires, which was resultant effect of increased heat feedback from tunnel sidewall and non-merging flames. Burning rates of single 10 cm pool fires could be compared with measurements by Zhu et. al [81] at similar pool size with bottom tray insulation and 95 g initial ethanol. Similar trends could be seen overall, across the airflow velocities such as steep increase in burning rates at 1.5 m/s. The cross section area of the tunnel model used in [81] was 42 x 60 cm which was similar to confined conditions of present study.

Figure 5.12 compares burn durations of single and dual pool fires as a function of pool depth and airflow velocity at two test points of 0.5 and 1.5 m/s. Burn duration was defined here as the time required for the fuel mass in the vessel to reach 1 g from initial state. Leaving aside the obvious conclusion of increased burn duration with fuel mass, it could be seen that 10 cm pool fires take longer to burn the same fuel mass which further backs the claim that the pool size can be categorized as the small pool where heat conduction from the vessel rim to the liquid fuel is the dominant factor in determining the burning rate.



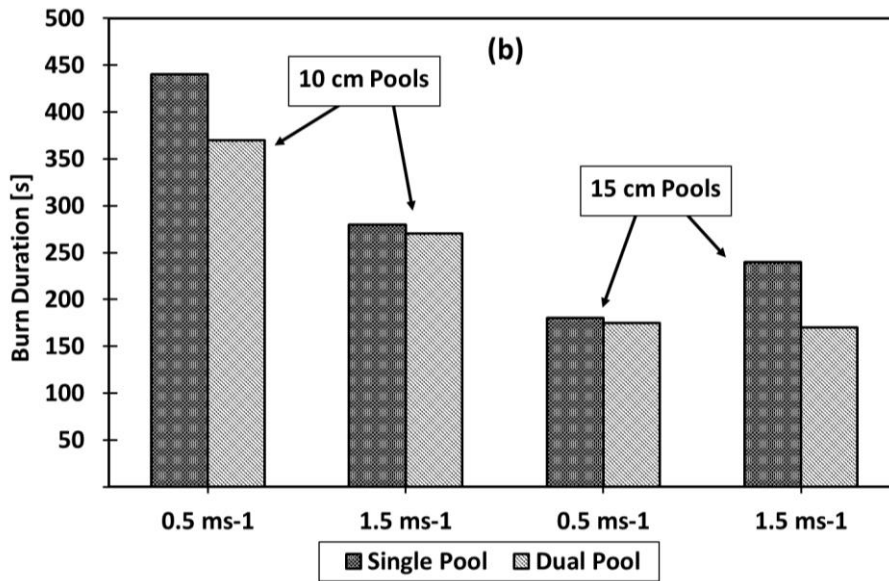


Figure 5.12. Burn duration of single and dual pool fires as a function of airflow velocity for (a) 40 g (b) 80 g initial fuel mass

The 15 cm pools burn durations seemed fairly invariant to the control parameters. The shorter onset of transition and the increased rate at which the burn rate reached its peak stage 4 value in 15 cm pool fires influenced the burn duration strongly. Figure 5.13 and 5.14 show captured flame images of 10 cm pool fires at 1.5 m/s airflow and initial fuel mass of 40 g for $S = 4$ cm and $S = 8$ cm respectively. There was a visible reflection of fire in the left side of photos, which was due to the glass observation opening, sealed during normal test measurements. The time stamps on figure 5.12 were given starting right after the ignition and are same in figure 5.13. Evolution of burning rate stages could be observed in figure 5.12 where duration from 110 to 160 s corresponded to the stage 4 as discussed in figure 5.8 in which fuel boiling and fire merging occurred. Increasing the separation distance to 8 cm results slightly increased flame height due to confinement effect of tunnel sidewall [82] with no observable physical interaction of the flames. Given the unchanged recording properties, luminosity of the flames was more visible in case of 4 cm separation distance during pool boiling phase (110–160 s).

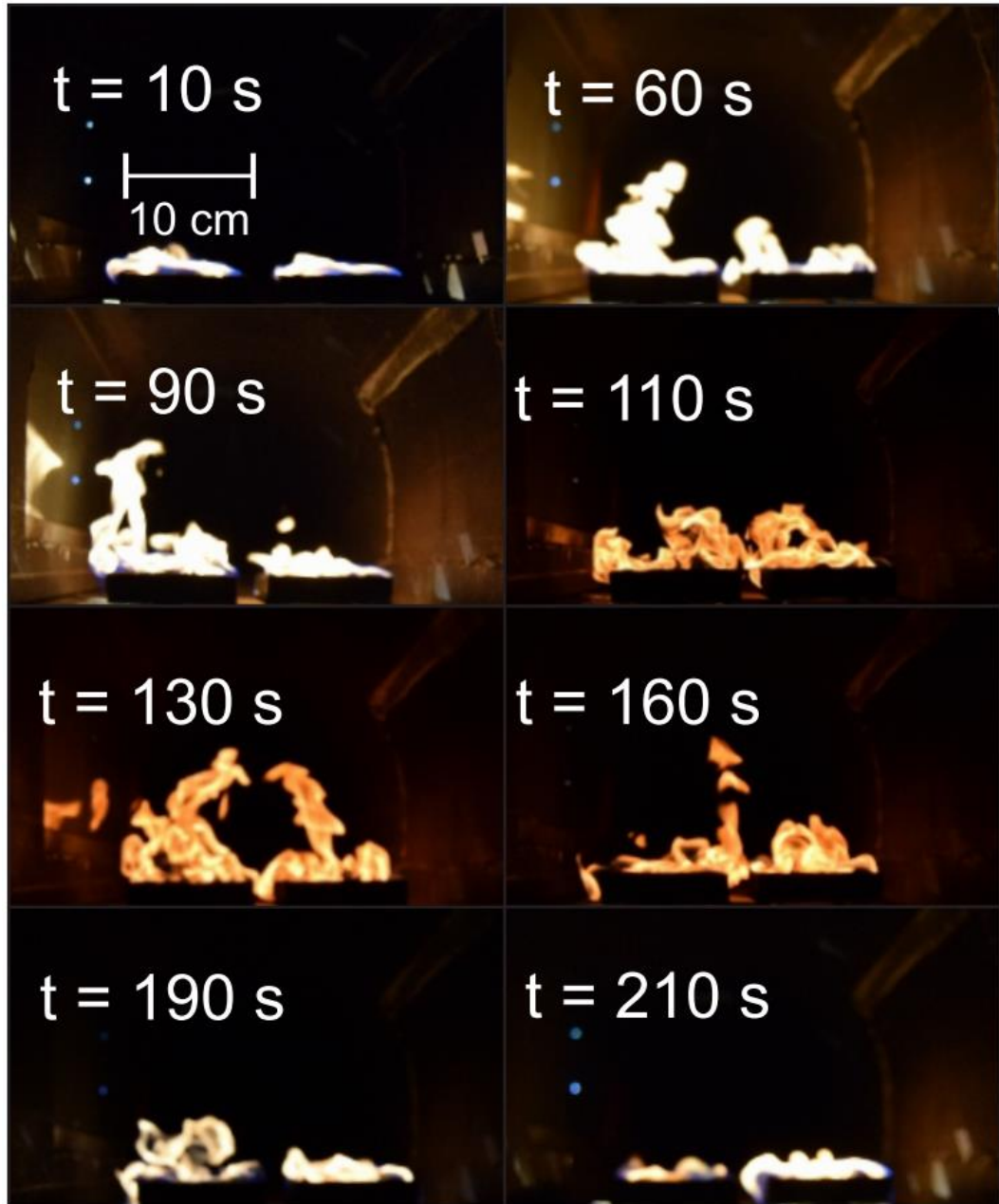


Figure 5.13. Flame captures of dual 10 cm pool fires at 1.5 m/s for $S = 4\text{ cm}$

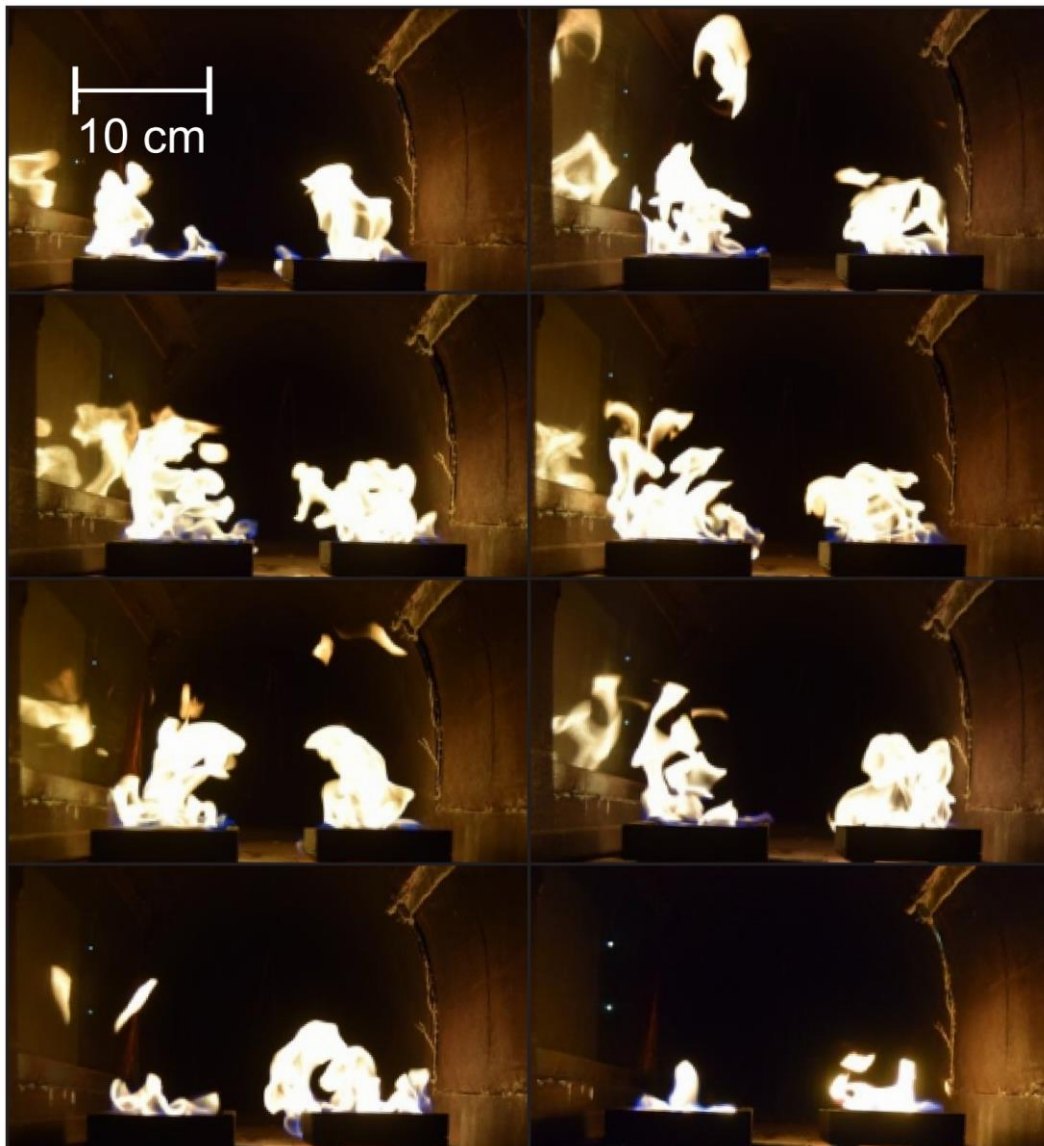


Figure 5.14. Flame captures of dual 10 cm pool fires at 1.5 m/s for $S = 8$ cm

5.2.2 HRR flux

HRR is believed to be a critical factor in evaluating fire safety, especially for the confined fire since heat feedback from walls is also an influential parameter [27]. To investigate effect of pool count on the HRR, figure 5.15 gives the normalized HRR values per unit area of the pools (HRR flux) as a function of airflow velocity.

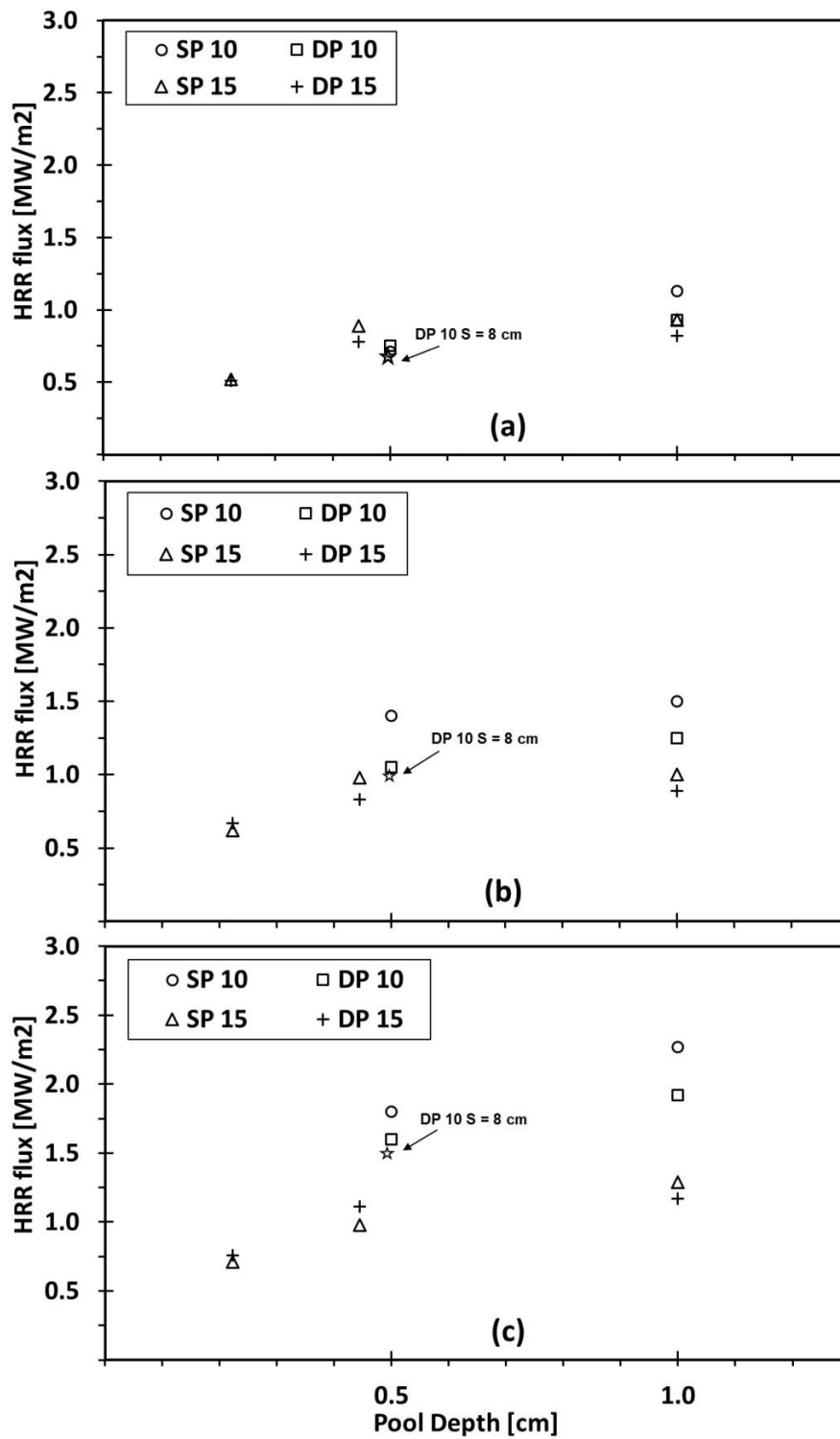


Figure 5.15. HRR flux of single and dual pool fires as a function of pool depth and airflow velocity (a) 0.5 m/s (b) 1 m/s (c) 1.5 m/s

As with the burning rates, the values of HRR were that of time-averaged quasi-steady burning period. It could be seen that increasing the airflow from 0.5 to 1.5 m/s and the pool depth had an enhancing effect on the HRR flux. This was more pronounced in case of 10 cm pools as the 15 cm pool fire HRR fluxes were fairly invariant to this range. The HRR in terms of kW for the dual pool fire cases showed a considerable increase with respect to single pool fires in the range of 50 % to 126 % considering 10 and 15 cm pool cases which further emphasized the effect of secondary fire on overall heat load.

5.3 Effect of tunnel blockage

It is believed that existence of an obstruction in the upstream of a tunnel fire may have considerable effects on the burning characteristics of the fire altering the safety measures that need to be accounted for. In this section, results of tests on blocked tunnel fire using a car and a metro carriage mockup with a blockage ratio of 14 % and 58 % are given. Ventilation to the model ranged from 0 (quiescent condition) to 1.5 m/s with pool depth of 0.45 cm fixed throughout the experiments. The details of experiment design parameters were given in section 3.3.3. The car blockage was denoted simply as ‘car’ and metro wagon blockage as ‘metro’ throughout the presented results. Results of some cases were also accompanied by FDS model predictions to justify the effect of blockage on flow field and burning rates of fires.

5.3.1 HRR and burning rate behavior

The blockage ratio was defined as the ratio of cross sectional area of the blockage to that of the tunnel. In order to facilitate interpretation of results, the ratio of the square pool size (L) to the blockage-fire separation distance (S) was used in presented results. In case of no blockage, the L/S ratio is zero assuming blockage was at infinity. The ratio entailed that as it increased, the separation distance became smaller. The HRR

flux from the pool fires were calculated and plotted against the L/S ratio for car and metro blockage in figure 5.16.

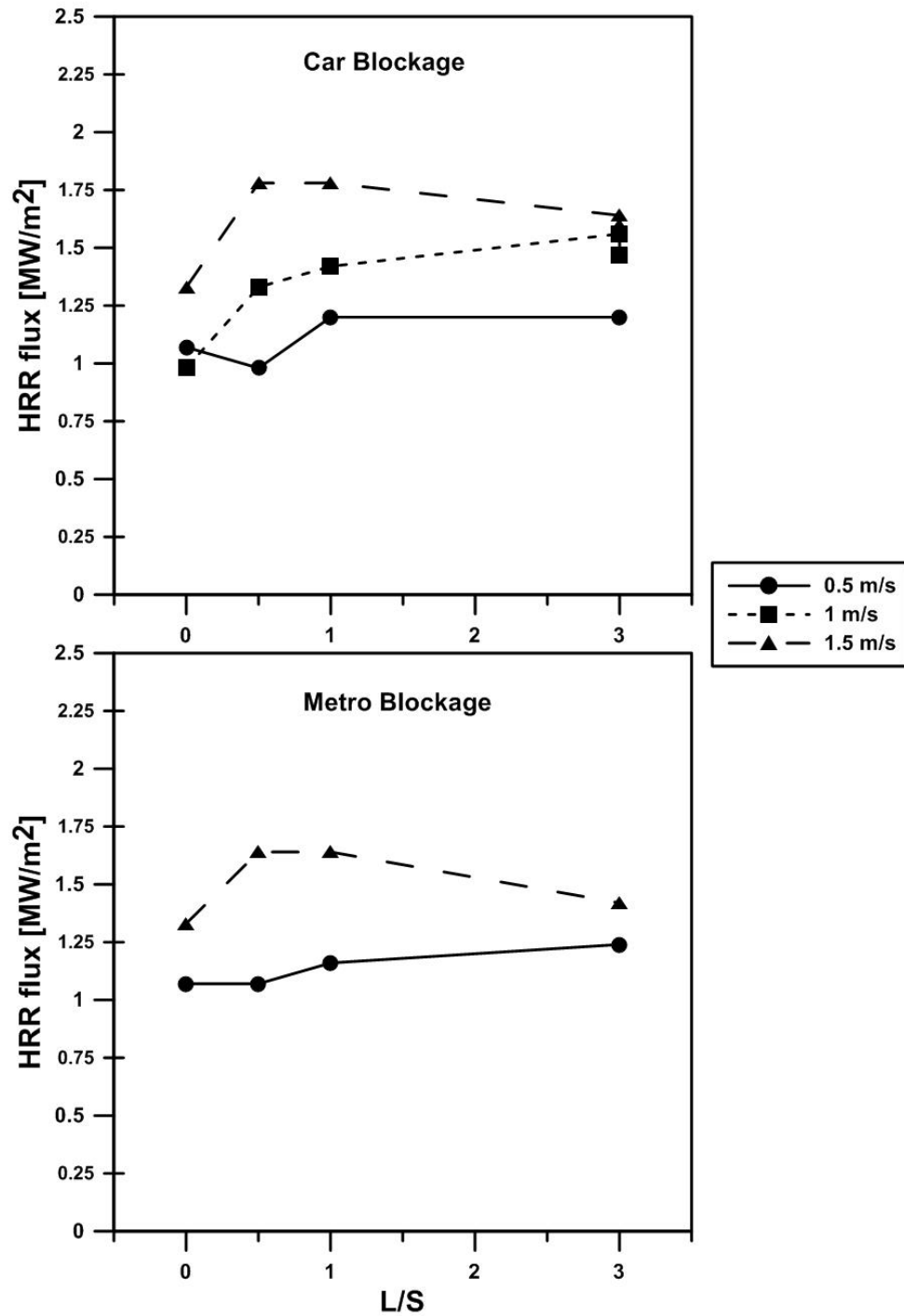


Figure 5.16. Effect of blockage and separation distance on HRR flux from the pool

The HRR was calculated based oxygen consumption calorimetry taking into account O₂, CO and CO₂ concentrations downstream of fire. The magnitude of HRR due to this method is influenced by oxygen concentration. This means that in blocked fire test cases, the flow pattern may have affected the flow distribution at the HRR measurement probe location. However, since all the measurements were performed at the same probe location, the results can be qualitatively compared. Also to double check the calorimetry, by checking the burning rate values along the HRR results, it can be concluded that the combustion is fuel controlled in the range of tested conditions. In order to do this, the mass loss rate of fire times heat of combustion of fuel was calculated at any test point on Fig 5.17 which ensured that the combustion is complete. Results established a general increase in the HRR flux at elevated ventilation velocities for constant L/S ratio.

For instance, at L/S = 0.5, the HRR flux showed an 80 % increase at 1.5 m/s car blockage case compared to 0.5 m/s. At S = 5 cm, the effect of ventilation was not as pronounced. Similar trends were spotted for metro blocked tunnel HRR flux. Although a general trend could not be observed regarding the separation distance, it was concluded that blocked fire affects the HRR considerably. At 0.5 and 1 m/s, reducing the separation distance resulted in increasing HRR flux. At 1.5 m/s, due to increased airflow, the maximum HRR flux occurred at L/S = 0.5. Similar trends were also observed in case of metro obstruction. The effect of blockage and separation distance on burning rates of the pool fires can be seen in figure 5.16. Following observations were made: (1) the burning rates showed a considerable increase in ventilated conditions compared to quiescent condition (almost twice) (2) the unblocked fire burning rates increased at 0.5 m/s due to ventilation, then decreased at 1 m/s and increase again at 1.5 m/s. This was also observed in results of part one and two of the experiments covered in sections 5.1 and 5.2. This was attributed to the cooling effect of ventilation at 1 m/s which reduced the burning rates (3) vortices were generated downstream of the car and metro obstruction which act as a bluff body.

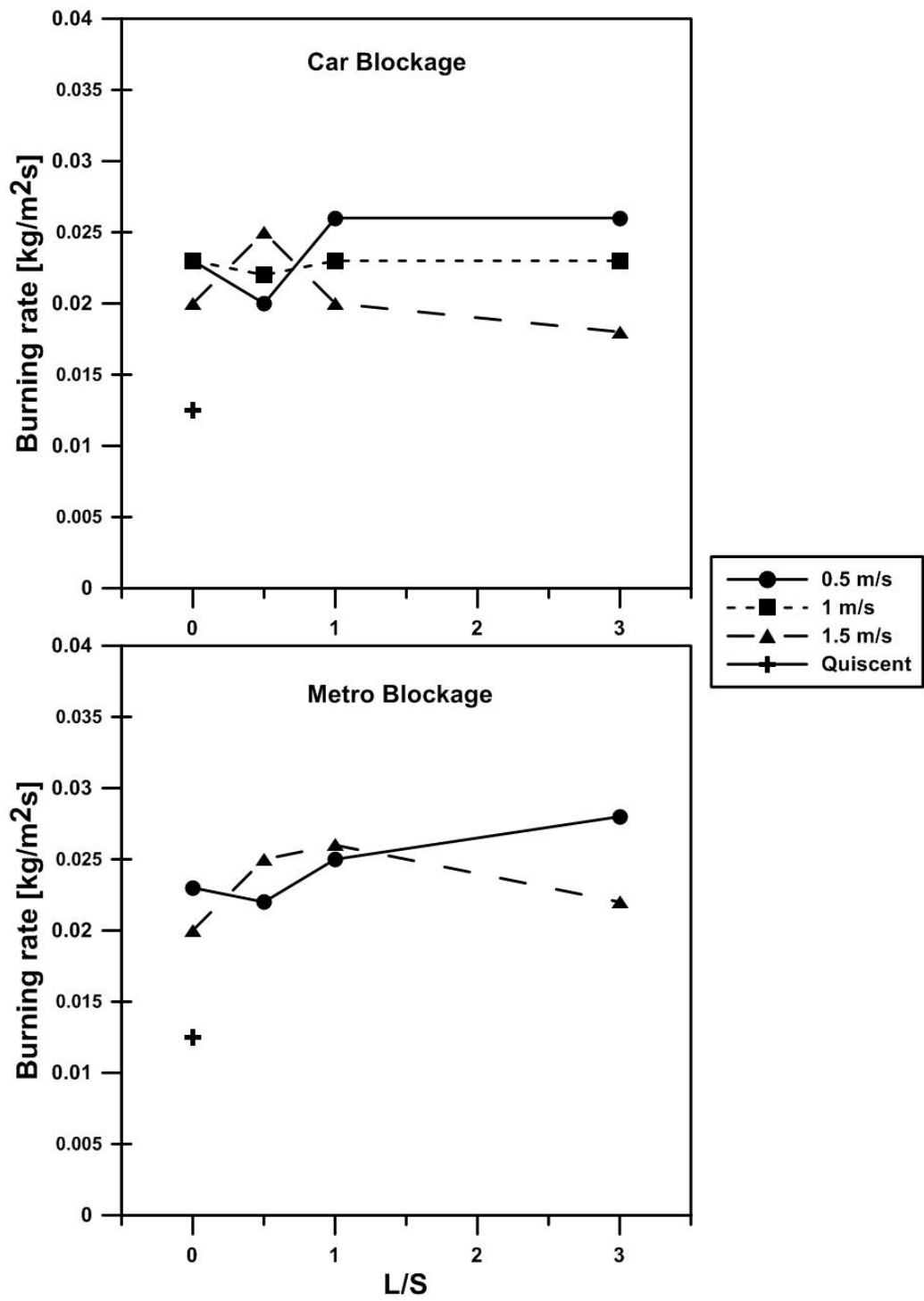


Figure 5.17. Effect of blockage and separation distance on burning rates from the pool fires

This was evident from the flame images as well as flow field predictions by FDS model. The generation of these vortices at the wake of blockage affected the burning rates considerably due to changes in the air entrainment and local ventilation velocity. For the car blocked pool fire, except the 1.5 m/s case, as the separation distance increased, the burning rate decreased. This trend was not seen at 1.5 m/s case where due to increased ventilation, the reattachment zone occurred upstream of pool fire at $S = 30$ cm, thus increasing the burning rates at higher L/S ratios. The recirculation zone effect could be seen in the velocity contours at half the height of the blockage on figure 5.18 where the blockage is identified as a white bluff body and the pool is the square transparent outline at the center. Vortices generated at the wake of the blockage can also be seen in this figure. As can be identified from the flame images, due to the recirculation zone in the low pressure wake of the blockage, the flame was elevated and attached to the blockage at $L/S = 1$ and $L/S = 3$ cases. Figure 5.19 shows the flame images and FDS predicted velocity field for $L/S = 0.5$ and 3 at limiting case of 0.5 m/s at similar conditions as in figure 5.18.

Under similar conditions, model predictions showed that at 0.5 m/s, the flow field is different compared to the 1.5 m/s case. It was seen that due to a smaller wake at this velocity, at higher L/S ratios in figure 5.18 (a), the average local ventilation velocity is greater compared to $L/S = 0.5$ case. At this velocity, there was no visible flame attachment to the blockage. This was an interesting finding since it showed that due to presence of tunnel blockage, the effect of ventilation velocity on the fire burning rates is not linear nor similar to the unblocked case and needs to be considered in the safety design parameters. Metro blocked pool fire burning rates showed trends similar to car blocked fires in terms of burning rates at tested conditions as seen in figure 5.17. However, due to increased blockage by metro carriage mock-up, the burning rates were generally lower compared to the car blocked cases and were not as sensitive to the separation distance.

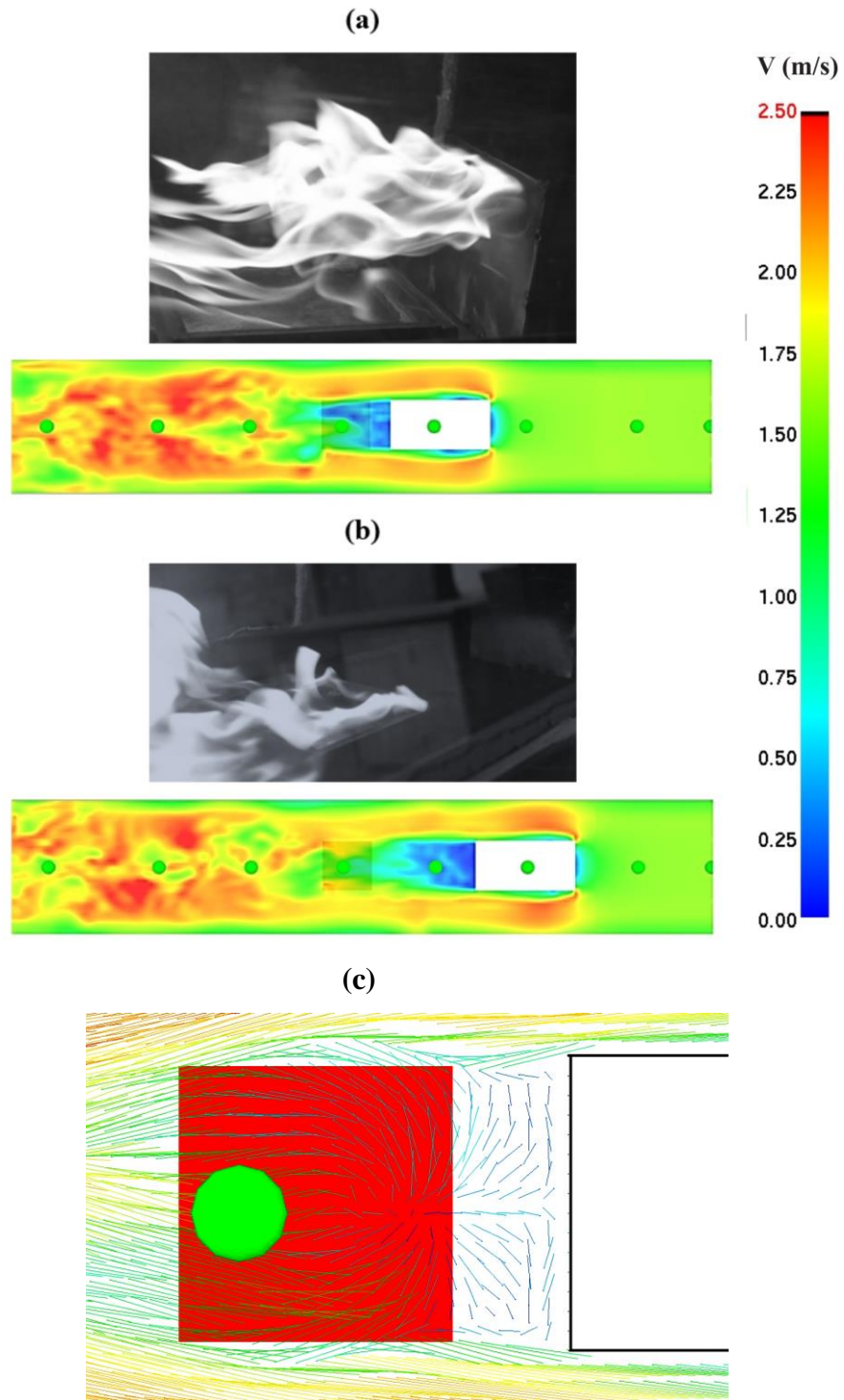


Figure 5.18. Flame images and FDS predicted velocity field for (a) $L/S = 3$ and (b) $L/S = 0.5$ (c) velocity vectors at the wake of blockage at 1.5 m/s ventilation velocity for car blockage at 80 s after ignition

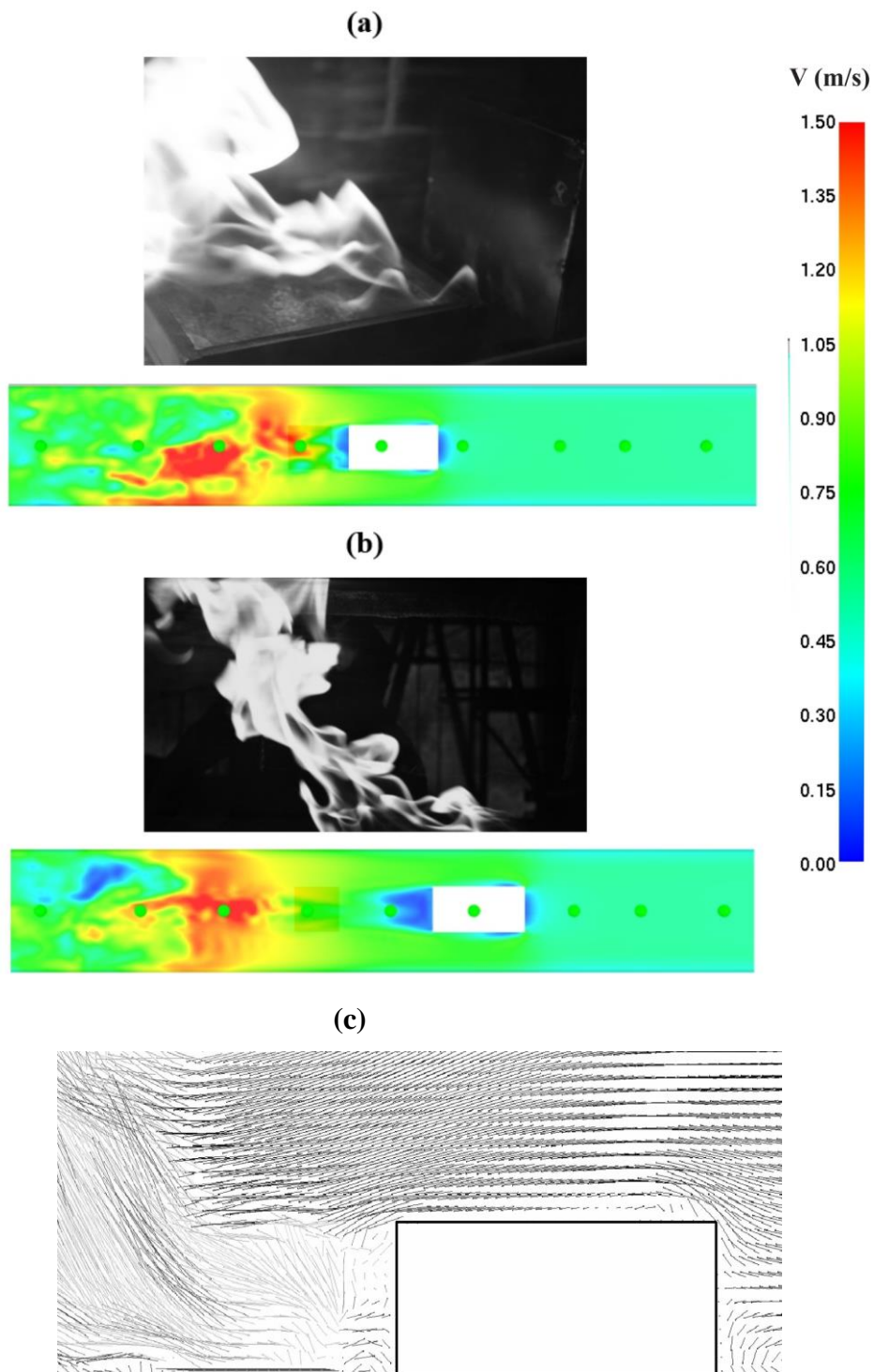


Figure 5.19. Flame images and FDS predicted velocity field for (a) $L/S = 3$ and (b) $L/S = 0.5$ and (c) velocity vectors at the wake of blockage at 0.5 m/s ventilation velocity for car blockage at 80 s after ignition

5.3.2 Temperature distribution

Maximum gas temperature beneath the tunnel ceiling is considered as an important parameter in the tunnel fire safety and designing of fire-proofing materials and tunnel structures and is influenced by several factors such as HRR of the fire, tunnel geometry and ventilation conditions [1,5]. The results of the EUREKA tests also showed that temperatures more than 300 ° C could damage the steel reinforcement of the tunnel lining concrete [40]. Measured maximum ceiling temperature along the tunnel for the car and metro blockage are plotted as a function of tunnel ventilation velocity and fire-blockage separation distance in figure 5.20. Measurements were made 4 cm below the arched ceiling of the tunnel. There are several general trends to be observed in this figure. The effect of blockage on fire dynamics was clear by comparing the temperature results for non-blocked and blocked fire. There was an increase in general for the temperature measurements of blocked fire, which agreed with previous results in the literature.

For instance, at $L/S = 3$, corresponding to the case of car blocked fire with a separation distance of 5 cm, a substantial increase in ceiling temperature was observed in the 300-700 °C region at pool location. It was seen that blockage affected area was mostly in -0.5 m and +0.25 m range with respect to pool center. At 0.5 m and further downstream of the fire, the blockage effect at different L/S values was less pronounced due to reattachment of flow. In general, increased blockage ratio using the metro block was seen to lower the measured temperatures they did not follow the trend seen at changing L/S ratios in car blockage cases especially at 1.5 m/s. The effect of ventilation on non-blocked fire was discussed as part of results in section 5.1. Several empirical equations have been proposed in the literature that predict maximum gas temperature below the tunnel ceiling accounting for fire load, tunnel geometry and ventilation factors.

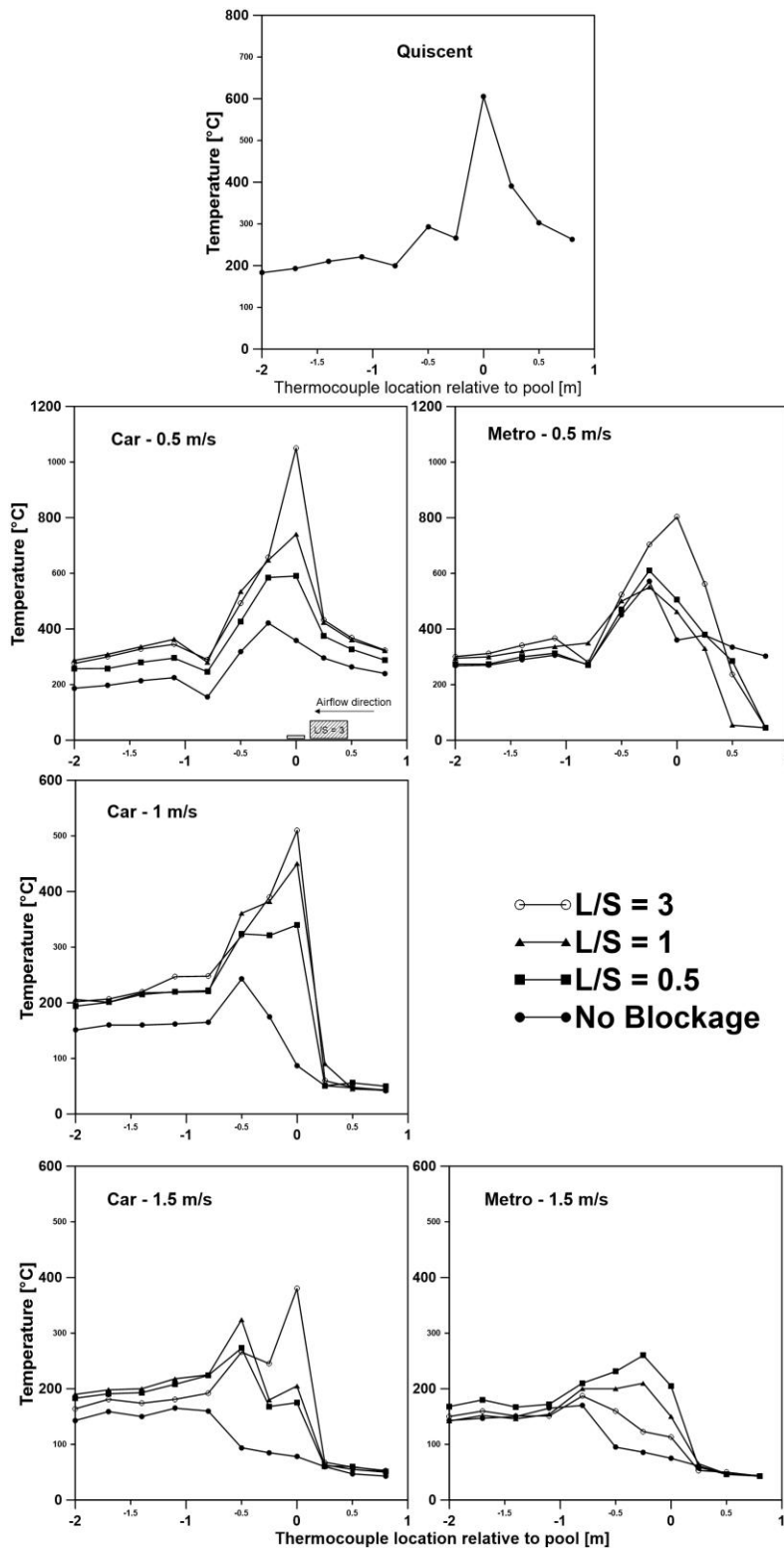


Figure 5.20. Maximum ceiling temperature along the tunnel for car and metro blockage as a function of tunnel ventilation velocity

Based on scaled model results, Kurioka et al. suggested equation (5.7) for the gas temperature in which ΔT_{\max} was defined as maximum excess temperature of smoke layer at downstream of fire and T_a as ventilation temperature [83].

$$\frac{\Delta T_{\max}}{T_a} = \gamma \left(\frac{\dot{Q}^{*2/3}}{Fr^{1/3}} \right)^\varepsilon \quad (5.7)$$

in which \dot{Q}^* is the Zukoski number, or non-dimensional HRR of fire defined in section 2.2.1. They suggested equation (5.8) for the coefficients as a function of Zukoski number and Froude number.

$$\begin{aligned} \gamma = 1.77, \varepsilon = 1.2 \text{ for } \frac{\dot{Q}^{*2/3}}{Fr^{1/3}} < 1.35 \\ \gamma = 2.54, \varepsilon = 0 \text{ for } \frac{\dot{Q}^{*2/3}}{Fr^{1/3}} \geq 1.35 \end{aligned} \quad (5.8)$$

Li et al. [50] proposed similar correlations for the maximum excess smoke layer temperature given in equation (5.9). In which $V' = V / V^*$ and V^* was calculated due to equation (5.10).

$$\Delta T_{\max} = \begin{cases} \frac{\dot{Q}}{Vr^{1/3} H^{5/3}}, V' > 0.19 \\ 17.5 \frac{\dot{Q}^{2/3}}{H^{5/3}}, V' \leq 0.19 \end{cases} \quad (5.9)$$

$$V^* = \left(\frac{\dot{Q}_c g}{r \rho_a c_p T_a} \right)^{1/3} \quad (5.10)$$

Figure 5.21 plots the predicted excess smoke layer temperature $(\Delta T_{\max} / T_a)_{Model}$ given by equations (5.7) through (5.10) versus $(\Delta T_{\max} / T_a)_{Measured}$ for all tested

considered in the range of $0 < L/S < 3$ and ventilation velocity of 0–1.5 m/s using car and metro blockage. The unblocked fire showed a good agreement with both the models with negligible differences (figure 5.21 (a)). The blocked fire temperature results showed a shift to the left hand side of the model line $y = x$ as seen in figure 5.22 (b) which indicates the increase of overall tunnel gas temperature with respect to free fire as discussed previously. A 4th degree polynomial fit could also be applied to the results as seen in figure 5.22 (b).

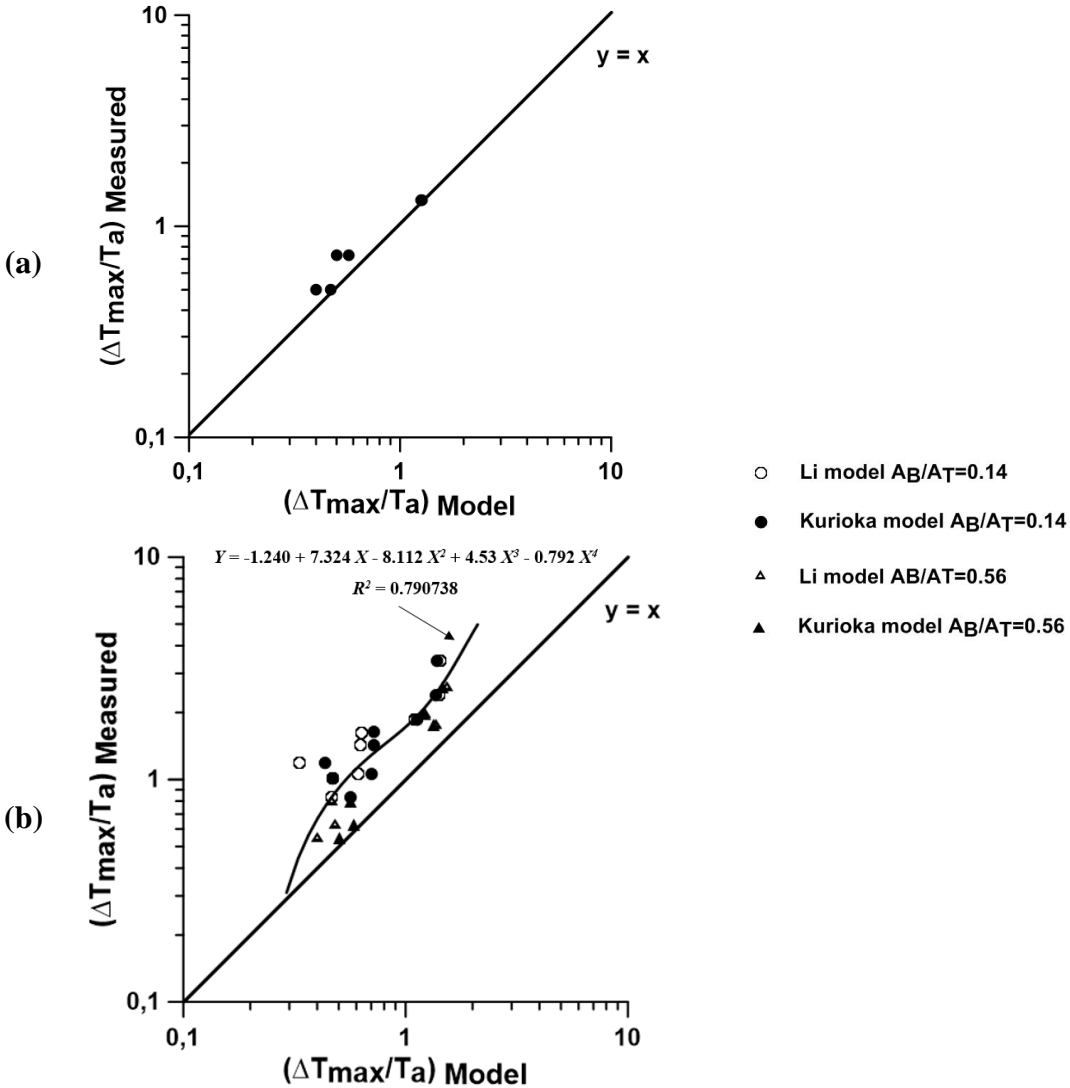


Figure 5.21. Predicted vs. measured excess smoke layer temperature due to Kurioka [83] and Li et al. [50] models for (a) free fire and (b) blocked fire

5.4 Effect of tunnel inclination

Tunnel slopes, negative or positive, could affect the smoke movement and thus the critical ventilation conditions required to prevent backlayering. For instance, due to the buoyancy effect of a negative slope, the critical ventilation velocity is expected to be greater compared to horizontal tunnel. In order to see these effects and how they influence other characteristics of tunnel fire such as burning rate and HRR, tests were performed and results are presented in this section. The fuel depth was constant throughout these experiments at 0.45 cm and square 15 cm pool size was used. The ventilation velocity was varied within 0-1.5 m/s with 0.25 m/s increments.

Figure 5.22 shows the effect of inclination on the burning rates and HRR flux of pool fires as a function of ventilation velocities as well as oxygen concentrations at probe location for the case of 1 m/s ventilation velocity. The decreasing trend shown in the burning rates at larger slopes such as 6 % was attributed to the interaction between cross airflow and fuel tray. Since the fuel tray was fixed at sloped conditions, the windward rim of the tray acts as a blockage in the flow direction and result in boundary layer development over the edge of rim. On the other hand, the fixed fuel tray increased the effective heat transfer area with the airflow from the bottom side at both positive and negative inclinations, compared to horizontal case, thus decreasing the burning rate of fire. The combustion is complete in the range of tested ventilation velocities as checked by the burning rate and HRR results. The maximum HRR occur at -3 % slope. The peak HRR flux of -3 % (downhill tunnel slope) was 1.42 MW/m² compared to 0.71 MW/m² at +6 % (uphill slope) at 1 m/s. The HRR was calculated due to oxygen consumption calorimetry method and is affected by oxygen concentration of the flue gas. In the downhill inclination, the buoyancy forces of the hot plume from pool fire propagated to the upstream of fire. In such case, the effect of incoming airflow was reduced on the pool fire and oxygen (air) fraction decreased in the downstream section (fire became under-ventilated) as seen in oxygen concentrations given in figure 5.22.

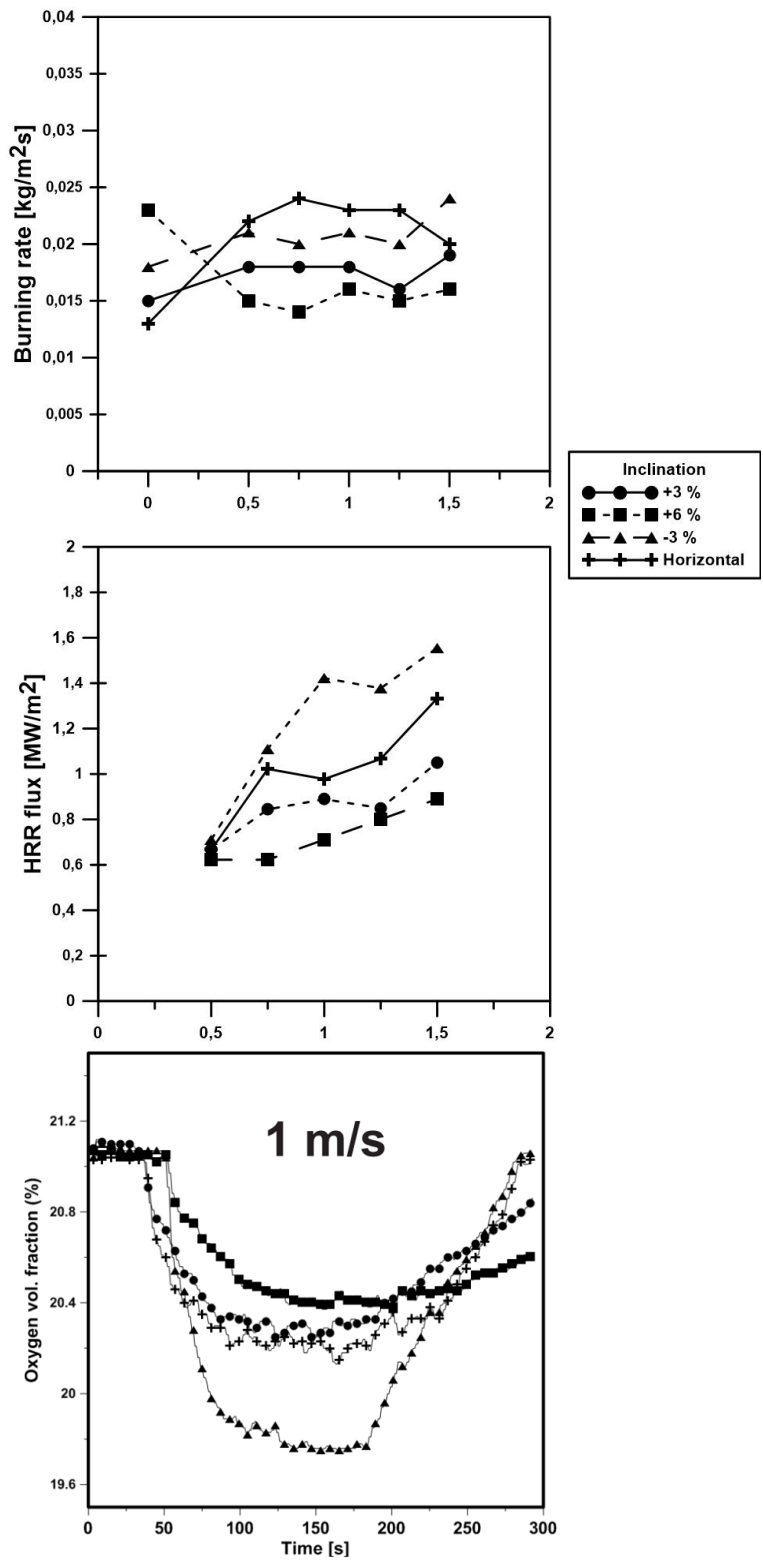


Figure 5.22. Effect of positive and negative inclination on the burning rates and HRR flux from fires and the oxygen concentration at probe location

In the uphill inclination cases, this smoke flow was reversed due to stack effect and resulted in decreased oxygen depletion factor of the fire and reduced HRR. Figure 5.23 presents the results of measured maximum ceiling temperatures in the tunnel, as a function of ventilation velocity and tunnel inclination. As with previous temperature figures, the x-axis represents the relative location of thermocouples to the pool (0 on x-axis). The figure demonstrated the following: (1) there was a general constant decreasing trend due to increased ventilation velocities at any inclination (2) except for the quiescent case tunnel temperature was increased at -3 % inclined case emphasizing the effect of downhill inclinations on the temperature distribution especially at 0.75-1.5 m/s range (3) uphill slopes resulted in increased airflow to the tunnel due to stack effect and decreased tunnel temperatures with this effect more pronounced at 0.75-1.5 m/s range (4) critical ventilation velocity was achieved around 0.75-1.25 m/s range for limiting cases of +6 % and -3 % inclinations which agrees with the data in the literature [4].

And (5) a minimum of 1 m/s ventilation velocity corresponding to 3.6 m/s in real scale was required to keep the ceiling temperature below 300 °C which is the safety limit for avoiding tunnel lining damage [7]. The effect of tunnel inclination on the backlayering length is depicted in figure 5.24. In this figure, the temperature difference between the tunnel ceiling and the ventilation flow temperature was defined as temperature over ambient (ΔT) and given at upstream locations corresponding to 0.7 H, 1.4 H and 2.2 H with H being the tunnel height. It was clearly seen from these results that at -3 % inclined case, the backlayering length extends to 2.2 H below 1.25 m/s ventilation velocity.

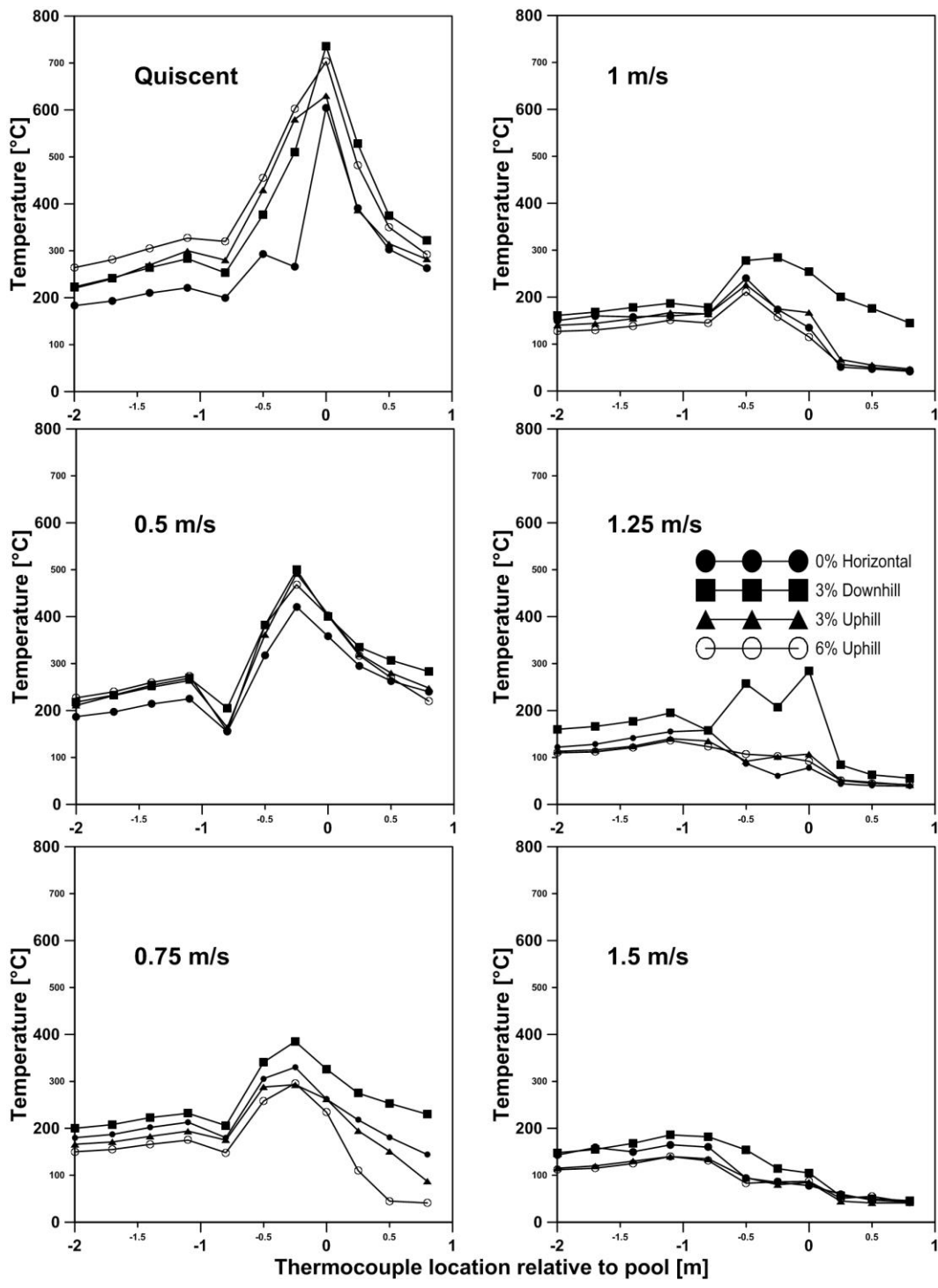


Figure 5.23. Effect of positive and negative inclination on the maximum ceiling temperature distribution as a function of ventilation velocity and inclination percentage

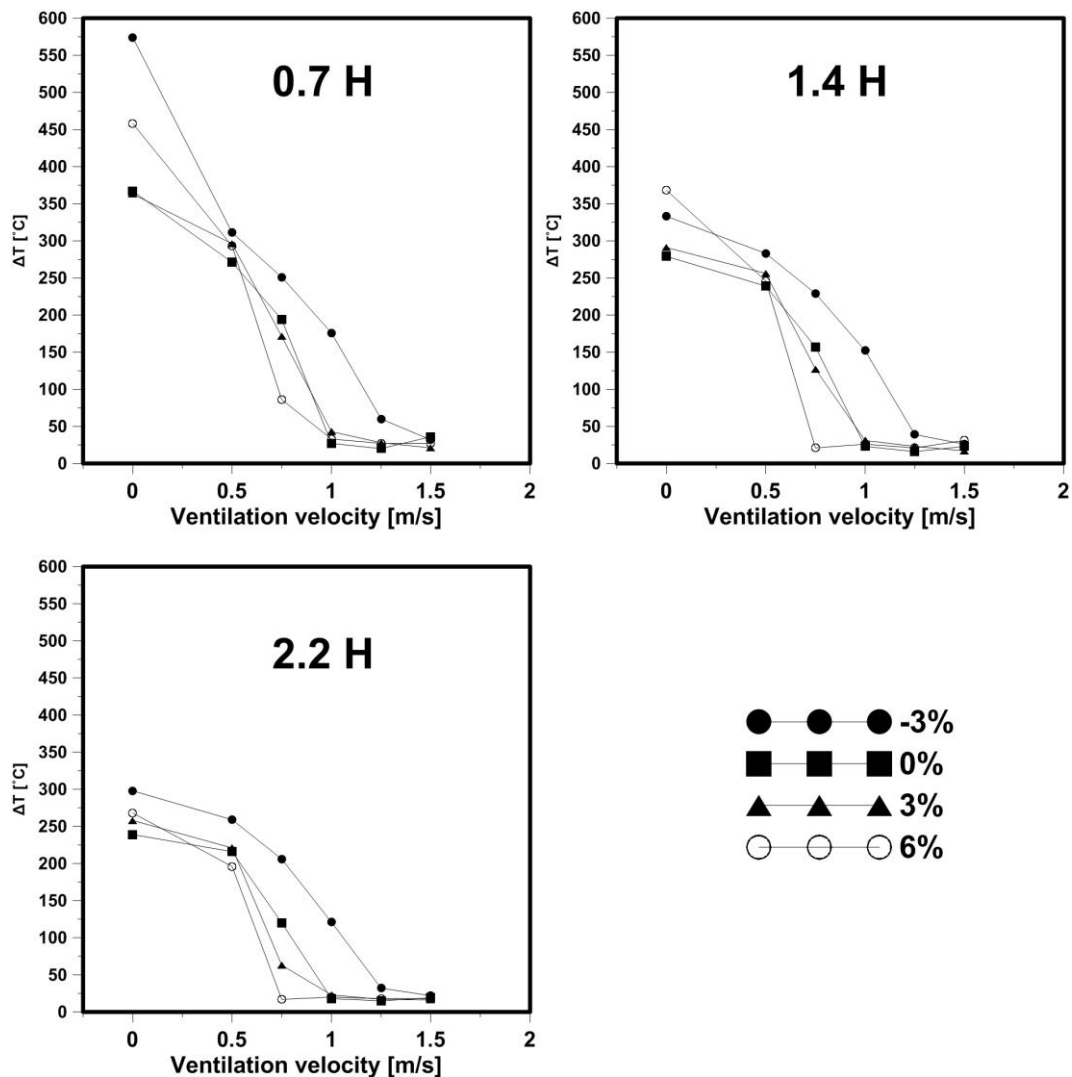


Figure 5.24. Temperature over ambient upstream of the pool fire as a function of ventilation velocity and tunnel slope at distances 0.7, 1.4 and 2.2 times height of the tunnel

It was seen that increasing the uphill inclination from horizontal position to 6 % resulted in a lower ventilation velocity of 0.75 m/s to prevent backlayering. However, it could be said that this value would be slightly larger considering ΔT for 6 % case at 0.7 H upstream position. Backlayering length of horizontal tunnel and 3 % inclined case was zero at 1 m/s ventilation velocity. Below 1 m/s, except for the 6 % uphill case, the temperature difference ranged between 220-320 °C in the upstream section

which is considered a safety hazard. In order to investigate the critical ventilation velocity variations at different sloping conditions more clearly, figure 5.25 compares the normalized critical ventilation velocity which was defined as the ratio of measured critical velocity of inclined tunnel to that of the horizontal case ($V_{cr}/V_{cr,0}$). Experimental measurements were tested against existing models in literature due to Atkinson & Wu model [4], Ko et al. model [84] and US Department of Transportation Subway Environment Simulation (SES) Computer Program equation [85] given for critical ventilation velocity of tunnels at inclined conditions. These relations are given in equation (5.11) as a function of tunnel inclination percentage.

$$\left\{ \begin{array}{l} \frac{V_{cr}}{V_{cr,0}} = 1.0 - 0.014\theta \quad \text{Atkinson \& Wu} \\ \frac{V_{cr}}{V_{cr,0}} = 1.0 - 0.033\theta \quad \text{Ko et al.} \\ \frac{V_{cr}}{V_{cr,0}} = 1.0 - 0.0374\theta^{0.8} \quad \text{SES} \end{array} \right. \quad (5.11)$$

The results indicated that the measured critical ventilation velocities for uphill inclinations (3 % and 6 %) agree better with the Atkinson model. However, there was a discrepancy between this model and measurements at -3 %, for which the SES and Ko et al. model compared better. It should be noted that due to 0.25 m/s increments of ventilation velocity, there is an added possibility of discrepancy between predicted and measured values. This could have been relaxed by using a reduced increment range. However, as it was discussed in section 3.1, fluctuations of the ventilation velocity measured by the hotwire anemometer meant that a 0.25 m/s increment was a safer choice rather than, say, 0.1 m/s. nevertheless, keeping this in mind, if the discussions regarding test points such as 6 % in are accounted for, the trend shown in figure 5.24 would be improved. A linear fit was proposed for the normalized critical ventilation velocity as a function of tunnel inclination grade for the tunnel model used in the study, which can be seen on figure 5.25.

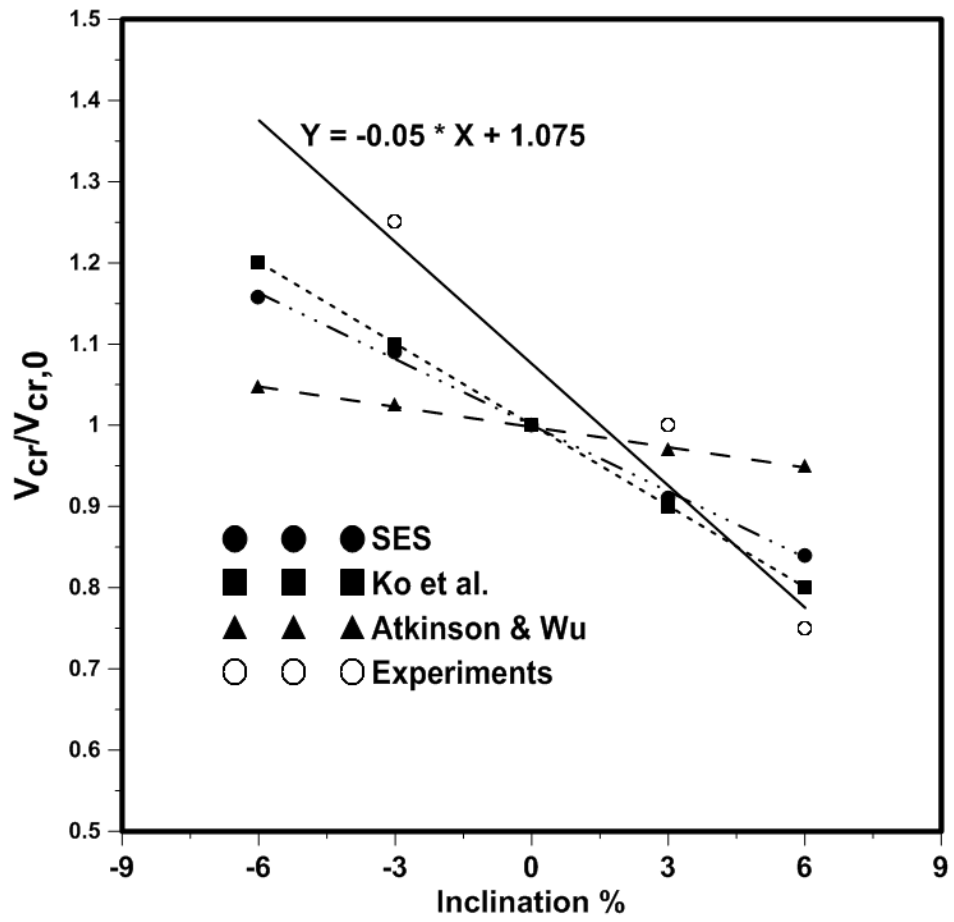


Figure 5.25. Comparison of measured normalized critical velocity with existing empirical model

CHAPTER VI

CONCLUSIVE REMARKS

Tunnel fires still remain an economical hurdle to the transportation industry as well as a threat to the lives of motorists and passengers. Design of tunnel fire safety features demands a deep knowledge on the fire burning behavior in confined spaces. There have been quite a number of researches that address different aspects of tunnel fires in the literature, however, there is still questions to be answered and gaps to be filled. The purpose of this research was to better understand fire dynamics in tunnels through a series of sought after experiments that covered a decent spectrum of fire scenarios. These experiments were categorized into four parts in which the effects of tunnel wall coating material, positive and negative slope, tunnel blockage due to upstream obstruction, and existence of secondary fire source in close vicinity on the fire characteristics were investigated. Recent literature shows that due to immense cost of large-scale tunnel fire tests, the attention was turned to reduced scale experiments, which favor a large portion of the fire research community.

Following this trend, a 1/13 reduced scale tunnel model, which was constructed based on Froude scaling technique was used in this study. Critical and appealing parameters to the fire safety research community were measured during experiments. These parameters included fire heat load, burning rate of fire, critical ventilation velocity, backlayering length and tunnel temperature distribution which were measured across a wide range of ventilation velocities and pool depth (initial fuel layer thickness). Longitudinal ventilation was applied to the model tunnel since it was identified as the most common fire safety system having easier maintenance and economical benefit over other ventilation systems. Application of liquid pool fire in the study was because it was a more practical solution for providing the fire source required to simulate fire scenarios with a wide fire load range. In order to alleviate the negative effects of pool fire of a sooting fuel such as heptane or diesel, ethanol was

utilized throughout the experiments, which resulted in a non-sooting cleaner combustion. The details of the obtained results for each of the four parts of this study were covered in Chapter V in separate sections. The major findings of the study are summarized in a conclusive fashion in the following section.

According to the experiments, the fire load and burning rate were considerably affected to various degrees by a number of factors including increasing pool depth of the fuel, longitudinal ventilation velocity, tunnel blockage and inclination. The pool depth is an equivalent of available burning material and was varied between 0.1 cm (i.e. spill fire or thin-layered pool fire) and 1 cm across different parts of the experiments. The square pool size was also varied between 0.1 m and 0.31 m limits which corresponds to small and large pool fires respectively. It was observed that the maximum burning rates of $15 \text{ g/m}^2\text{s}$ associated with 0.31 m pool size at 0.3 cm depth corresponded to a lower burning rates of $12 \text{ g/m}^2\text{s}$ at 0.15 m pool size at similar pool depth conditions (0.223 cm). This signified the effect of increased fuel surface area (i.e. exposed burning area) that resulted in increased burning rates of fire. It was demonstrated that there is a general decreasing trend in burning rates of fires when the ventilation velocity increased from 0.5 to 1 m/s, after which point it increased again. This was explained by competing effects of airflow cooling and oxygen availability due to increased flow, which was in agreement with other results in the literature.

The HRR ranged within limits of 7-85 kW in the experiments which was well within the range of the normalized HRR results from large scale experiments by Ingason [41] also given in table 2.6. The burning rates varied within $8\text{-}35 \text{ g/m}^2\text{s}$ across tested conditions. It was seen that critical velocity was achieved around 1 m/s for all tested cases except for 3 % downhill tunnel, where the critical ventilation occurred around 1.25 m/s, and the 6 % uphill inclined tunnel, where this value was measured to be around 0.75 m/s. This demonstrated that a longitudinal ventilation velocity around 1 m/s for the model, corresponding to 3.6 m/s for the real scale tunnel would be sufficient to meet critical ventilation requirements. The effect of tunnel inclination was emphasized as being an influential factor that should be considered in tunnel safety design. Temperatures as high as 250-350 °C measured in the pool upstream showed

existence of backlayering flow at ventilation velocities below the critical values associated with different experiments. At such conditions, the overall tunnel temperature exceeded the maximum allowed temperatures established by fire safety standards in order to avoid tunnel lining and construction damage [7]. It was shown that upstream thermal radiation flux, having been identified as an important safety factor was considerably reduced by increasing the ventilation velocity to the tunnel due to increased fire tilt angle and retarded smoke plume further downstream of fire. It was demonstrated that using a highly emissive black-painted anodized wall coating could also reduce the radiative flux up to 45% while having no apparent effect on ventilation requirements.

The case of adjacent pool fires occurring in confined spaces in which coupled effects of interacting fires as well as airflow ranging from quiescent condition up to 1.5 m/s were investigated on the burning rates using 10 and 15 cm square pools with varying initial depth. Temporal evolution of the burning rates was observed and associated with pool size and count. It was shown that a secondary pool fire in close vicinity intensifies the burn rate considerably with the m_{DP}''' / m_{SP}''' ratio ranging between 1.375 and 2.25 for 10 cm pools and 1.06 and 1.73 for 15 cm pools. The heat overall load of the fire also tended to increase as high as 126 % for the cases of dual pool fires which further emphasized the effect of the secondary fire. Increasing airflow speed was shown to have a monotonously enhancing effect on burning rates of 10 cm pool cases whereas 15 cm pool cases are affected non-linearly with a peak value reached at 0.025 kg/m²s across tested conditions. This was explained by effect of pool size on dominant heat transfer regime as well as competing effects of cooling and increased air entrainment (enhanced burning) at increased airflow speeds. However, it was seen that increasing the airflow velocity decreases quasi-steady burning rate of single pool fires.

Effect of tunnel upstream obstruction effect on the fire burning characteristics and heat load was also investigated using two types of obstruction, a car and a metro wagon with respectively 14 % and 56% blockage ratio. It was shown that due to the bluff

body effect of the blockage, a low-pressure wake with vortexes were generated downstream of the car and metro blockage. This was evident from the flame images as well as FDS model predictions. The generation of these vortexes at the wake of blockage affected the burning rates considerably due to changes in the air entrainment and flame dragging and the local ventilation velocity. As the separation distance increased the burning rate decreased except for 1.5 m/s case where due to increased ventilation, the reattachment zone occurred upstream of pool fire at $S = 30$ cm, thus increasing the burning rates at higher L/S ratios. Blockage fire resulted in increased overall tunnel temperature. Results from these series of experiments were tested against empirical correlations by Kurioka et al. [83] and Li et al. [50].

Results from tunnel inclination tests revealed that due to buoyancy forces of the hot plume from pool fire propagating to the upstream of fire in downhill inclination, the heat load from fires might vary considerably. For instance, it was shown that the peak HRR flux of -3 % (downhill tunnel) was 1.42 MW/m^2 compared to 0.71 MW/m^2 at +6 % (uphill tunnel) at 1 m/s. Measured maximum ceiling temperature results also indicated that there was a general increase in tunnel temperature at -3 % inclined case emphasizing the effect of downhill inclinations on the temperature distribution especially at 0.75-1.5 m/s range. Critical ventilation velocity was achieved around 0.75-1.25 m/s range for limiting cases of +6 % and -3 % inclinations which agreed with the data in the literature [4]. Backlayering length of fires were also investigated at different sloping conditions and it was demonstrated that below 1 m/s, except for the 6 % uphill case, the temperature difference ranged between 220 and 320 °C in the upstream section which was considered a safety hazard. Measurements normalized critical ventilation velocities were tested against existing models in literature due to Atkinson & Wu [4], Ko et al. [84] and SES equation [85] and they agreed well with the SES and Ko et al. model in general. A fit was proposed for the normalized critical ventilation velocity as a function of tunnel grade.

Recommendations for future work can be summarized as below.

1. Increasing the cross sectional area of model by upscaling the construction to better accommodate for specific experiments for which physical restrictions did not allow a thorough investigation such as case of dual pool fires or obstructed tunnel, or,
2. Increasing the length of the model tunnel,
3. Investigation of the pool fire characteristics at steady state phase by implementing a fuel feeding system to keep pool depth constant at desired level, thus, eliminating the transient behavior of batch pool fires,
4. Investigating the smoke layer density and visibility using light extinction methods,
5. Expanding the range of tested ventilation velocities as well as pool size and depth, tunnel inclination grade and also investigating the case of multiple pool fires (more than two),
6. Conducting the blockage tests with a more realistic representation of the obstruction and/or wider range of blockage ratio,
7. Improvement is needed to be done on the FDS model which was developed in current work to integrate better sub-models as well as an adapted grid,
8. As an alternative, other open source codes such as OpenFoam/FireFoam could be used to develop sophisticated CFD models to investigate tunnel fires,
9. Measurement of hazardous emission concentrations and their distribution inside the tunnel due to different ventilation velocities and fire loads,
10. General improvement of the current state of test setup such as renewing and addition of new thermocouples, better tunnel isolation and mounted radiometers.

REFERENCES

- [1] Beard, A., & Carvel R. The handbook of tunnel fire safety. London: Thomas Telford; 2005.
- [2] Yalçın, E., Akpınar, E., Hakan, O.A., Ertürk A. Soma kömür işletmeleri a.ş. Tarafından işletilen manisa ili soma ilçesi,eynez köyündeki kömür madeninde 13.05.2014 tarihinde meydana gelen maden kazasi ile ilgili bilirkişi raporu. 2014.
- [3] Hu LH, Zhao XY, Zhu W, Tang F. An experimental investigation and characterization on flame bifurcation and leaning transition behavior of a pool fire in near wake of a square cylinder. *Int J Heat Mass Transf* 2012;55:7024–35. doi:10.1016/j.ijheatmasstransfer.2012.07.015.
- [4] Atkinson GT, Wu Y. Smoke control in sloping tunnels. *Fire Saf J* 1996;27:335–41. doi:10.1016/S0379-7112(96)00061-6.
- [5] Hu LHH, Huo R, Peng W, Chow WKK, Yang RXX. On the maximum smoke temperature under the ceiling in tunnel fires. *Tunn Undergr Sp Technol* 2006;21:650–5. doi:10.1016/j.tust.2005.10.003.
- [6] Barbato L, Cascetta F, Musto M, Rotondo G. Fire safety investigation for road tunnel ventilation systems – An overview. *Tunn Undergr Sp Technol* 2014;43:253–65. doi:10.1016/j.tust.2014.05.012.
- [7] National Fire Protection Association. NFPA 502: Standard for Road Tunnels,

Bridges, and Other Limited Access Highways, 2011 Edition 2011;2458000:51.

- [8] AIPCR. Fire and Smoke Control in Road Tunnels. 1999.

- [9] Carvel RO, Beard AN, Jowitt PW, Drysdale DD. Variation of heat release rate with forced longitudinal ventilation for vehicle fires in tunnels. *Fire Saf J* 2001;36:569–96. doi:10.1016/S0379-7112(01)00010-8.

- [10] Li JS., Chow W. Numerical studies on performance evaluation of tunnel ventilation safety systems. *Tunn Undergr Sp Technol* 2003;18:435–52. doi:10.1016/S0886-7798(03)00023-3.

- [11] Vauquelin O. Parametrical study of the back flow occurrence in case of a buoyant release into a rectangular channel. *Exp Therm Fluid Sci* 2005;29:725–31. doi:10.1016/j.expthermflusci.2005.01.002.

- [12] Hu LH, Huo R, Chow WK. Studies on buoyancy-driven back-layering flow in tunnel fires. *Exp Therm Fluid Sci* 2008;32:1468–83. doi:10.1016/j.expthermflusci.2008.03.005.

- [13] Walton WD, Thomas PH, Ohmiya Y. Estimating Temperatures in Compartment Fires. *SFPE Handb. Fire Prot. Eng.*, New York, NY: Springer New York; 2016, p. 996–1023. doi:10.1007/978-1-4939-2565-0_30.

- [14] Peacock RD, Jones WW, Reneke PA, Forney GP. CFAST – Consolidated Model of Fire Growth and Smoke Transport (Version 6) User’s Guide. NIST Spec Publ 1041.

- [15] McGrattan K, Hostikka S, Floyd J. Fire Dynamics Simulator, User's Guide. NIST Spec Publ 2000.
- [16] Greenshields C. OpenFOAM The OpenFOAM Foundation User Guide 2011.
- [17] Quintiere JG. Fundamental of Fire Phenomena. 2006.
- [18] Yi L, Xu Q, Xu Z, Wu D. An experimental study on critical velocity in sloping tunnel with longitudinal ventilation under fire. *Tunn Undergr Sp Technol* 2014;43:198–203. doi:10.1016/j.tust.2014.05.017.
- [19] Kang K. Characteristic length scale of critical ventilation velocity in tunnel smoke control. *Tunn Undergr Sp Technol* 2010;25:205–11. doi:10.1016/j.tust.2009.11.004.
- [20] Roh JS, Yang SS, Ryou HS, Yoon MO, Jeong YT. An experimental study on the effect of ventilation velocity on burning rate in tunnel fires-heptane pool fire case. *Build Environ* 2008;43:1225–31. doi:10.1016/j.buildenv.2007.03.007.
- [21] Li YZ, Lei B, Ingason H. Study of critical velocity and backlayering length in longitudinally ventilated tunnel fires. *Fire Saf J* 2010;45:361–70. doi:10.1016/j.firesaf.2010.07.003.
- [22] Quintiere JG. Scaling applications in fire research. *Fire Saf J* 1989;15:3–29. doi:10.1016/0379-7112(89)90045-3.
- [23] Tang W, Hu LH, Chen LF. Effect of blockage-fire distance on buoyancy driven

- back-layering length and critical velocity in a tunnel: An experimental investigation and global correlations. *Appl Therm Eng* 2013;60:7–14. doi:10.1016/j.applthermaleng.2013.06.033.
- [24] Lee Y-P, Tsai K-C. Effect of vehicular blockage on critical ventilation velocity and tunnel fire behavior in longitudinally ventilated tunnels. *Fire Saf J* 2012;53:35–42. doi:10.1016/j.firesaf.2012.06.013.
- [25] Kayili S, Yozgatligil A, Eralp OC. Effect of Ventilation and Geometrical Parameters of the Burning Object on the Heat Release Rate in Tunnel Fires. *Combust Sci Technol* 2012;184:165–77. doi:10.1080/00102202.2011.625371.
- [26] Kayili S, Yozgatligil A, Cahit Eralp O. An experimental study on the effects of blockage ratio and ventilation velocity on the heat release rate of tunnel fires. *J Fire Sci* 2011;29:555–75. doi:10.1177/0734904111416336.
- [27] Babrauskas V, Peacock RD. Heat release rate: The single most important variable in fire hazard. *Fire Saf J* 1992;18:255–72. doi:10.1016/0379-7112(92)90019-9.
- [28] Parker WJ. Calculations of the Heat Release Rate by Oxygen Consumption for Various Applications. *J Fire Sci* 1984;2:380–95. doi:10.1177/073490418400200505.
- [29] Huggett C. Estimation of rate of heat release by means of oxygen consumption measurements. *Fire Mater* 1980;4:61–5. doi:10.1002/fam.810040202.

- [30] Brohez S, Delvosalle C, Marlair G, Tewarson a. The Measurement of Heat Release from Oxygen Consumption in Sooty Fires. *J Fire Sci* 2000;18:327–53. doi:10.1177/073490410001800501.
- [31] Brohez S, Delvosalle C, Marlair G, Tewarson a. Soot Generation In Fires: An Important Parameter For Accurate Calculation Of Heat Release. *Fire Saf Sci* 2000;6:265–76. doi:10.3801/IAFSS.FSS.6-265.
- [32] Hamins A, Johnsson E, Donnelly M, Maranghides A. Energy balance in a large compartment fire. *Fire Saf J* 2008;43:180–8. doi:10.1016/j.firesaf.2007.08.002.
- [33] Pretrel H, Saux W Le, Audouin L. Experimental determination of fire heat release rate with OC and CDG calorimetry for ventilated compartments fire scenario 2014:474–506. doi:10.1002/fam.
- [34] Bryant R, Mulholland G. A guide to characterizing heat release rate measurement uncertainty for full- scale fire tests. *Fire Mater* 2008:121–39. doi:10.1002/fam.
- [35] Janssens ML. Measuring rate of heat release by oxygen consumption. *Fire Technol* 1991;27:234–49. doi:10.1007/BF01038449.
- [36] Sensenig DL, States. U, (U.S.) C for FR. An oxygen consumption technique for determining the contribution of interior wall finishes to room fires 1980:86 in various pagings.
- [37] Thomas PH, Committee M of T and FO. The Movement of Smoke in Horizontal

Passages Against an Air Flow. 1968.

- [38] Kennedy WD. Critical Velocity: Past, Present and Future. Semin. Smoke Crit. Veloc. Tunnels, London: JFL Lowndes; 1996, p. 305–22.

- [39] Wu Y, Bakar MZ. Control of smoke flow in tunnel fires using longitudinal ventilation systems – a study of the critical velocity. *Fire Saf J* 2000;35:363–90. doi:10.1016/S0379-7112(00)00031-X.

- [40] Stahlanwendung S. Fires in Transport Tunnels: Report on Full-scale Tests ; Eureka-Project EU 499: FIRETUN ; Conducted by the Following 9 European Countries: Austria, Finland, France, Germany, Great Britain, Italy, Norway, Sweden, Switzerland. 1995.

- [41] Ingason H. State of the Art of Tunnel Fire Research. *Fire Saf Sci* 2008;9:33–48. doi:10.3801/IAFSS.FSS.9-33.

- [42] Bechtel P. Memorial Tunnel Fire Ventilation Test Program Test Report. 1995.

- [43] Lemaire T, Kenyon Y. Large Scale Fire Tests in the Second Benelux Tunnel. *Fire Technol* 2006;42:329–50. doi:10.1007/s10694-006-8434-4.

- [44] Lönnermark A, Ingason H. Gas temperatures in heavy goods vehicle fires in tunnels. *Fire Saf J* 2005;40:506–27. doi:10.1016/j.firesaf.2005.05.003.

- [45] Ingason H, Lönnermark A. Heat release rates from heavy goods vehicle trailer fires in tunnels. *Fire Saf J* 2005;40:646–68. doi:10.1016/j.firesaf.2005.06.002.

- [46] Lönnermark A, Ingason H. Fire Spread and Flame Length in Large-Scale Tunnel Fires. *Fire Technol* 2006;42:283–302. doi:10.1007/s10694-006-7508-7.
- [47] Roh JS, Ryou HS, Kim DH, Jung WS, Jang YJ. Critical velocity and burning rate in pool fire during longitudinal ventilation. *Tunn Undergr Sp Technol* 2007;22:262–71. doi:10.1016/j.tust.2006.08.003.
- [48] Hu LH, Liu S, Peng W, Huo R. Experimental study on burning rates of square/rectangular gasoline and methanol pool fires under longitudinal air flow in a wind tunnel. *J Hazard Mater* 2009;169:972–9. doi:10.1016/j.jhazmat.2009.04.050.
- [49] Li L, Li S, Wang X, Zhang H. Fire-induced flow temperature along tunnels with longitudinal ventilation. *Tunn Undergr Sp Technol* 2012;32:44–51. doi:10.1016/j.tust.2012.05.003.
- [50] Li YZ, Lei B, Ingason H. The maximum temperature of buoyancy-driven smoke flow beneath the ceiling in tunnel fires. *Fire Saf J* 2011;46:204–10. doi:10.1016/j.firesaf.2011.02.002.
- [51] Chen B, Lu S, Li C, Kang Q, Yuan M. Unsteady burning of thin-layer pool fires. *J Fire Sci* 2011;30:3–15. doi:10.1177/0734904111415807.
- [52] Wang C, Guo J, Ding Y, Wen J, Lu S. Burning rate of merged pool fire on the hollow square tray. *J Hazard Mater* 2015;290:78–86. doi:10.1016/j.jhazmat.2015.02.069.

- [53] Ji J, Fan CG, Li YZ, Ingason H, Sun JH. Experimental study of non-monotonous sidewall effect on flame characteristics and burning rate of n-heptane pool fires. *Fuel* 2015;145:228–33. doi:10.1016/j.fuel.2014.12.085.
- [54] Dlugogorcki B, Wilson M. Effect Of Lip Ieiget On Properties Of Small Scale Pool Fires. *AOFST 2* 1995:129–40.
- [55] Hu L, Wu L, Liu S. Flame length elongation behavior of medium hydrocarbon pool fires in cross air flow. *Fuel* 2013;111:613–20. doi:10.1016/j.fuel.2013.03.025.
- [56] Miloua H, Azzi a. Evaluation of different numerical approaches for a ventilated tunnel fire. *J Fire Sci* 2011;29:403–29. doi:10.1177/0734904111400976.
- [57] Nilsen a. R, Log T. Results from three models compared to full-scale tunnel fires tests. *Fire Saf J* 2009;44:33–49. doi:10.1016/j.firesaf.2008.03.001.
- [58] Wang HY. Numerical and theoretical evaluations of the propagation of smoke and fire in a full-scale tunnel. *Fire Saf J* 2012;49:10–21. doi:10.1016/j.firesaf.2011.12.012.
- [59] Jain S, Kumar S, Kumar S, Sharma TP. Numerical simulation of fire in a tunnel: Comparative study of CFAST and CFX predictions. *Tunn Undergr Sp Technol* 2008;23:160–70. doi:10.1016/j.tust.2007.04.004.
- [60] Steinhaus T, Welch S, Carvel R, Torero J. Large-scale pool fires. *Therm Sci* 2007;11:101–18. doi:10.2298/TSCI0702101S.

- [61] Blinov VI, Khudiakov GN. Certain Laws In The Diffusion Burning Of Liquids. Dokl Akad Nauk SSSR 1957;113:1094–7.
- [62] Rasbash DJ, Rogowski ZW, Stark GW V. Properties of fires of liquids. Fuel 1956;35:94–132.
- [63] De Ris J, Orloff L. A dimensionless correlation of pool burning data. Combust Flame 1972;18:381–8. doi:10.1016/S0010-2180(72)80189-5.
- [64] Babrauskas V. Estimating large pool fire burning rates. Fire Technol 1983;19:251–61. doi:10.1007/BF02380810.
- [65] Koseki H. Combustion properties of large liquid pool fires. Fire Technol 1989;25:241–55. doi:10.1007/BF01039781.
- [66] Mudan KS. Thermal radiation hazards from hydrocarbon pool fires. Prog Energy Combust Sci 1984;10:59–80. doi:10.1016/0360-1285(84)90119-9.
- [67] Ditch BD, de Ris JL, Blanchat TK, Chaos M, Bill RG, Dorofeev SB. Pool fires - An empirical correlation. Combust Flame 2013;160:2964–74. doi:10.1016/j.combustflame.2013.06.020.
- [68] Hayasaka H. Unsteady Burning Rates Of Small Pool Fires. Fire Saf Sci 1997;5:499–510. doi:10.3801/IAFSS.FSS.5-499.
- [69] Drysdale D. Steady Burning of Liquids and Solids. An Introd to Fire Dyn 2011:181–223. doi:10.1002/9781119975465.ch5.

- [70] Wheeler, Anthony J.; Ganji AR. Introduction to Engineering Experimentation. 3rd ed. New Jersey: Pearson; 2010.
- [71] Fox, Robert; McDonald, Alan; Pritchard PJ. Introduction to Fluid Mechanics, 6th Edition. 6th ed. Wiley; n.d.
- [72] Brohez S. Uncertainty analysis of heat release rate measurement from oxygen consumption calorimetry. *Fire Mater* 2005;29:383–94. doi:10.1002/fam.895.
- [73] Enright PA, Fleischmann CM. Uncertainty of Heat Release Rate Calculation of the ISO5660--1 Cone Calorimeter Standard Test Method. *Fire Technol* 1999;35:153–69. doi:10.1023/A:1015416005888.
- [74] McGrattan K, Hostikka S, Floyd J, Baum H. NIST Special Publication 1018-5. Fire Dynamics Simulator (version 5). Technical Reference Guide. *Math Model* 2008;1.
- [75] McGrattan K, McDermott R, Floyd J, Hostikka S, Forney G, Baum H. Computational fluid dynamics modelling of fire. *Int J Comput Fluid Dyn* 2012;26:349–61. doi:10.1080/10618562.2012.659663.
- [76] Anderson DA (Dale A, Pletcher RH, Tannehill JC. Computational fluid mechanics and heat transfer. n.d.
- [77] Glassman I. Combustion. Academic Press; 1996.

- [78] Spalding DB. The combustion of liquid fuels. *Symp Combust* 1953;4:847–64. doi:10.1016/S0082-0784(53)80110-4.
- [79] Chen B, Lu SX, Li CH, Kang QS, Lecoustre V. Initial fuel temperature effects on burning rate of pool fire. *J Hazard Mater* 2011;188:369–74. doi:10.1016/j.jhazmat.2011.01.122.
- [80] Hamins A, Fischer SJ, Kashiwagi T, Klassen ME, Gore JP. Heat Feedback to the Fuel Surface in Pool Fires. *Combust Sci Technol* 1994;97:37–62. doi:10.1080/00102209408935367.
- [81] Zhu P, Wang X, Tao C. Experiment study on the burning rates of ethanol square pool fires affected by wall insulation and oblique airflow. *Exp Therm Fluid Sci* 2015;61:259–68. doi:10.1016/j.expthermflusci.2014.11.006.
- [82] Gao ZH, Liu ZX, Ji J, Fan CG, Li LJ, Sun JH. Experimental study of tunnel sidewall effect on flame characteristics and air entrainment factor of methanol pool fires. *Appl Therm Eng* 2016;102:1314–9. doi:10.1016/j.applthermaleng.2016.03.025.
- [83] Kurioka H, Oka Y, Satoh H, Sugawa O. Fire properties in near field of square fire source with longitudinal ventilation in tunnels. *Fire Saf J* 2003;38:319–40. doi:10.1016/S0379-7112(02)00089-9.
- [84] Gwon Hyun Ko GH, Seung Ryul Kim SR, Hong Sun Ryou HS. An Experimental Study on the Effect of Slope on the Critical Velocity in Tunnel Fires. *J Fire Sci* 2010;28:27–47. doi:10.1177/0734904109106547.

- [85] Quade PB. D. Subway Environmental Design Handbook. Volume II. Subway Environment Simulation Computer Program (SES). Part 1. User's Manual. vol. II. 1980.

CURRICULUM VITAE

PERSONAL INFORMATION

Surname, Name: Shafee, Sina
Nationality: Iranian
Date and Place of Birth: 5 May 1986, Maragheh-Iran
E-mail: sina.shafee@metu.edu.tr

EDUCATION

Degree	Institution	Year of Graduation
MSc.	Sahand University of Technology Mechanical Engineering Department	2011
BSc.	Urmia University Mechanical Engineering Department	2007
High School	Nemune Azadegan	2003

FOREIGN LANGUAGES

Fluent English, Fluent Turkish

PUBLICATIONS

- Shafee S., Yamali U., Yozgatligil A., Experimental Investigation on the Mass Loss Rates of Thin-Layered n-Heptane Pool Fires in Longitudinally Ventilated Reduced Scale Tunnel, (2017) *Combustion Science and Technology*, DOI: 10.1080/00102202.2017.1338693.
- Shafee S., Yozgatligil A., A Scaled Study on The Effect of Blockage on Tunnel Fires, Accepted for oral presentation at Tenth Mediterranean Combustion Symposium (MCS-10), 17–21 Sept. 2017, Flegrea Area, Napoli, Italy.
- Shafee S., Yozgatligil A., A scaled study on pool fire characteristics in longitudinally ventilated tunnels, Under review at *Thermal Science*, ThSci2017.072.

- Shafee S., Yozgatligil A., Burning Rate of Confined Pool Fires Affected by Adjacent Fire Source, Ready for submission to Fire Safety Journal.
- Shafee S., Yozgatligil A., An Experimental Investigation on the Effect of Inclination and Blockage Ratio on the Combustion Characteristics of Tunnel Fires, In preparation
- Shafee S., Yozgatligil A., An experimental study on the effect of wall coating material on the radiative heat loss from ethanol pool fires in tunnels, 13th International Combustion Symposium, Sept. 9-11, 2015, Bursa, Turkey.
- Maghbouli A., Yang W., An H., Li J., Shafee S. Effects of injection strategies and fuel injector configuration on combustion and emission characteristics of a D.I. diesel engine fueled by bio-diesel, (2015) Renewable Energy, 76, pp. 687-698.
- Maghbouli A., Shafee S., Saray R.K., Yang W., Hosseini V., An H. A Multi-Dimensional CFD-Chemical Kinetics Approach in Detection and Reduction of Knocking Combustion in Diesel-Natural Gas Dual-Fuel Engines Using Local Heat Release Analysis (2013) SAE International Journal of Engines, 6 (2), pp. 777-787.
- A. Maghbouli, R. Khoshbakhti Saray, Shafee S., J. Ghafouri, Numerical study of combustion and emission characteristics of dual-fuel engines using 3D-CFD models coupled with chemical kinetics, FUEL, 106 (2013) 98–105
- R. Barzegar, Shafee S., Sh. Khalilarya, CFD simulation of the combustion process, emission formation and the flow field in an in-direct injection diesel engine, Thermal Science Intl. Scientific Journal (2012), DOI: 10.2298/TSCI111218108B.
- Shafee S., R. Khoshbakhti Saray, A. Maghbouli, J. Ghafouri, 3-D Modeling of Combustion in a Natural Gas Fuelled HCCI Engine, Proceedings of the 7th CICE, Olympic Hotel, Tehran, Iran, Nov.2011, A-10-102-1.

HOBBIES

Squash, Motor sport, Languages, Travel